



ScienceDirect®

AEU - International Journal of Electronics and Communications

Supports *open access*

7.2

CiteScore

3.169

Impact Factor

[Submit your article ↗](#)[Guide for authors ↗](#)

Menu

[Search in this journal](#)Latest
issue**Volume 170***In progress* • October 2023**About the journal**

International Journal of Electronics and Communications

AEÜ is an international scientific journal which publishes original works, invited tutorials, and special issues on the state-of-the art research areas. The journal's scope covers design and implementation of electronic devices, circuits, and communication systems, including but not limited to:

- ...

[View full aims & scope](#)[VDE Homepage ↗](#)**1.3 weeks**

Time to First Decision

2.1 weeks

Review Time

1.1 weeks

Publication Time

[View all insights](#)**Editor-in-Chief** | [View full Editorial Board](#)**Shahram MINAEI, Prof. Dr.**

Dogus University, İstanbul, Turkey

FEEDBACK

[Recent Advances in the Design and Applications of Fractional-Order Circuits and Systems](#)

Edited by Prof. Costas Psychalinos, Prof. Ahmed S. Elwakil, Assist. Prof. Anis Allagui, Dr. Aleksei Tepljakov

19 April 2022

[RF and Antenna Devices and Techniques for Emergent Communication Systems](#)

Edited by Angel-Antonio San-Blas, Andrea Francesco Morabito, Mohammad H Neshati

29 November 2021

[> View all special issues and article collections](#)

[> View all issues](#)

Print ISSN: 1434-8411
Online ISSN: 1618-0399

Copyright © 2023 Elsevier GmbH. All rights reserved

For Authors

[Track your accepted paper](#)

[Journal Finder](#)

[Researcher Academy](#)

[Rights and permissions](#)

[Journal Article Publishing Support Center](#)

For Editors

[Publishing Ethics Resource Kit](#)

[Guest Editors](#)

For Reviewers

[Reviewer recognition](#)



Copyright © 2023 Elsevier B.V. or its licensors or contributors.
ScienceDirect® is a registered trademark of Elsevier B.V.



[> Aims and scope](#)[> Editorial board](#)[> Call for papers](#)[> News](#)[> Announcements](#)

Editorial board by country/region

51 editors and editorial board members in 20 countries/regions

1 India (7)

2 Italy (7)

3 Spain (6)

[> See more editors by country/region](#)

Editorial board

Editor-in-Chief

Shahram MINAEI, Prof. Dr.

Dogus University, İstanbul, Turkey

[> View full biography](#)

Area Editors

[Submit your article](#) ↗

Leila Safari

L'Aquila AQ, Italy

Devices, Circuits and Electronics

Andrea Francesco Morabito

Reggio Calabria, Italy

Antennas

[View full biography](#)

Assistant to Editor-in-Chief

Erkan Yuce

Denizli, Turkey

Editorial Board

Ana Vazquez Alejos

Vigo, Spain

Ali Ialbaksh, PhD

Sydney, New South Wales, Australia

Anis Allagui, Ph.D

Sharjah, United Arab Emirates

[View full biography](#)

Karine Amis

Brest, France

Stéphane Azou, PhD

Brest, France

[View full biography](#)

Leyre Azpilicueta, PhD

Pamplona, Spain

[Submit your article](#) ↗

Reggio Calabria, Italy

Petros S Bithas

Athens, Greece

Fabiola Colone, PhD

Roma, Italy

Angela Coves, PhD

Elx, Spain

Mauro Cuevas

Buenos Aires, Argentina

Ahmed Elwakil, PhD

Sharjah, United Arab Emirates

Parul Garg, PhD

New Delhi, India

Jorge Guilherme, PhD

Tomar, Portugal

Khaled Hayatleh, BEng, PhD

Oxford, United Kingdom

Sajad Jafari, PhD

Tehran, Iran

Binod Kumar Kanaujia

New Delhi, India

Rakesh Kshetrimayum, PhD

Guwahati, India

[Submit your article](#) ↗

Saeed Latif, Ph.D.

Mobile, Alabama, United States of America

Chunguo Li, PhD

Nanjing, China

[View full biography](#)

Chao Lu, PhD

Carbondale, Illinois, United States of America

Mahsa Mehrad

Damghan, Iran

Giuseppina Monti

Lecce, Italy

Mohammad Neshati, PhD

Mashhad, Iran

[View full biography](#)

Sima Noghianian, Dr.

San Diego, California, United States of America

Thomas Noulis, PHD

Thessaloniki, Greece

[View full biography](#)

Irena Orovic

Podgorica, Montenegro

Roberta Palmeri

Reggio Calabria, Italy

Neeta Pandey, PhD

New Delhi, India

[Submit your article](#) ↗[View full biography](#)

Lobna Said, PhD

Cairo, Egypt

[View full biography](#)

Angel-Antonio San-Blas, PhD

Elx, Spain

Fabrizio Santi, PhD

Rome, Italy

[View full biography](#)

Prabhat Sharma, PhD

Nagpur, India

[View full biography](#)

Neeta Singh, Ph.D

New Delhi, India

Qingquan Sun, Ph.D.

San Bernardino, California, United States of America

Norikazu Takahashi

Okayama, Japan

Germán Torregrosa Penalva, PhD

Elx, Spain

Weimin Wang

Beijing, China

[View full biography](#)

Yongle Wu

Beijing, China

[Submit your article](#) ↗

Xian, China

Erkan Yuce

Denizli, Turkey

[View full biography](#)

Emeritus Editor-in-Chief

Ralf Lehnert

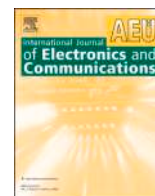
Dresden, Germany

All members of the Editorial Board have identified their affiliated institutions or organizations, along with the corresponding country or geographic region. Elsevier remains neutral with regard to any jurisdictional claims.



Copyright © 2023 Elsevier B.V. or its licensors or contributors.
ScienceDirect® is a registered trademark of Elsevier B.V.





Regular paper



Modeling of quasi-tapered microstrip antenna based on expansion-exponential tapered method and its application for wideband MIMO structure

Teguh Firmansyah^{a,*}, Supriyanto Praptodiyono^a, Jaka Permana^a, Syah Alam^b,
Toto Supriyanto^c, Ken Paramayudha^d, Yuyu Wahyu^d, Mudrik Alaydrus^e, Jun Kondoh^{f,g}

^a Department of Electrical Engineering, Universitas Sultan Ageng Tirtayasa, Cilegon, Indonesia

^b Department of Electrical Engineering, Universitas Trisakti, Jakarta, Indonesia

^c Department of Telecommunication Engineering, Politeknik Negeri Jakarta, Jakarta, Indonesia

^d Research Center for Electronics and Telecommunication, Indonesian Institute of Sciences, Bandung, Indonesia

^e Department of Electrical Engineering, Universitas Mercu Buana, Jakarta, Indonesia

^f Graduate School of Science and Technology, Shizuoka University, 3-5-1 Johoku, Naka-ku, Hamamatsu-shi 432-8561, Japan

^g Graduate School of Integrated Science and Technology, Shizuoka University, 3-5-1 Johoku, Naka-Ku, Hamamatsu-shi, Shizuoka 432-8561, Japan

ARTICLE INFO

Keywords:

4G/WLAN/X-band/5G
Expansion-exponential
MIMO antenna
Quasi-tapered structure

ABSTRACT

In this paper, a quasi-tapered wideband antenna using a circular-shaped with an inverted-omega ground structure is presented. A tapered antenna is usually developed based on linear-shape, exponential-shape, or Klopfenstein-shape taper. Here, we proposed an expansion of the exponential tapered model to investigate the circular-shaped tapered structure. In detail, the proposed antenna is divided into circular divergent and circular convergent-tapered sections. Then, the impedance ratio is utilized to analyze the tapered structure. Moreover, the ABCD parameter based on the transmission line model is used to investigate the overall antenna structure. The proposed model was verified by finite element method and also step impedance resonance evaluation. Furthermore, the proposed wideband antenna is also developed with multiple input multiple output (MIMO) and mutual coupling reduction structure. The antenna was fabricated on a Rogers RT/Duroid 5880 substrate with $\epsilon_r = 2.2$, thickness of $h = 1.6$ mm, and dielectric loss $\tan \delta = 0.0009$. As a result, the proposed MIMO antenna can successfully cover the 4G (3.3 GHz), mid-band 5G (3.4–3.8 GHz), WLAN (5.8 GHz), X-band (10–11 GHz), and high-band 5G (24.5–26 GHz) communications. A good agreement between the simulated and measured results validates the proposed method.

1. Introduction

A massive communication network with high data-rate capability is required to support 5G technology [1,2]. This challenging requirement has forced the development of 5G technology to work at the millimeter-wave (mmW) band to accommodate an enormous number of users with a wide bandwidth availability [3,4]. Several interesting methods of wideband antenna design working at mmW band have been investigated such as the substrate integrated cavity (SIC) antenna [5] and double-sided substrate-integrated waveguide (SIW) antenna [6]. They operate at the mmW band with a gain of 12 dBi and 8 dBi, respectively. Moreover, a monopole-like antenna structure [7] and a magneto-electric antenna [8] were introduced to combine 4G/WLAN and 5G

communications. Furthermore, antennas based on a tapered structure were proposed in [9–12].

In addition, another fundamental characteristic of 5G antennas is the multiple-input multiple-output (MIMO) capability. A well-designed MIMO antenna should deliver excellent particular performances, such as mutual coupling (MC), envelope correlation coefficient (ECC), and diversity gain (DG) [13–15]. Several methods were proposed for development of MIMO antennas including quasi-Yagi structure [16], metal frame structure [17], vertical stubs [18], fractal [19], and Y-shape structure [20]. Nonetheless, although these methods offer a good MIMO performance, they were only applicable for a single band 5G application. Then, a dual-loop antenna structure [21], step impedance [22], and a double-oval shaped antenna [23] were introduced for 4G and 5G

* Corresponding author.

E-mail address: teguhfirmansyah@untirta.ac.id (T. Firmansyah).

<https://doi.org/10.1016/j.aeue.2023.154745>

Received 7 March 2023; Accepted 24 May 2023

Available online 2 June 2023

1434-8411/© 2023 Elsevier GmbH. All rights reserved.

implementation with MIMO capability [24,25]. Nevertheless, these antennas did not target the mmWave band. Therefore, we can see the gap in the development of the MIMO antenna that can handle 4G, WLAN, X-band, and mid-high band 5G communications from S-band to mmW-band.

In addition to wideband performance and MIMO capability, the modeling of an antenna is essential for understanding and investigating its behavior. Therefore, many researchers proposed and derived models for antennas based on recursive convex optimization [26], equivalent circuit modeling [27], cavity model [28], and stepped-impedance resonator [29]. However, these proposed modeling techniques were focused on a narrow bandwidth antenna. To model wideband antennas, other methods such as space-mapping with kriging surrogates [30], linear elements [31], equivalent circuit model [32] have been successfully applied with slightly complex calculations. Furthermore, the MIMO antenna applications were investigated using various modeling techniques, namely a statistical analysis model [33], equivalent circuit model [34], effective length matrices [35], and eigen-analysis [36]. Nevertheless, these models were applied for narrowband applications. It is important to note that the design of antennas with wideband characteristics and suitable MIMO capability remains an open issue in antenna engineering. The study presented in this paper made several contributions, which are listed as follows:

1. A wideband antenna based on a quasi-tapered structure using a circular shape is proposed. A quasi-tapered characteristic was obtained by integrating a circular-shaped patch antenna with an inverted omega ground plane as shown in Fig. 1(a).
2. We also proposed an expansion-exponential tapered model to investigate the quasi-tapered structure based on a circular shape. This proposed model was utilized due to the limitation of the traditional linear, exponential, and Klopfenstein tapering methods. It is important to note that our circular tapered structure diverges from the conventional linear, exponential, or Klopfenstein shapes typically employed in tapering.
3. To obtain the mathematical model of for the circular shape tapered structure, we expand the the existing exponential shape tapered model. In detail, Fig. 1(b) illustrates the proposed circular tapered structure which is divided into two halves circular shapes. It is seen that the physical dimension of the left-side of the half-circular shape is increasing. However, if we investigate the impedance characteristic, the impedance value is decreasing. Therefore, the left side structure has a convergent behavior. Vice versa, the right side of the half-circular shape has a divergent characteristic.
4. The study employs the ABCD parameter based on the transmission line model to investigate the overall antenna structure. The proposed model was verified by the finite element method (FEM). Following

the verification process, the proposed antenna was then applied to a MIMO structure. The fabrication of the antenna was carried out on a Rogers RT/Duroid 5880 substrate with $\epsilon_r = 2.2$, thickness of $h = 1.6$ mm, and dielectric loss $\tan \delta = 0.0009$.

5. In addition, we also proposed a multislot defected ground structure (DGS) structure to reduce the mutual coupling parameter in the MIMO antenna system. As a result, the proposed MIMO antenna demonstrated wide bandwidth and excellent performance across various communication bands. The antenna is capable of operating in the S-band to mmW band, effectively covering a broad frequency range. This wide frequency coverage enabled the antenna to support multiple communication standards, including 4G (3.3 GHz), mid-band 5G (3.4–3.8 GHz), WLAN (5.8 GHz), and high-band 5G (24.5–26 GHz) concurrently. Table 1 provides an overview of the proposed research positioning.

This article has structures as follows. The first section describes the research position and the proposed method. The second section focuses on the quasi-tapered investigation based on the convergent/divergent-tapered model with ABCD parameters. The third section highlights the design and measurement of the proposed quasi-tapered MIMO antenna. Then, it is followed by the results/discussions and the MIMO performance investigation. Finally, the last section concludes this research.

2. Quasi-tapered antenna based on circular-shaped patch with inverted-omega ground structure

Several methods have been studied to predict the operation frequency of an antenna, namely the lumped circuit modelling [40,41] and the transmission line approach [13]–[17]. Fig. 1(a) shows the main part of the antenna structure including the patch plane, ground plane, and excitation port. It should be noted that the proposed antenna has a direct excitation configuration. Hence, we can extract the antenna structure as several parts: a source impedance (Z_S), an excitation line, a convergent-tapered section, a divergent-tapered section, and a load-impedance (Z_L). Here, we use air impedance as the load impedance [42,43], as depicted in Fig. 1(b). The followed section describes the expanded exponential-shape taper to get the circular-shape taper model.

2.1. Half-circular shaped tapered with expansion-exponential tapered model

The proposed half-circular shape tapered configuration with the expansion-exponential tapered model is shown in Fig. 2(a). It has a radius of R and has convergent-tapered behavior. The input part was directly connected to the source impedance of $Z_{S(2)}$ and the end part is connected to the load impedance of $Z_{L(2)}$. It has a length of l_A from the

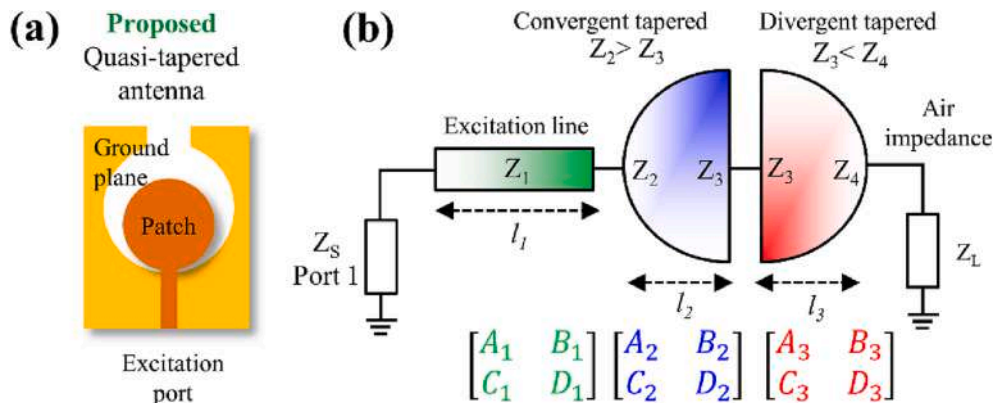


Fig. 1. (a) the proposed antenna based on quasi-tapered structure using circular-shaped patch with inverted-omega ground, (b) the ABCD parameters of proposed quasi-tapered antenna based on exponential tapered transmission lines approach.

Table 1
Research position.

Ref	Freq. (GHz)	Antenna structure	Proposed methods	Applications Narrow-band	Wide-band	MIMO antenna	Mutual coupling reduction	Advantages
[26]	2.50	Microstrip slot dipole	Recursive convex optimization	Yes	-	-	-	The proposed model has the capability to make predictions for the near field.
[27]	30.0	Micro-coaxial collinear	Equivalent circuit modeling	Yes	-	-	-	The calculation model is capable of identifying the equivalent circuit.
[28]	2.47-2.56	Stacked Microstrip Ring	Cavity model	Yes	-	-	-	The proposed model can predict the near field.
[29]	1.50-2.50	Stepped-Impedance Slot Antenna	Stepped-Impedance Resonator	Yes	-	-	-	The proposed model is capable of predicting the dualband impedance characteristics.
[30]	2.00-8.00	CPW-fed slot antenna with monopole	Space-mapping with kriging surrogates	-	Yes	-	-	The proposed model has the ability to forecast the value of reflection coefficient.
[31]	3.00	Conventional dipole	Linear elements	-	Yes	-	-	The model can estimate the radiation pattern.
[32]	2.51-6.55	Linear tapered slot	Equivalent circuit model	-	Yes	-	-	The calculation model has the potential to determine the equivalent circuit.
[33]	3.50-8.50	Monopole UWB	Statistical analysis model	-	Yes	-	-	The proposed model can make predictions for the value of reflection coefficient.
[34]	2.20	Monopole	Equivalent circuit model	Yes	-	Yes	-	The network parameters can be utilized for the prediction of S-parameters performance.
[35]	5.15-5.35	Monopole	The effective length matrices	Yes	-	Yes	-	The effective length matrices demonstrate good agreement with the method of moments.
[36]	5.20	FIFA-monopole	Eigen-Analysis	Yes	-	Yes	-	The model can determine the radiation pattern.
[37]	2.90-18.00	Circular shaped monopole	N.R.	-	Yes	Yes	Yes	The proposed antenna exhibits wideband performance.
[38]	3.00-30.0	Monopole with slot	N.R.	-	Yes	Yes	Yes	The proposed antenna possesses good isolation.
[39]	3.30-8.50	L-shaped branch	N.R.	-	Yes	Yes	Yes	The proposed antenna has wideband performance.
This paper	3.30-26.0	Quasi-tapered using circular shaped	Expansion-exponential tapered model	-	Yes	Yes	Yes	The proposed antenna design combines wideband performance, a simple impedance calculation model, and low mutual coupling in a MIMO configuration.

Note: N.R. = not reported.

input-port to the output-port. Moreover, Fig. 2(b). show the approximation characteristic of the impedance ratio (K) with different length of the taper. Here, we used the widest dimension of taper as the reference hence it has a unity value. Then, we can see that the impedance is increasing due to the decrease in the taper width.

To investigate the half-circular tapered configuration, we expand the exponential tapered model by introduce the term of impedance ratio with the expansion-exponential tapered model. The K can be written as:

$$K = a(e^{b(1-l_A)} + c) \tag{1}$$

where the a , b , and c are the adjustable constant parameters that follow the impedance curve of the circular shape. The intrinsic characteristic of the exponential-taper model is defined by the taper factor (b). Therefore, the impedance value of $Z_{(l=l_A)}$ at the length of l_A can be determined as:

$$Z_{(l=l_A)} = Z_{(l=0)}a(e^{b(1-l_A)} + c) \tag{2}$$

where $Z_{(l=0)}$ is the impedance at the initial position. Here, we state the initial impedance value as Z_0 . Then, the ABCD matrix of the half circular taper can be determined by:

$$\begin{bmatrix} A & B \\ C & D \end{bmatrix} = \frac{1}{\sqrt{Z_A Z_B}} \times \begin{bmatrix} Z_A \cosh \gamma l_A - Z_A \frac{d}{2\gamma} \sinh \gamma l_A & j Z_A Z_B \frac{\beta}{\gamma} \sinh \gamma l_A \\ j \frac{\beta}{\gamma} \sinh \gamma l_A & Z_B \cosh \gamma l_A + Z_B \frac{d}{2\gamma} \sinh \gamma l_A \end{bmatrix} \tag{3}$$

where

$$\gamma = \sqrt{\beta^2 - \left(\frac{d}{2}\right)^2} \tag{4}$$

$$d = \frac{\ln(a(e^{b(1-l_A)} + c))}{l_A} \tag{5}$$

$$\beta = \frac{2\pi}{\lambda} \tag{6}$$

with γ is the propagation constant. Moreover, the input impedance $Z_{IN(A)}$ can be calculated as:

$$Z_{IN(A)} = Z_A \frac{2Z_L \gamma + (j2Z_B \beta - Z_L d) \tanh \gamma l_A}{2Z_B \gamma + (j2Z_L \beta + Z_B d) \tanh \gamma l_A} \tag{7}$$

The next step is to investigate the antenna structure using the expansion-exponential taper model approximation, as depicted in Fig. 3 (a)-(b).

2.2. Quasi-tapered antenna with expansion-exponential tapered model

In detail, the proposed antenna structure can be separated into three important parts including excitation line, convergent-taper, and divergent taper, as shown in Fig. 3(a). It is important to note that eventhough the physical dimension becomes narrow or converging the impedance value becomes higher or diverging. Therefore, we called it as a divergent-taper and vice versa. Fig. 3(b) shows that the excitation line width is constant. Therefore, the impedance ratio is also constant. In addition, we introduce K_1 and K_2 as the impedance ratio for convergent-taper and divergent-taper, respectively. In detail, the investigation of the structure will be started by the excitation line followed by the convergent taper and divergent taper.

2.2.1. The excitation line

For more convenience and detail of the tapered structure, we can see Fig. 3(a)-(3b). The excitation line has directly connected to the input

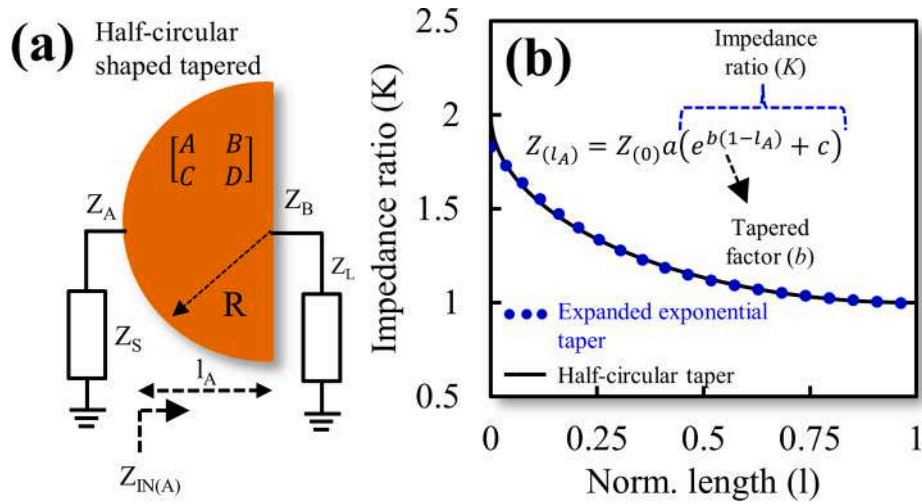


Fig. 2. (a) The proposed of half-circular shaped taper configuration with convergent tapered behavior. (b) Approximation of impedance ratio with widest dimension of taper as the reference.

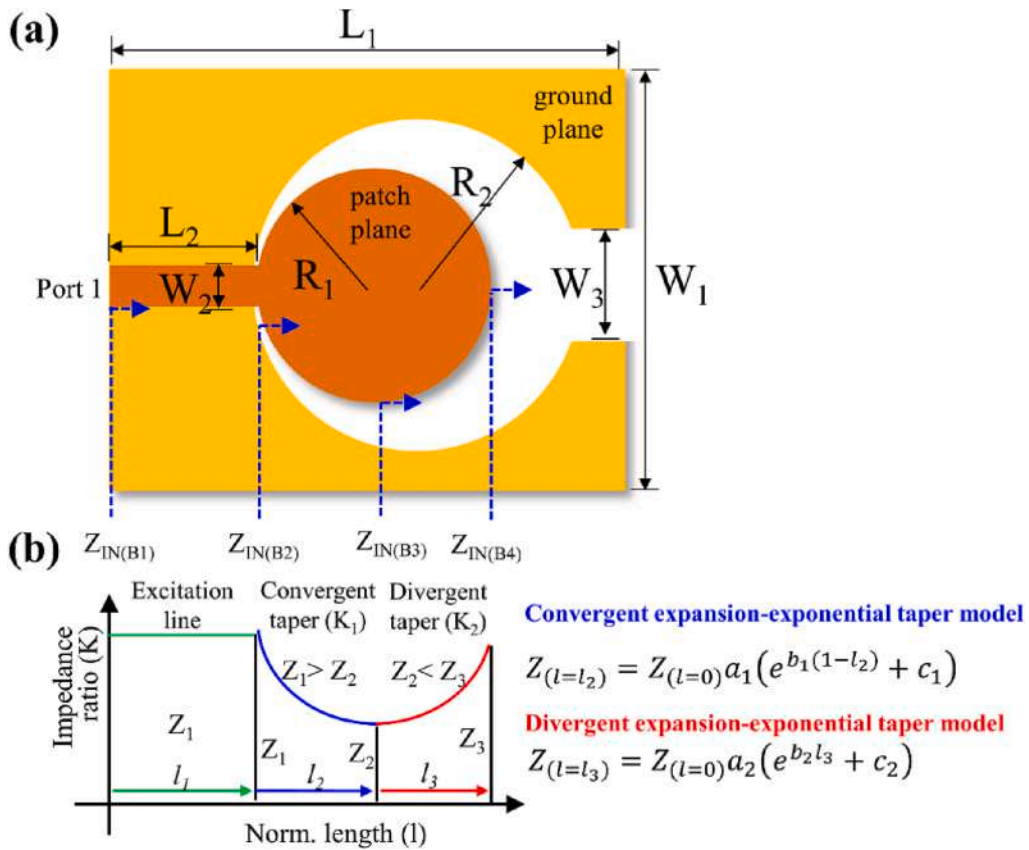


Fig. 3. (a) Quasi-tapered antenna based on circular-shaped with inverted-omega ground structure, (b) the approximation of impedance ratio and the electrical length of the proposed antenna structure.

impedance (Z_S) which is usually called as port 1. Moreover, the excitation line has the impedance characteristic (Z_1) and electrical length (l_1). They correspond to the width (W_2) and the length (L_1), respectively. To simplify the investigation, we assume the impedance of the excitation line (Z_1) is equal to the source impedance (Z_S).

2.2.2. The half-circular shaped convergent-tapered

The convergent-tapered is focused on decreasing of impedance values. Therefore, the impedance ratio (K_1) for the convergent taper of

the proposed antenna is determined by:

$$K_1 = a_1(e^{b_1(1-l_2)} + c_1) \tag{8}$$

where the a_1 , b_2 , and c_2 are constant parameters and the value follows the impedance curve. Moreover, b_2 is the convergent taper ratio for the proposed antenna.

Then, the impedance value of $Z_{(l=l_2)}$ at the length of l_2 can be calculated as:

$$Z_{(l=l_2)} = Z_{(l=0)} a_1 (e^{b_1(1-l_2)} + c_1) \quad (9)$$

where $Z_{(l=0)}$ is the impedance at the initial position. The ABCD matrix of half-circular taper with convergent structure can be determined by:

$$\begin{bmatrix} A_2 & B_2 \\ C_2 & D_2 \end{bmatrix} = \frac{1}{\sqrt{Z_1 Z_2}} \times \begin{bmatrix} Z_1 \cosh \gamma_2 l_2 - Z_1 \frac{d_1}{2\gamma} \sinh \gamma_2 l_2 & j Z_1 Z_2 \frac{\beta}{\gamma} \sinh \gamma_2 l_2 \\ j \frac{\beta}{\gamma} \sinh \gamma_2 l_2 & Z_2 \cosh \gamma_2 l_2 + Z_2 \frac{d_1}{2\gamma} \sinh \gamma_2 l_2 \end{bmatrix} \quad (10)$$

where

$$\gamma_2 = \sqrt{\beta^2 - \left(\frac{d_1}{2}\right)^2} \quad (11)$$

$$d_1 = \frac{\ln(a_1(e^{b_1(1-l_2)} + c_1))}{l_2} \quad (12)$$

with γ_2 is the propagation constant of the convergent taper with circular shape. Then, Fig. 4(a)-4(c) show the relation between normalized length (l_2) with the impedance ratio (K_1) for convergent taper with different value of a_1 , c_1 , and b_1 .

In detail, the normalized length of l_2 value was analyzed between 0 and 1. It can be seen that the a_1 and c_1 have a similar effect to the impedance ratio (K_1). The a_1 and c_1 have linear effects to the impedance ratio value. Moreover, K_1 was highly influenced by coefficient b_1 . Therefore, by adjusting the value of a_1 , c_1 , and b_1 , we can obtain the impedance ratio that is similar to the circular part.

2.2.3. The half-circular shaped divergent-tapered

The impedance ratio (K_2) for the divergent taper part of the proposed antenna design is determined by:

$$K_2 = a_2 (e^{b_2 l_3} + c_2) \quad (13)$$

where a_1 , b_2 , and c_2 are the adjustable constant parameters that follows the impedance curve. Moreover, b_2 is the convergent taper ratio for the proposed antenna. The impedance value of $Z_{(l=l_2)}$ at the length of l_2 can be calculated as:

$$Z_{(l=l_3)} = Z_{(l=0)} a_2 (e^{b_2 l_3} + c_2) \quad (14)$$

Then, the ABCD matrix of half-circular taper with convergent structure can be determined by:

$$\begin{bmatrix} A_3 & B_3 \\ C_3 & D_3 \end{bmatrix} = \frac{1}{\sqrt{Z_2 Z_3}} \times \begin{bmatrix} Z_2 \cosh \gamma_3 l_3 + Z_2 \frac{d_2}{2\gamma_3} \sinh \gamma_3 l_3 & j Z_2 Z_3 \frac{\beta}{\gamma_3} \sinh \gamma_3 l_3 \\ j \frac{\beta}{\gamma_3} \sinh \gamma_3 l_3 & Z_3 \cosh \gamma_3 l_3 - Z_3 \frac{d_2}{2\gamma_3} \sinh \gamma_3 l_3 \end{bmatrix} \quad (15)$$

where

$$\gamma_3 = \sqrt{\beta^2 - \left(\frac{d_2}{2}\right)^2} \quad (16)$$

$$d_2 = \frac{\ln(a_2(e^{b_2 l_3} + c_2))}{l_3} \quad (17)$$

with γ_2 is the propagation constant of the circular shape. Moreover, Fig. 5(a)-5(c) show the relation between normalized length (l_2) with the impedance ratio (K_1) of the convergent taper for different value of a_1 , c_1 , and b_1 , respectively. In details, the normalized length l_2 value was plotted from 0 to 1. Then, a_1 is varied from 0.028 to 0.038 with a step value of 0.002. Therefore, we can see that the value of K_1 decreases exponentially.

Overall, by adjusting the values of a_1 , b_1 , and c_1 , we can get the impedance ratio values of half-circular shaped using exponential taper model approach.

3. Comparison model

To verify the proposed model, the comparison of the impedance ratio of the expanded exponential model and finite element method (FEM) is presented in Fig. 6(a). We can see that the models are in good agreement and fit with each other. This means that the proposed model can be used to calculate the impedance ratio of circular-shaped taper. Moreover, the proposed model can be also implemented and verified using simple case, such as when $K = 1$ and the length of l between 0.5 and 1, d_1 and d_2 will become 0 as shown in Fig. 6(b). The model can be also utilized for the calculation of input impedance of step impedance resonator. In detail, by using $d = 0$ and the loss-less case of $\gamma = j\beta$, it will lead to the equation of input impedance of step impedance resonator as follows:

$$Z_{IN(B1)} = Z_1 \frac{Z_{IN(B2)} + j Z_1 \tan \beta l_1}{Z_1 + j Z_{IN(B2)} \tan \beta l_1} \quad (18)$$

$$Z_{IN(B2)} = Z_1 \frac{Z_{IN(B3)} + j Z_2 \tan \beta l_2}{Z_2 + j Z_{IN(B3)} \tan \beta l_2} \quad (19)$$

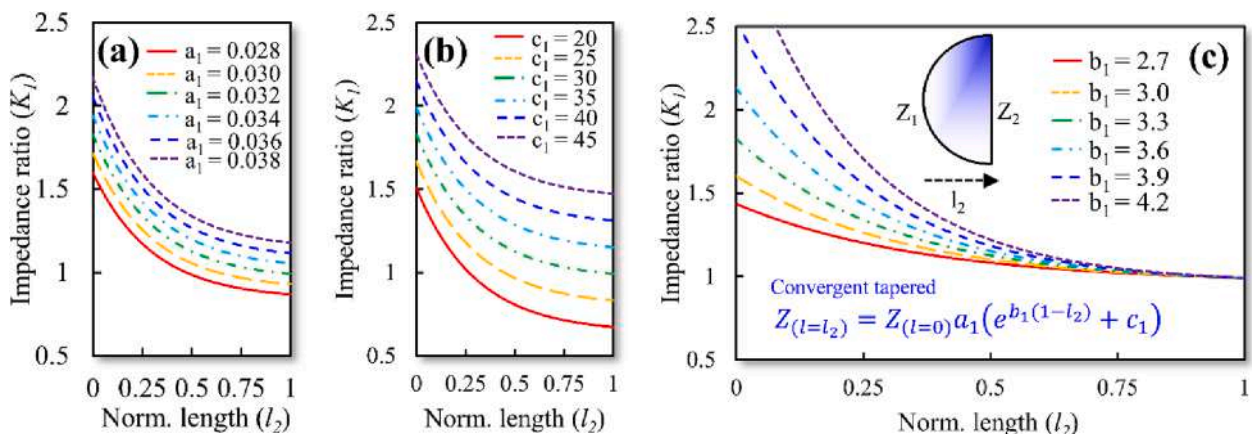


Fig. 4. (a) The relation between normalized length (l_2) with the impedance ratio (K_1) for different value of (a) a_1 , (b) c_1 , and (c) b_1 .

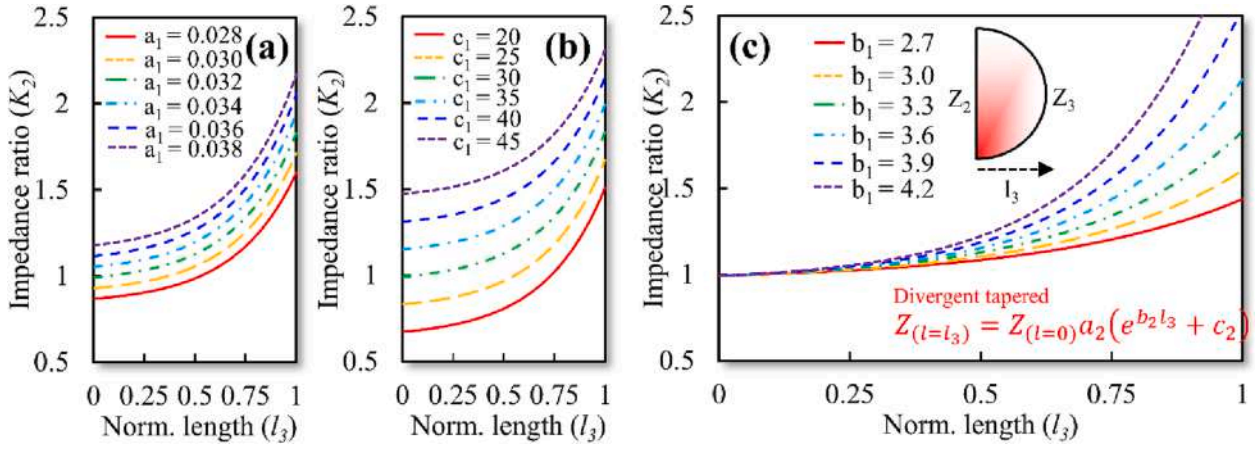


Fig. 5. (a) The relation between normalized length (l_3) with the impedance ratio (K_2) for different value of (a) a_2 , (b) c_2 and (c) b_1 .

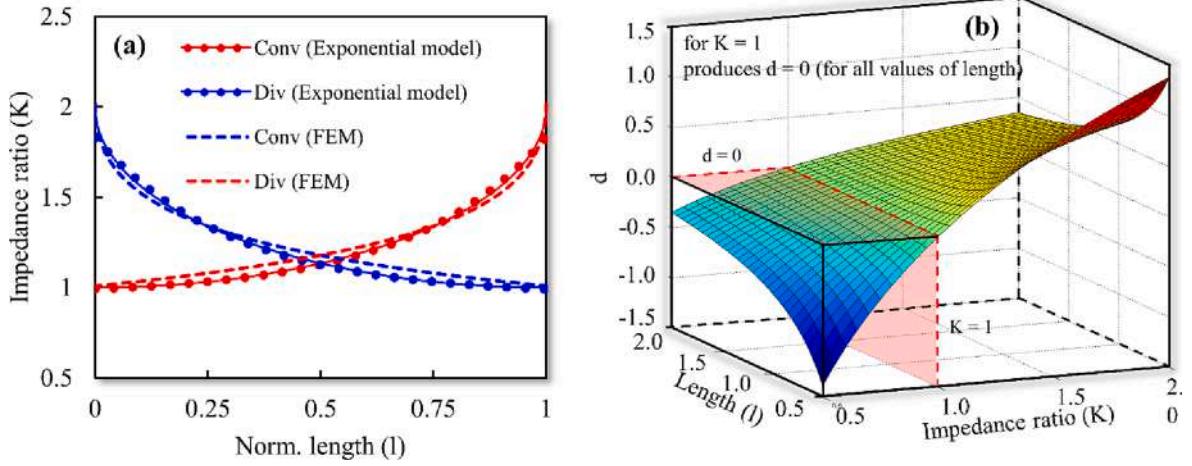


Fig. 6. (a) Comparison of circular shape-tapper using expanded exponential model, and finite element method (FEM) (b) a generalized for case $K = 1$ and its relations between l and d value.

$$Z_{IN(B3)} = Z_2 \frac{Z_{IN(B4)} + jZ_3 \tan \beta l_3}{Z_3 + jZ_{IN(B4)} \tan \beta l_3} \quad (20)$$

$$Z_{IN(B4)} = Z_L \quad (21)$$

Finally, the proposed exponential tapered transmission line model can be used for impedance calculation of circular shape resonator and step impedance resonator.

Fig. 7(a) and 7(b) show the results comparison between the expansion-exponential tapered method and conventional tapered method for circular convergent-taper and circular divergent-taper configurations, respectively. MATLAB software was used to perform the calculations for both the expansion-exponential and conventional tapered methods. In addition to MATLAB, the transmission line electromagnetics modeling tool suite of TNT 1.2.2 was utilized for the FEM based calculations. It is observed that the proposed method exhibited greater consistency and better fit with the FEM results. These results look similar for circular-convergent taper and circular-divergent taper. However, if we compare it with the conventional tapered methods, the deviation is significant. This results suggests that the proposed expansion-exponential tapered method offers distinct advantages and a more suitable design approach compared to conventional methods. Additionally, it is important to note that further detailed investigations of the antenna characteristics were conducted using CST Microwave Studio software.

The next step is antenna dimension optimization and MIMO

characterization. The antenna dimension can be optimized to obtain working frequencies ranging from S-band to mmWave band with $|S_{11}| < -10$ dB. To reduce the mutual coupling effect of this proposed MIMO antenna, we include a structure that is based on multi-slot configuration. This multi-slot structure was positioned at the middle part of the antenna ground plane. To evaluate the MIMO performance of the antenna, several additional parameters should also be considered. The parameters are $|S_{21}|$, ECC, and DG. ECC can be determined using S-parameters [44]. Then, the DG can be derived from the ECC equation [44].

4. Design of quasi-tapered wideband MIMO antenna

The design steps of the proposed antenna can be divided into two main parts. The first part focuses on the modelling of the quasi-tapered antenna using the transmission line model approach. Then, the second part focuses on the optimization of the MIMO antenna. In detail, the design procedures of the quasi-tapered antennas have several steps including a conventional circular shape monopole microstrip antenna design, feeding length modification, and ground-plane modification into an inverted omega-ground structure as illustrated as antenna A#, B#, and C# in Fig. 8(a)-8(c), respectively.

The substrate geometry of antenna A# is rectangular with a length of L_1 and a width of W_1 . The radiating part of the antenna A# structure is developed from a circular-shaped patch with radius of R_1 and is fed by a direct-excitation feed with a length of L_{3A} and width of W_2 . At the

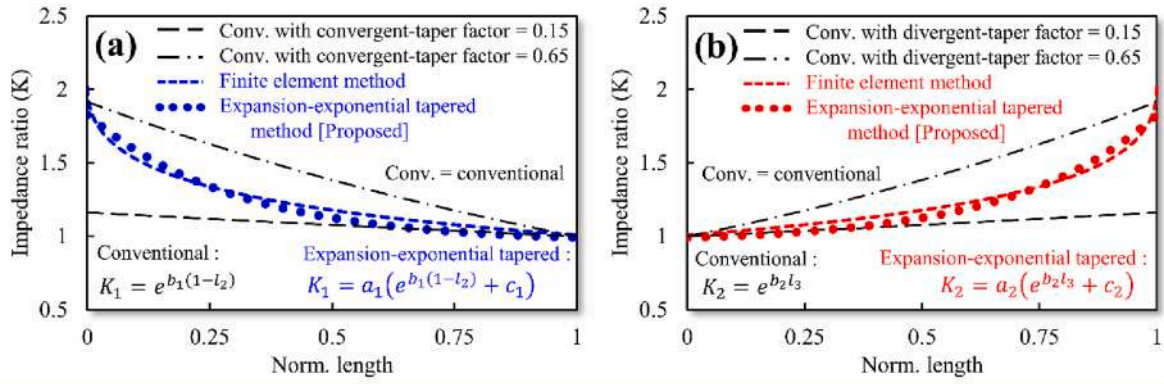


Fig. 7. Results comparison between the proposed method expansion-exponential tapered method and conventional tapered method (a) circular convergent-taper, and (b) circular divergent-taper.

ground plane side, a circular ground slot with the radius of R_2 is included. This ground slot is positioned at distances of L_2 and L_4 from the bottom and the top side of the substrate, respectively. It should be mentioned that the position of the circular patch and the circular ground slot are centrally aligned. Fig. 9(a) shows the reflection coefficient of antenna A# with variation of R_1 . In this scenario, R_1 is varied from 3 mm to 15 mm. We can see that the change of R_1 leads to the variation of antenna frequency and the return loss. However, we note that the antenna still has a poor matching impedance at several desired frequencies as shown in the reflection coefficient value. Hence, in the next step we investigate the effect of excitation length (L_2) variation on the resonant frequency as antenna B#. The simulation result of the effect of L_2 variation is shown in Fig. 9(b). The result indicates that the length of L_2 has a significant effect on the return loss of the antenna. Next, we add an upper part slot with a width of W_3 . This antenna is called antenna C#.

Fig. 10(a) shows that by using this additional slot, the antenna has a better reflection coefficient compared to antenna B#. Furthermore, Fig. 10(b) shows the comparison of the return loss of antenna A#/B#/C#. We can see that antenna C# has a better reflection coefficient compared to antenna A# or B#. Therefore, we decide to expand antenna C# into a MIMO structure. The design evolution of the MIMO antenna structure is shown in Fig. 11(a), 11(b), 11(c), and 11(d) as MIMO antenna C1#, C2#, C3#, and C4#. The C1# antenna represents a conventional MIMO antenna which comprises two identical antennas without any structural modification as depicted in Fig. 11(a).

In MIMO antenna C2#, an additional single DGS slot-ground

structure with a length of L_{D1} and width of W_{D1} is introduced at the top part of the ground plane as depicted in Fig. 11(b). the MIMO antenna C3# has a dual slots ground structure. The additional slot is positioned at the middle part of the ground plane with a length of L_{D2} and a width of W_{D2} , as shown in Fig. 11(c). Finally, a third ground slot is included in MIMO antenna C4#. This slot is introduced at the bottom part of the ground plane with a length of L_{D3} and width of W_{D3} , as illustrated in Fig. 11(d). The complete dimension and 3D view of MIMO antenna C4# can be seen in Fig. 12(a) and Fig. 12(b), respectively.

Moreover, Fig. 13(a) shows the comparison of the reflection coefficient of the MIMO antennas. We can see that a return loss of under -10 dB at the desired frequencies is achieved for all MIMO antennas C1#/C2#/C3#/C4#. This indicates that the proposed MIMO configurations have no significant effect on the operation frequency of the antenna. Lastly, Fig. 13(b) shows the comparison of the mutual coupling of MIMO antenna C1#/C2#/C3#/C4#. The results indicate that the MIMO antenna C4# provides the best isolation with a mutual coupling lower than -20 dB. Next, the proposed antenna is fabricated and measured to verify the simulation results.

5. Result and discussion

The proposed antennas C# and C4# were fabricated on Rogers RT/Duroid 5880 substrate with $\epsilon_r = 2.2$, thickness of $h = 1.6$ mm, and dielectric loss $\tan d = 0.0009$. The complete dimensions are as follows (in millimeter): $R_1 = 9$, $R_2 = 15$, $W_1 = 40$, $W_2 = 2.6$, $W_3 = 10$, $W_T = 85$,

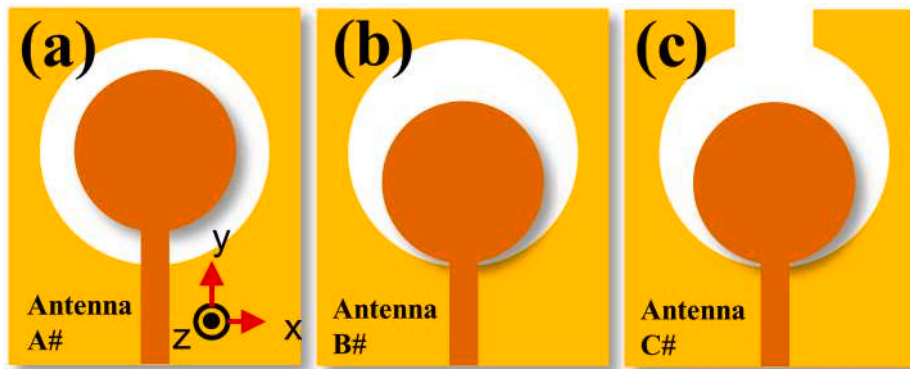


Fig. 8. (a) Conventional circular shape antenna, (b) modification the feeding length of L_2 , (c) modification of ground-plane and became inverted omega-ground structure by added W_3 .

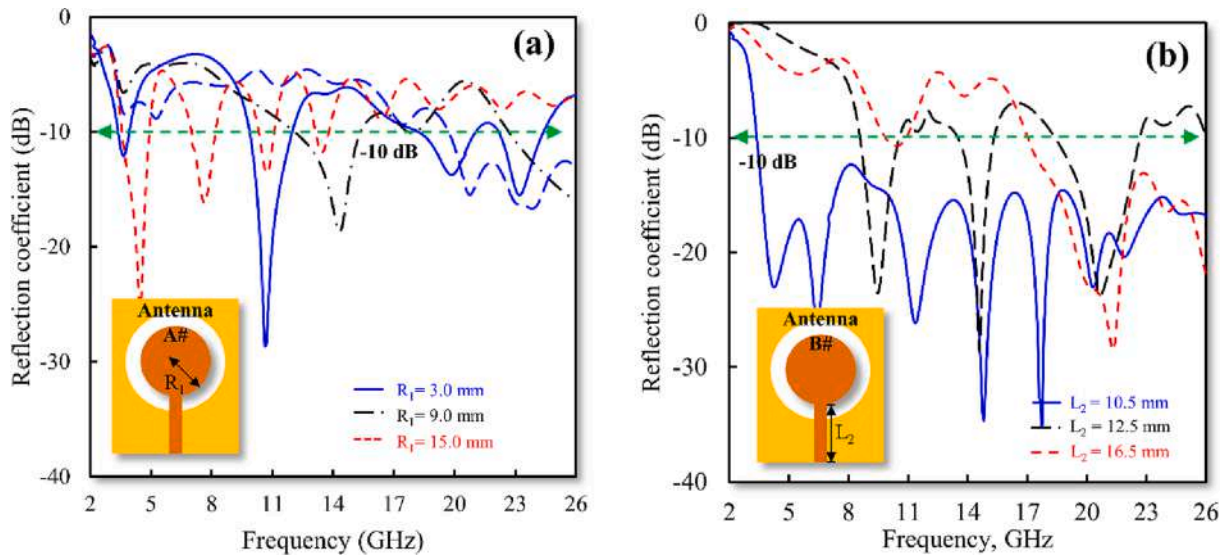


Fig. 9. (a) Reflection coefficient of antenna A# with varied of R_1 , (b) Reflection coefficient of antenna B# with varied of L_2 .

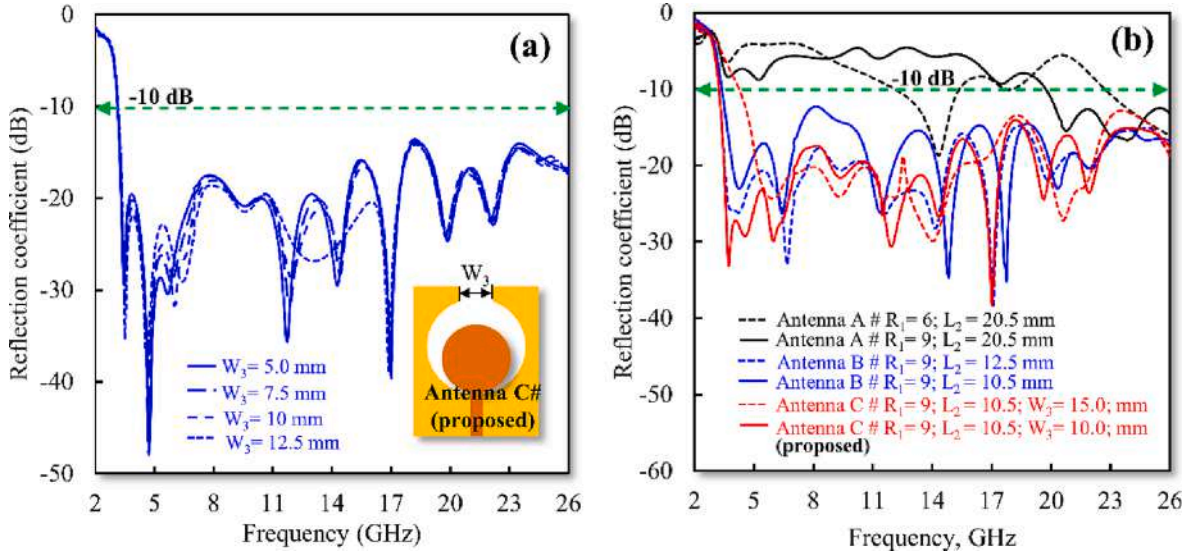


Fig. 10. (a) Reflection coefficient of antenna C# with varied of W_3 , (b) comparison of reflection coefficient of antenna A#/B#/C#.

$W_{D1} = 5, W_{D2} = 5, W_{D3} = 5, L_1 = 45, L_2 = 10.4, L_3 = 4.6, L_{3A} = 15.5, L_{3B} = 10.5, L_{D1} = 6, L_{D2} = 29.5, L_{D3} = 5$. In detail, Fig. 14(a), 14(b), 14(c), and 14(d) show the photographs of fabricated antenna C# and C4# with view from the patch and the ground side. The measurement of the proposed antenna's performance up to 26 GHz was facilitated by using the first-generation of super SMA female connectors from HASCO. Based on the data sheet, this connector has good performance from DC up to 27 GHz [45]. Furthermore, an R&S ZVA67 VNA is used to measure the antenna performance.

Fig. 14(e) shows the reflection coefficient comparison between the simulation and measurement of antenna C#. We can see that at several frequencies points the measured return losses are higher than those from the simulation. Nevertheless, they are still under -10 dB and hence the antenna C# can successfully cover a wide range from S-band to mmW band. Fig. 14(f) shows a comparison of the reflection coefficient between the simulation and measurement of MIMO antenna C4#. In line with the antenna C#, the MIMO configuration does not change the reflection

coefficients significantly. The return loss of the proposed MIMO antenna is still under -10 dB.

The mutual coupling (MC) comparison between simulation and measurement of MIMO antenna C4# is depicted in Fig. 14(g). In MIMO antenna, MC is generally used to evaluate the interaction of the antennas. We can see that the MIMO antenna C4# has MC values lower than -20 dB in all desired frequencies. Therefore, we can conclude that the interferences between antennas are insignificant. It should be noted that, in principle, this antenna has the potential to operate across wide frequency bands. However, in this paper, the focus was directed towards specific frequency bands in order to position the study within the context of future communication technologies. We have selected several specific bands such as the 4G (3.3 GHz), mid-band 5G (3.4–3.8 GHz), WLAN (5.8 GHz), X-band (10–11 GHz), and high-band 5G (24.5–26 GHz) communications.

Fig. 15 (a-j) presents the normalized co-and cross-polarization radiation patterns of the proposed antenna. Specifically, Fig. 15 (a-e) display

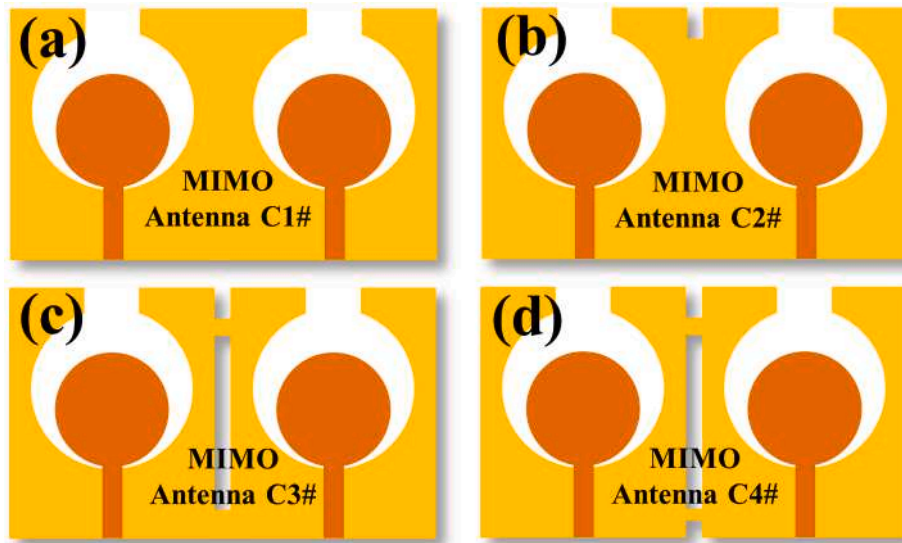


Fig. 11. (a) MIMO antenna C4#, and (b) 3D view of proposed MIMO antenna C4#.

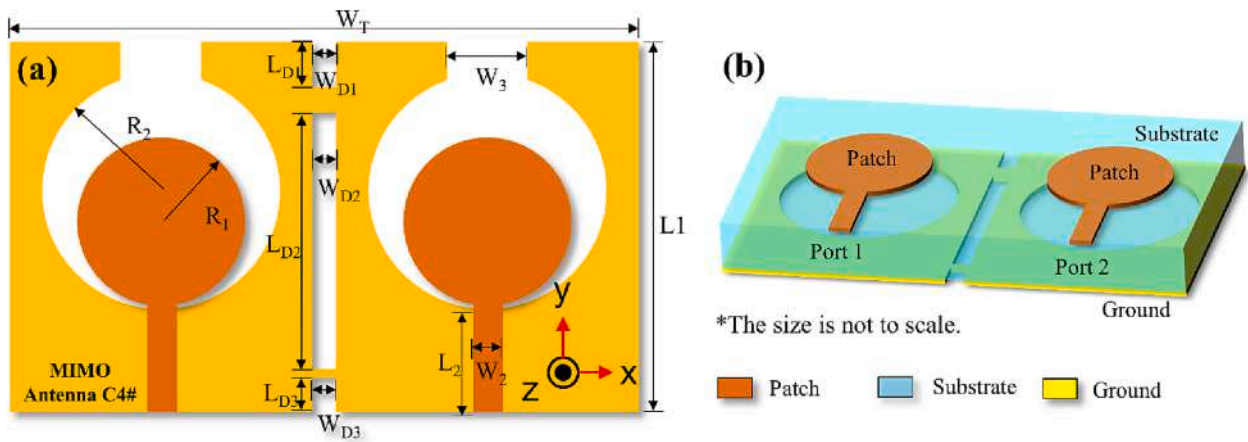


Fig. 12. (a) MIMO antenna C4#, and (b) 3D view of proposed MIMO antenna C4#.

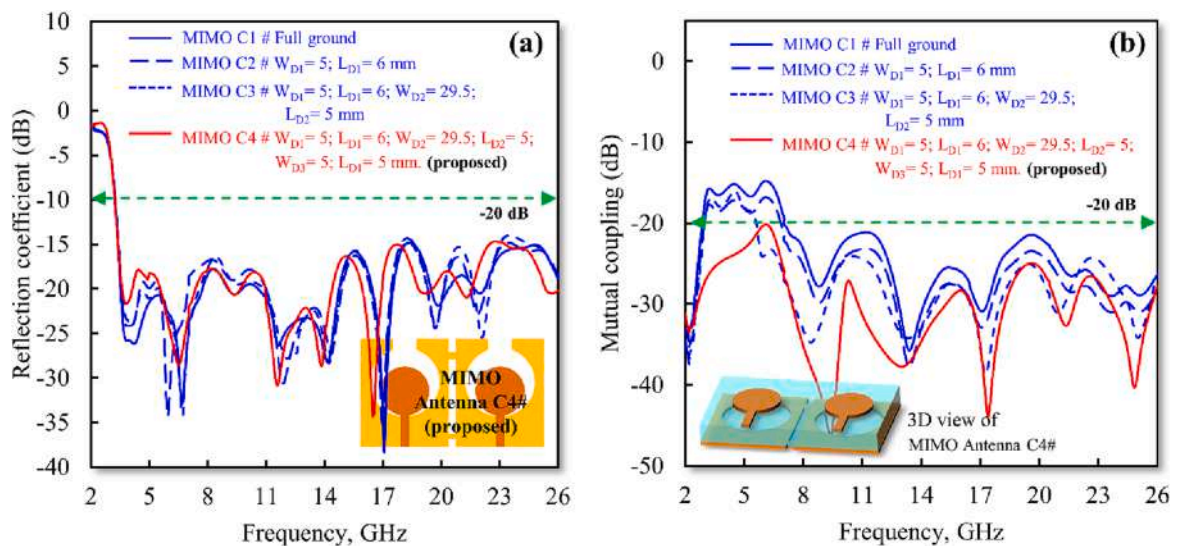


Fig. 13. (a) A comparison of reflection coefficient of MIMO antenna C1#/C2#/C3#/C4#, (b) comparison of mutual coupling of MIMO antenna C1#/C2#/C3#/C4#.

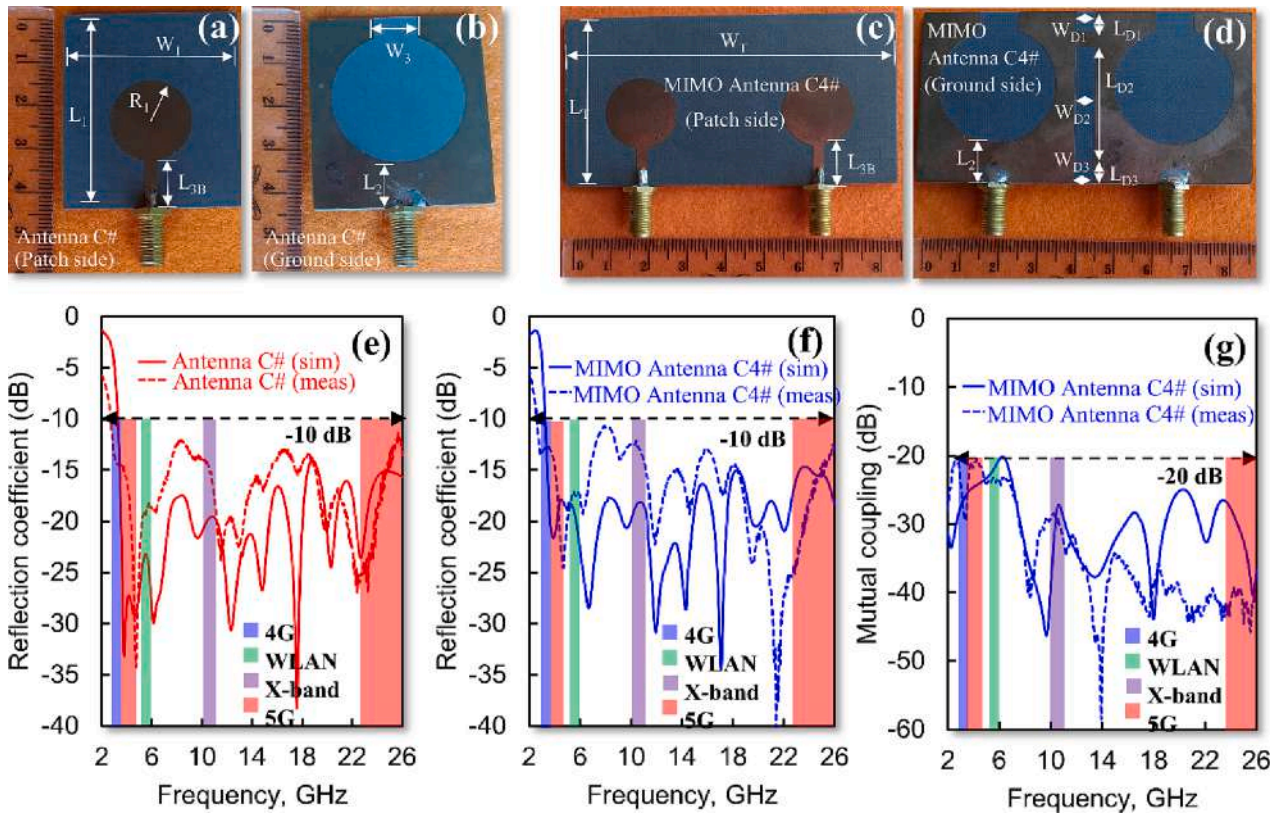


Fig. 14. (a) Fabrication result of antenna C# (a) view from patch side, (b) view from ground side. Fabrication result of MIMO antenna C4# (c) view from patch side, (d) view from ground side. The reflection coefficient comparison between simulation and measurement of (e) antenna C#, (f) MIMO antenna C4#, (g) a mutual coupling comparison between simulation and measurement of MIMO antenna C4#.

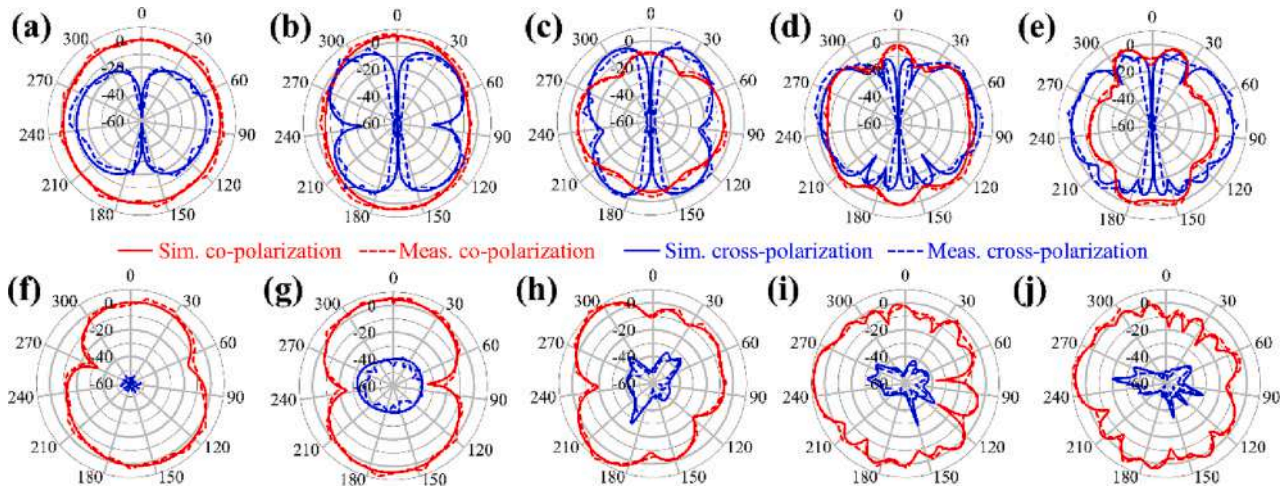


Fig. 15. Co- and cross-polarization normalized radiation patterns at XOZ-plane at frequency of (a) 3.3 GHz, (b) 5.8 GHz, (c) 10 GHz, (d) 24 GHz, and (e) 26 GHz. Then, Co- and cross-polarization normalized radiation patterns at YOZ-plane at frequency of (f) 3.3 GHz, (g) 5.8 GHz, (h) 10 GHz, (i) 24 GHz, and (j) 26 GHz.

the normalized co- and cross-polarization radiation patterns at the XOZ-plane for frequencies of 3.3 GHz, 5.8 GHz, 10 GHz, 24 GHz, and 26 GHz, respectively. It is seen at the XOZ-plane, the cross-polarization values are relatively large. However, the main beam at 0 degree exhibits a very low cross-polarization value. Moreover, Fig. 15 (a-e) show the normalized co- and cross-polarization radiation patterns at YOZ-plane for frequencies of 3.3 GHz, 5.8 GHz, 10 GHz, 24 GHz, and 26 GHz, respectively. At the YOZ-plane direction, the proposed antenna exhibits a very low cross-polarization value. Therefore, it can be concluded the proposed antenna has omni-directional pattern at the YOZ-plane.

As an additional explanation, there are several reasons that the monopole antenna can generate circular polarization such as ground-plane's position and antenna shape [46–48]. The ground-plane plays an important role in determining the polarization of an antenna. In the specific case of a monopole antenna, the ground plane can cause the polarization of the signal to change from its original orientation, with a larger ground plane providing more reflection and resulting in a more significant change in polarization [46–48].

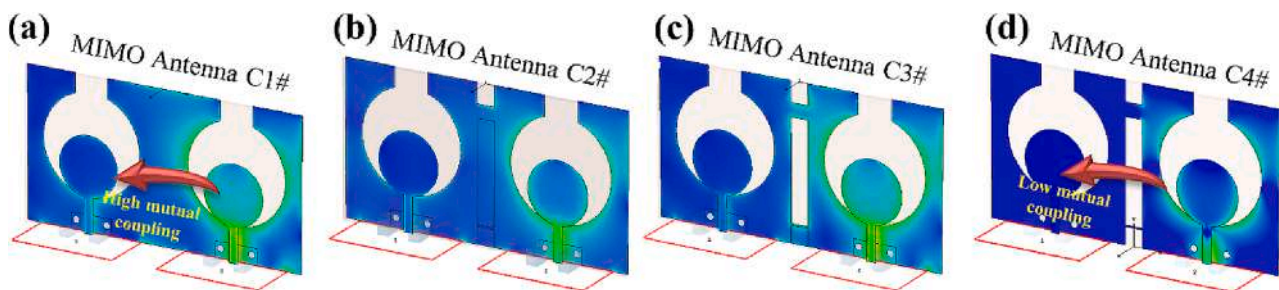


Fig. 16. Surface current density of (a) MIMO antenna C1#, (b) MIMO antenna C2#, (c) MIMO antenna C3#, (d) MIMO antenna C4#.

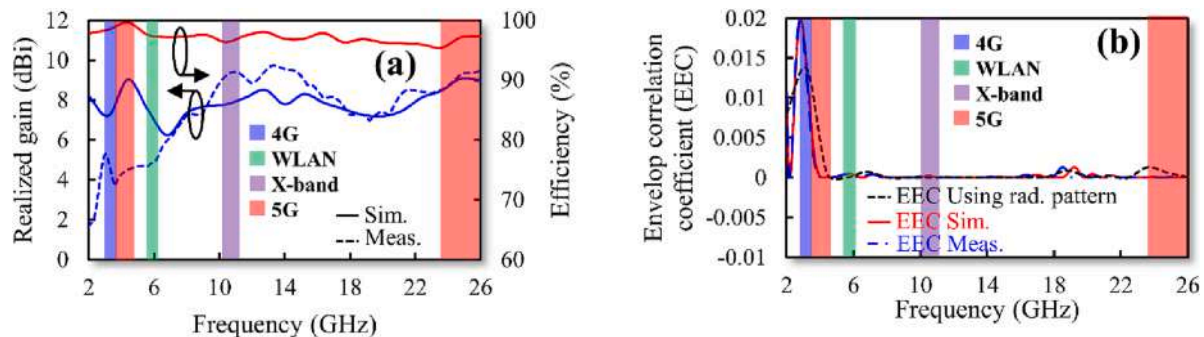


Fig. 17. Comparison result of (a) realized gain and efficiency, (b) enveloped correlation coefficient.

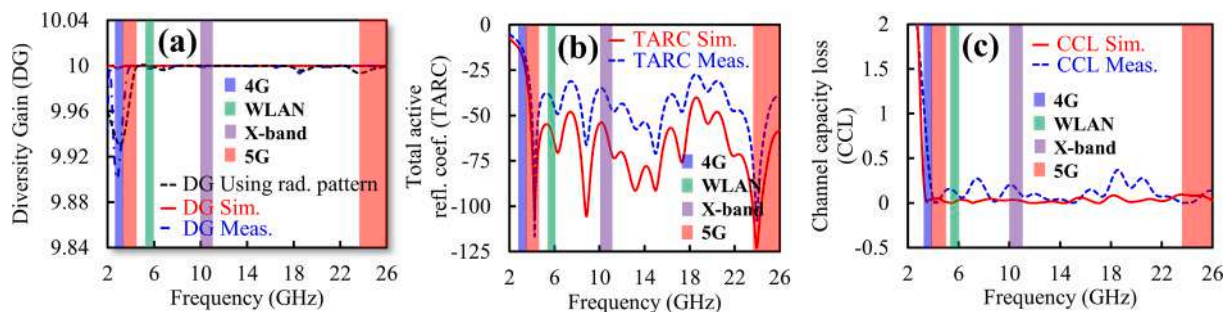


Fig. 18. Comparison result of (a) diversity gain, (b) total active reflection coefficient, and (c) channel capacity loss.

6. MIMO performances

The evaluation of surface current density distribution is crucial to understand the behavior of the proposed MIMO antenna. This surface current density distribution can be used to explain the MC between closely spaced antennas. Fig. 16(a), 16(b), 16(c), and 16(d) illustrate the surface current density of MIMO antenna C1#, C2#, C3#, and C4#, respectively. We can see that the MIMO antenna C1# has the highest mutual coupling among others. The MCs are qualitatively decreased after ground slots were included. This can be seen in Fig. 16(d) where the MIMO antenna C4# generates the lowest mutual coupling, as indicated by the blue color in the subsequent antenna. Then, Fig. 17 (a-b) show the results comparison of realized gain and efficiency, and enveloped correlation coefficient, respectively.

A realized gain and efficiency of MIMO antenna C4# is shown in Fig. 17(a). As depicted in the graph, the antenna has a realized gain ranging from 2.0 dBi to 9.5 dBi. The efficiency value range from 95.4% to 98.2%. It is important to note that only simulation data for efficiency are presented due to the limitations of the measurement device. However, the obtained results indicate good performance in terms of efficiency. This is attributed due to the low loss of Rogers RT/Duroid 5880 substrate which has a dielectric loss tangent ($\tan \delta$) of 0.0009. Furthermore, the envelope correlation coefficient (ECC) of the antenna

is illustrated in Fig. 17(b). The ECC value can be calculated using radiation patterns or scattering parameters [4,49,50]. The result shows that the ECC is slightly increased around the S-band. This occurrence is correlated with the MC, as a higher MC between antennas will have a more significant effect on the ECC. Nonetheless, we can see that the ECCs are still under 0.02 at all frequencies. Therefore, it is indicated that the antenna has a small correlation coefficient.

Fig. 18(a-c) show comparison result of diversity gain (DG), total active reflection coefficient (TARC), and channel capacity loss (CCL) of the MIMO antenna C4#, respectively. Moreover, we can also calculate the DG value using the ECC obtained from the radiation patterns. The DG maximum value achieved is 10 dB, while the proposed MIMO antenna C4# has a high DG of above 9.9 dB. This means the proposed antenna performs well in terms of MIMO performance. Additionally, the TARC value which is a metric to relates the reflection power an N-port microwave component can be calculated using equations from [4,49,50]. The TARC value of the proposed antenna is lower than -10 dB which indicates that the reflection power is very low. Then, the CCL value is lower than 0.4, which is suitable for MIMO applications. Table 2 shows the comparison between our proposed design and previous published antennas. The result shows that the proposed structure has many advantages that are suitable for 5G applications.

Table 2
Performance comparison of the proposed antenna with published antennas.

Ref.	Antenna structure	f_c / BW (GHz)	Proposed application	Size (λ_0)	Substrate	Shape of rad. pattern	Port	Isolation (dB)	Realized Gain (dBi)	Efficiency (%)	CCL	EEC	DG
[51]	Quasi self complementary	6.85/7.50	WLAN, UWB	0.73×0.73	FR4, $\epsilon_r = 4.4$, $h = 1.57$, $\tan \delta = 0.02$	Omni directional	4	< -15	1.7 – 4.2	60–90	N.R	N.R	N.R
[52]	Planar-monopole	7.40/9.20	UWB	0.64×0.76	RTDuroid4350B, $\epsilon_r = 3.5$, $h = 0.8$, $\tan \delta = 0.004$	Omni directional	2	< -20	-2 – 5.8	95–99	N.R	N.R	N.R
[53]	Koch fractal monopole	7.5/9.0	C-Band, UWB	1.12×0.62	FR4, $\epsilon_r = 4.4$, $h = 1.57$, $\tan \delta = 0.02$	Omni directional	2	< -19	1.0 – 5.0	N.R	N.R	0.17	N.R
[54]	Monopole with floating parasitic	6.85/7.50	UWB	0.80×0.91	RTDuroid4003, $\epsilon_r = 4.3$, $h = 1.57$, $\tan \delta = 0.0024$	Omni directional	2	< -16	3.4 – 6.5	N.R	N.R.	0.2	N.R
[55]	Single-dipole	3.65/0.30	5G	1.70×2.06	FR4, $\epsilon_r = 4.4$, $h = 1$, $\tan \delta = 0.02$	Directional	2	< -18	N.R.	80–90	N.R.	0.1	N.R.
[56]	Dual monopole	7.55/8.90	WLAN and 5G	0.55×0.90	RTDuroid5880, $\epsilon_r = 2.2$, $h = 1.57$, $\tan \delta = 0.0009$	Omni directional	2	< -18	N.R	N.R	N.R	0.35	N.R.
[57]	Monopole with EBG	2.42/0.15	WLAN	0.23×0.30	FR4, $\epsilon_r = 4.4$, $h = 1$, $\tan \delta = 0.02$	Directional	2	< -24	~ 4.25	50 – 58	N.R	0.008	9.99
[58]	Circular monopole	2.50/0.60	WLAN	0.58×0.33	JC, $\epsilon_r = 1.6$, $h = 1$, $\tan \delta = 0.02$	Omni directional	2	< -16	~ 3.0	N.R	N.R	0.05	N.R
[59]	CPW Asymmetric EBG	4.75/2.90	Sub-6 GHz 5G	0.34×0.66	FR4, $\epsilon_r = 4.4$, $h = 1.57$, $\tan \delta = 0.02$	Omni directional	2	< -18	N.R	N.R	N.R	0.025	~ 10.0
[60]	O-shaped monopole	4.10/3.40	WLAN and 5G	0.13×0.62	FR4, $\epsilon_r = 4.4$, $h = 1.57$, $\tan \delta = 0.02$	Omni directional	2	< -23	2 – 4	20.0–65.0	N.R	N.R	N.R
[61]	Octagonal-elips shaped	11.0/18.0	UWB and 5G	1.46×1.61	FR4, $\epsilon_r = 4.4$, $h = 1.57$, $\tan \delta = 0.02$	Omni directional	2	< -15	~ 10.0	90–92	N.R	0.02	9.80–10.00
[62]	Octagonal-shaped radiating	6.85/7.50	UWB with noeth	0.43×0.68	FR4, $\epsilon_r = 4.4$, $h = 1.57$, $\tan \delta = 0.02$	Omni directional	2	< -18	1.2 – 2.91	70–90	<0.05	<0.02	9.40–10.00
[63]	Metamaterial and SIW	9.00/14.00	UWB	1.05×1.08	FR4, $\epsilon_r = 4.4$, $h = 1.57$, $\tan \delta = 0.02$	Omni directional	2	< -23	3.7 – 4.3	65–80	<0.04	0.04	1.5–10
This paper	Quasi-tapered using circular shaped	14.65/22.70	4G / Mid-band 5G / WLAN /X-Band / High band 5G	4.15×2.09	RTDuroid5880, $\epsilon_r = 2.2$, $h = 1.57$, $\tan \delta = 0.0009$	Omni directional	2	< -20	2.0–9.5	95.4 – 98.2	<0.04	<0.02	9.88–10

Note: f_c = frequency center, BW = bandwidth, CCL = channel capacity loss, EEC = envelop correlation coefficient, DG = diversity gain, and N.R = not reported.

7. Conclusion

We have successfully designed a quasi-tapered wideband MIMO antenna by combining a circular-shaped patch and an inverted omega ground structure. An expansion of the exponential tapered model was used to investigate the circular-shaped tapered structure. In detail, the proposed antenna is divided into circular divergent and circular convergent-tapered sections. Then, a transmission lines approach was utilized to analyze and optimize the antenna structure. The proposed model was verified by FEM simulation and also step impedance calculation. Moreover, the proposed MIMO antenna can successfully cover the at 4G (3.3 GHz), mid-band 5G (3.4–3.8 GHz), WLAN (5.8 GHz), X-band (10–11 GHz), and high-band 5G (24.5–26 GHz) communications. A good agreement between the simulated and measured results validates the proposed method. A good agreement between the simulated and measured results validates the proposed method.

Declaration of Competing Interest

The authors declare that they have no known competing financial interests or personal relationships that could have appeared to influence the work reported in this paper.

Data availability

Data will be made available on request.

Acknowledgment

This work is supported by the Kementerian Pendidikan, Kebudayaan, Riset, dan Teknologi of Indonesia. Universitas Sultan Ageng Tirtayasa. 2023.

References

- B. Aghoutane, S. Das, M. EL Ghzaoui, B. T. P. Madhav, and H. El Faylali, "A novel dual band high gain 4-port millimeter wave MIMO antenna array for 28/37 GHz 5G applications," *AEU - Int. J. Electron. Commun.*, vol. 145, no. December 2021, p. 154071, 2022, <https://doi.org/10.1016/j.aeue.2021.154071>.
- B. Feng, Y. Tu, J. Chen, K. L. Chung, and S. Sun, "High-performance dual circularly-polarized antenna arrays using 3D printing for 5G millimetre-wave communications," *AEU - Int. J. Electron. Commun.*, vol. 130, no. June 2020, p. 153569, 2021, 10.1016/j.aeue.2020.153569.
- Yadav V, Yadav RS, Yadav P, Mishra B, Kumar A. "Dual and wideband 6-port MIMO antenna for WiFi, LTE and carrier aggregation systems applications", *AEU - Int J Electron Commun* 2023;162. <https://doi.org/10.1016/j.aeue.2023.154576>.
- Cunera K, Akcam N, Okan T, Arican GO. "28/38 GHz dual-band MIMO antenna with wideband and high gain properties for 5G applications", *AEU - Int J Electron Commun* 2023;vol. 162:154553. <https://doi.org/10.1016/j.aeue.2023.154553>.
- Mao CX, Khalily M, Xiao P, Brown TWC, Gao S. Planar sub-millimeter-wave array antenna with enhanced gain and reduced sidelobes for 5G broadcast applications. *IEEE Trans Antennas Propag* 2019;67(1):160–8. <https://doi.org/10.1109/TAP.2018.2874796>.
- Di Renna RB, Magri Souza VPR, Ferreira TN, Matos LJ, Souza JAM, Siqueira GL. A new double-sided substrate-integrated waveguide slot array antenna for 5G applications. *Microw Opt Technol Lett* 2019;61(3):682–7. <https://doi.org/10.1002/mop.31617>.
- Wen S, Dong Y. A low-profile wideband antenna with monopolelike radiation characteristics for 4G/5G indoor micro base station application. *IEEE Antennas Wirel Propag Lett* 2020;19(12):2305–9. <https://doi.org/10.1109/LAWP.2020.3030968>.
- Sun K, Yang D, Liu S. A wideband hybrid feeding circularly polarized magneto-electric dipole antenna for 5G Wi-Fi. *Microw Opt Technol Lett* 2018;60(8): 1837–42. <https://doi.org/10.1002/mop.31259>.
- Al-Rawi A, Hussain A, Yang J, Franzen M, Orlenius C, Kishk AA. A new compact wideband MIMO antenna - the double-sided tapered self-grounded monopole array. *IEEE Trans Antennas Propag* 2014;62(6):3365–9. <https://doi.org/10.1109/TAP.2014.2309985>.
- Ma TG, Jeng SK. A printed dipole antenna with tapered slot feed for ultrawideband applications. *IEEE Trans Antennas Propag* 2005;53(11):3833–6. <https://doi.org/10.1109/TAP.2005.858819>.
- Allen CM, Eldek AA, Elsherbeni AZ, Smith CE, Huang CWP, Lee KF. Dual tapered meander slot antenna for radar applications. *IEEE Trans Antennas Propag* 2005;53(7):2324–8. <https://doi.org/10.1109/TAP.2005.850757>.
- Ren J, et al. Large Frequency Ratio Vivaldi Antenna System With Low-Frequency Gain Enhancement Utilizing Dual-Function Taper Slot. *IEEE Trans Antennas Propag* 2022;70(6):4854–9.
- Ding T, Wang M, Xiao J, Shu J, Ye Q. A Wrench-Shaped Monopole-Like Slot Antenna For UWB Applications. *Cross Strait Radio Science & Wireless Technology Conference (CSRSWTC):9–11*. <https://doi.org/10.1109/CSRSWTC50769.2020.9372582>.
- Ling CW, Lo WH, Yan RH, Chung SJ. Planar binomial curved monopole antennas for ultrawideband communication. *IEEE Trans Antennas Propag* 2007;55(9): 2622–4. <https://doi.org/10.1109/TAP.2007.904140>.
- Wang L, et al. Compact UWB MIMO antenna with high isolation using fence-type decoupling structure. *IEEE Antennas Wirel Propag Lett* 2019;18(8):1641–5. <https://doi.org/10.1109/LAWP.2019.2925857>.
- Nouri M, Abazari Aghdam S, Jafarih A, Bagby J, Sahebghalam S. A wideband millimeter-wave antenna based on quasi-Yagi antenna with MIMO circular array antenna beamforming for 5G wireless networks. *Microw Opt Technol Lett* 2019;61(7):1810–4. <https://doi.org/10.1002/mop.31790>.
- Chen HD, Tsai YC, Sim CYD, Kuo C. Broadband eight-antenna array design for Sub-6 GHz 5G NR bands metal-frame smartphone applications. *IEEE Antennas Wirel Propag Lett* 2020;19(7):1078–82. <https://doi.org/10.1109/LAWP.2020.2988898>.
- Zhao A, Ren Z. Size reduction of self-isolated MIMO antenna system for 5G mobile phone applications. *IEEE Antennas Wirel Propag Lett* 2019;18(1):152–6. <https://doi.org/10.1109/LAWP.2018.2883428>.
- S. Alam, I. Surjati, A. Ferawan, and T. Firmansyah, "Design and realization of compact microstrip antenna using fractal sierpinski carpet for wireless fidelity application," *Indones. J. Electr. Eng. Informatics*, vol. 6, no. 1, pp. 70–78, 2018, 10.11591/ijeii.v6i1.390.
- Multi-output Y.S.M. Three wideband monopolar patch antennas in a Y-shape structure for 5G multi-input–multi-output access points. *IEEE Antennas Wirel Propag Lett* 2020;19(3):393–7. <https://doi.org/10.1109/LAWP.2020.2967354>.
- Hu WEI, et al. Dual-Band Eight-Element MIMO Array Using Multi-Slot Decoupling Technique for 5G Terminals. *IEEE Access* 2019;7:153910–20. <https://doi.org/10.1109/ACCESS.2019.2948639>.
- Wibisono G, Firmansyah T. "Concurrent multiband low noise amplifier with multisection impedance transformer", in *Asia-Pacific Microwave Conference Proceedings*. APMC 2012. <https://doi.org/10.1109/APMC.2012.6421776>.
- Hua Q, Huang YI, Member S, Alieldin A. A dual-band dual-polarized base station antenna using a novel feeding structure for 5G communications. *IEEE Access* 2020; 8:63710–7. <https://doi.org/10.1109/ACCESS.2020.2984199>.
- Mohanty A, Sahu S. "Bio-inspired maple-leaf viburnum shaped 4-port compact wideband MIMO antenna with reinforced interleaved SIW cavity integration", *AEU - Int J Electron Commun* 2022;vol. 156:154383. <https://doi.org/10.1016/j.aeue.2022.154383>.
- Wu T, Wang MJ, Chen J. Decoupling of MIMO antenna array based on half-mode substrate integrated waveguide with neutralization lines. *AEU - Int J Electron Commun* 2022;157:154416. <https://doi.org/10.1016/j.aeue.2022.154416>.
- Yang SJ, Kim YD, Yun DJ, Yi DW, Myung NH. Antenna modeling using sparse infinitesimal dipoles based on recursive convex optimization. *IEEE Antennas Wirel Propag Lett* 2018;17(4):662–5. <https://doi.org/10.1109/LAWP.2018.2810289>.
- S. Lin, H. Dong, Y. Liu, X. Y. Zhang, and X. Zhang, "Equivalent Circuit Modeling and Radiation Analysis of a Micro-Coaxial Collinear Antenna," *2022 IEEE Int. Symp. Antennas Propag. Usn. Radio Sci. Meet. AP-S/URSI 2022 - Proc.*, pp. 199–200, 2022, 10.1109/AP-S/USNC-URSI47032.2022.9886416.
- Gómez-Tagle J, Christodoulou CG. Extended cavity model analysis of stacked microstrip ring antennas. *IEEE Trans Antennas Propag* 1997;45(11):1626–35. <https://doi.org/10.1109/8.650074>.
- Wang CJ, Chen LT. Modeling of stepped-impedance slot antenna. *IEEE Trans Antennas Propag* 2014;62(2):955–9. <https://doi.org/10.1109/TAP.2013.2291906>.
- S. Koziel, S. Ogurtsov, and J. P. Jacobs, "Modeling of wideband antennas using space-mapping-corrected kriging surrogates," *2013 7th Eur. Conf. Antennas Propagation, EuCAP 2013*, pp. 1540–1543, 2013.
- Lu G, Korisich I, Greenstein L, Spasojevic P. "Antenna modelling using linear elements, with applications to UWB", *IEEE Antennas Propag. Soc AP-S Int Symp* 2004;3:2544–7. <https://doi.org/10.1109/aps.2004.1331892>.
- Nayak U, Chongder P, Biswas A. "Novel filtering and diplexing linear tapered slot antenna with high-selectivity", *AEU - Int J Electron Commun* 2022;156. <https://doi.org/10.1016/j.aeue.2022.154363>.
- Roblin C, D'Errico R. Statistical analysis of a parametric model of a 'population' of UWB antennas. *Eur Conf Antennas Propagation, EuCAP 2009:3343–7*.
- Wallace JW, Mehmood R. On the accuracy of equivalent circuit models for multi-antenna systems. *IEEE Trans Antennas Propag PART 1* 2012;vol. 60(2):540–7. <https://doi.org/10.1109/TAP.2011.2152339>.
- Papamichael V, Soras C. MIMO antenna modelling using the effective length matrices. *Prog Electromagn Res C* 2009;10:111–27. <https://doi.org/10.2528/PIERC09061903>.
- Papamichael VC. Eigen-analysis of lossy compact multielement antenna systems. *IEEE Antennas Wirel Propag Lett* 2009;8:1334–6. <https://doi.org/10.1109/LAWP.2009.2038288>.
- S. Kareemulla and V. Kumar, "Diversity performance of band notched ultra-wideband MIMO antenna," *Optik*, vol. 272, no. August 2022, p. 170128, 2023, <https://doi.org/10.1016/j.jlileo.2022.170128>.
- F. Wang, Z. Duan, Q. Li, Y. Wei, and Y. Gong, "Compact wideband MIMO antenna for 5G communication," *2017 IEEE Antennas Propag. Soc. Int. Symp. Proc.*, vol. 2017-Janua, no. c, pp. 939–940, 2017, 10.1109/APUSNCURSINRSM.2017.8072512.

- [39] Chen Z, Yuan XT, Ren J, Yuan T. "An ultra-wideband MIMO antenna for 5G smartphone", *AEU - Int J Electron Commun* 2022;vol. 154:154301. <https://doi.org/10.1016/j.aeue.2022.154301>.
- [40] Ansarizadeh M, Ghorbani A, Abd-Alhameed RA. An approach to equivalent circuit modeling of rectangular microstrip antennas. *Prog Electromagn Res B* 2008;8: 77–86. <https://doi.org/10.2528/pierb08050403>.
- [41] Adams JJ, Bernhard JT. Broadband equivalent circuit models for antenna impedances and fields using characteristic modes. *IEEE Trans Antennas Propag* 2013;61(8):3985–94. <https://doi.org/10.1109/TAP.2013.2261852>.
- [42] N. M. Din, C. K. Chakrabarty, A. Bin Ismail, K. K. A. Devi2, and W.-Y. Chen, "Design of RF Energy Harvesting System for energizing low power devices," *Prog. Electromagn. Res.*, vol. 132, no. July, pp. 49–69, 2012.
- [43] Devi KKA, Sadasivam S, Din NM, Chakrabarty CK, Rajib SK. Design of a wideband 377 Ohm E-Shaped patch antenna for RF energy harvesting. *Microw Opt Technol Lett* 2013;55(3):569–73. <https://doi.org/10.1002/mop>.
- [44] Iqbal A, Saraereh OA, Ahmad AW, Bashir S. Mutual Coupling Reduction Using F-Shaped Stubs in UWB-MIMO Antenna. *IEEE Access* 2017;6:2755–9. <https://doi.org/10.1109/ACCESS.2017.2785232>.
- [45] Technologies L. SMA Connectors [Online]. Available: SMA Connectors 2012. <https://www.hasco-inc.com/categories/connectors/sma-connectors.html>.
- [46] Chang TN, Lin JM. Dual-band circularly polarized monopole antenna. *J Electromagn Waves Appl* 2015;29(7):843–57. <https://doi.org/10.1080/09205071.2015.1022265>.
- [47] Liang Z, Li Y, Long Y. Multiband monopole mobile phone antenna with circular polarization for GNSS application. *IEEE Trans Antennas Propag* 2014;62(4): 1910–7. <https://doi.org/10.1109/TAP.2014.2299821>.
- [48] M. H. Shih, K. L. Hsiao, and C. J. Wang, "A monopole antenna with circular polarization," *ISAP 2014 - 2014 Int. Symp. Antennas Propagation, Conf. Proc.*, pp. 609–610, 2015, 10.1109/ISANP.2014.7026798.
- [49] Li Y, et al. "Mutual coupling reduction for monopole MIMO antenna using L-shaped stubs, defective ground and chip resistors", *AEU - Int J Electron Commun* 2023; vol. 160:154524. <https://doi.org/10.1016/j.aeue.2022.154524>.
- [50] A. Khan, A. Wakeel, L. Qu, and Z. Zahid, "Dual-band 8 × 8 MIMO antenna with enhanced isolation and efficiency for 5G smartphone applications," *AEU - Int. J. Electron. Commun.*, vol. 163, no. December 2022, p. 154600, 2023, 10.1016/j.aeue.2023.154600.
- [51] Liu L, Cheung SW, Yuk TI. Compact MIMO antenna for portable devices in UWB applications. *IEEE Trans Antennas Propag* 2013;61(8):4257–64. <https://doi.org/10.1109/TAP.2013.2263277>.
- [52] Zhu J, Li S, Feng B. Compact dual-polarized UWB quasi-self-complementary MIMO / Diversity. *IEEE Antennas Wirel Propag Lett* 2016;15:905–8. <https://doi.org/10.1109/LAWP.2015.2479622>.
- [53] Irene G, Rajesh A. A penta-band reject inside cut Koch fractal hexagonal monopole UWB MIMO antenna for portable devices. *Prog Electromagn Res C* 2018;82: 225–35. <https://doi.org/10.2528/pierc18020604>.
- [54] Khan MS, Capobianco A, Najam AI, Shoaib I, Autizi E, Shafique MF. Compact ultra-wideband diversity antenna with a floating parasitic digitated decoupling structure. *IET Microwaves, Antennas Propag* 2014;8(10):747–53. <https://doi.org/10.1049/iet-map.2013.0672>.
- [55] Qu L, Piao H. A dual-port single-dipole MIMO antenna pair based on selective modal excitation for 5G metal-rimmed terminals. *IEEE Access* 2022;10:100208–14. <https://doi.org/10.1109/ACCESS.2022.3188017>.
- [56] A. Qudus and R. Saleem, "Dual Port UWB Diversity/MIMO Antenna with Dual Band-Notch Characteristics," in *International Conference on Signal Processing and Communication Systems (ICSPCS)*, 2016, pp. 7–10. <https://doi.org/10.1109/ICSPCS.2016.7843320>.
- [57] Sharma K, Pandey GP. Two port compact MIMO antenna for ISM band applications. *Prog Electromagn Res C* 2020;100:173–85. <https://doi.org/10.2528/pierc20011504>.
- [58] Raviteja GV, Kumar PP, Ramesh G, Prasad BG, Sai RV. Wearable Dual-port MIMO antenna for On-body applications," in *International Conference on Elect. Electron Inform Commun Technol (ICEEICT)* 2022:7–11. <https://doi.org/10.1109/ICEEICT53079.2022.9768416>.
- [59] A. I. Afifi, A. S. Abd El-Hameed, A. Allam, S. M. Ahmed, and A. B. Abdel-Rahman, "Dual Port MIMO Antenna with Low Mutual Coupling Based on Asymmetric EBG Decoupling Structure," *15th Eur. Conf. Antennas Propagation, EuCAP 2021*, pp. 5–9, 2021, 10.23919/EuCAP51087.2021.9411149.
- [60] Soltani S, Lotfi P, Murch RD. Design of compact dual-band dual-port WLAN MIMO antennas using slots. *IEEE Antennas Propag Soc AP-S Int Symp* 2015;vol. 2015: 924–5. <https://doi.org/10.1109/APS.2015.7304849>.
- [61] Gireesh P, Sandeep Kumar P, Malathi K, Khanra I, Agarwal A, Sivakumar K. Design and analysis of dual port super wideband antenna set for MIMO applications. *J Phys Conf Ser* 2021;1964(6):pp. <https://doi.org/10.1088/1742-6596/1964/6/062051>.
- [62] Kumar A, Ansari AQ, Kanaujia BK, Kishor J, Kumar S. An ultra-compact two-port UWB-MIMO antenna with dual band-notched characteristics. *AEU - Int J Electron Commun* 2020;114:152997. <https://doi.org/10.1016/j.aeue.2019.152997>.
- [63] Anand S, Theetharappan R. "Metamaterial and SIW inspired isolating fences for lateral de-coupling in MIMO antenna", *AEU - Int J Electron Commun* 2023;vol. 166:154667. <https://doi.org/10.1016/j.aeue.2023.154667>.



Teguh Firmansyah <teguhfirmansyah@untirta.ac.id>

AEUE-D-23-00484 - Confirming your submission to AEUE - International Journal of Electronics and Communications

1 pesan

AEUE - International Journal of Electronics and Communications <em@editorialmanager.com>

7 Maret 2023 pukul 22.06

Balas Ke: AEUE - International Journal of Electronics and Communications <support@elsevier.com>
Kepada: Teguh Firmansyah <teguhfirmansyah@untirta.ac.id>

This is an automated message.

Modeling of Quasi-tapered Microstrip Antenna Based on Expansion-exponential Tapered Method and Its Application for Wideband MIMO Structure

Dear Mr Firmansyah,

We have received the above referenced manuscript you submitted to AEUE - International Journal of Electronics and Communications. It has been assigned the following manuscript number: AEUE-D-23-00484.

To track the status of your manuscript, please log in as an author at <https://www.editorialmanager.com/aeue/>, and navigate to the "Submissions Being Processed" folder.

Thank you for submitting your work to this journal.

Kind regards,
AEUE - International Journal of Electronics and Communications

More information and support

You will find information relevant for you as an author on Elsevier's Author Hub: <https://www.elsevier.com/authors>FAQ: How can I reset a forgotten password?
https://service.elsevier.com/app/answers/detail/a_id/28452/supporthub/publishing/kw/editorial+manager/For further assistance, please visit our customer service site: <https://service.elsevier.com/app/home/supporthub/publishing/>. Here you can search for solutions on a range of topics, find answers to frequently asked questions, and learn more about Editorial Manager via interactive tutorials. You can also talk 24/7 to our customer support team by phone and 24/7 by live chat and email.

This journal uses the Elsevier Article Transfer Service. This means that if an editor feels your manuscript is more suitable for an alternative journal, then you might be asked to consider transferring the manuscript to such a journal. The recommendation might be provided by a Journal Editor, a dedicated Scientific Managing Editor, a tool assisted recommendation, or a combination. For more details see the journal guide for authors.

#AU_AEUE#

To ensure this email reaches the intended recipient, please do not delete the above code

In compliance with data protection regulations, you may request that we remove your personal registration details at any time. ([Remove my information/details](#)). Please contact the publication office if you have any questions.



Teguh Firmansyah <teguhfirmansyah@untirta.ac.id>

Confirming handling editor for submission to AEUE - International Journal of Electronics and Communications

1 pesan

AEUE - International Journal of Electronics and Communications <em@editorialmanager.com>
Balas Ke: AEUE - International Journal of Electronics and Communications <support@elsevier.com>
Kepada: Teguh Firmansyah <teguhfirmansyah@untirta.ac.id>

8 Maret 2023 pukul 06.03

This is an automated message.

Manuscript Number: AEUE-D-23-00484

Modeling of Quasi-tapered Microstrip Antenna Based on Expansion-exponential Tapered Method and Its Application for Wideband MIMO Structure

Dear Mr Firmansyah,

The above referenced manuscript will be handled by Editor-in-Chief Professor Shahram MINAEI.

To track the status of your manuscript, please log into Editorial Manager at <https://www.editorialmanager.com/aeue/>.

Thank you for submitting your work to this journal.

Kind regards,

AEUE - International Journal of Electronics and Communications

More information and support

You will find information relevant for you as an author on Elsevier's Author Hub: <https://www.elsevier.com/authors>

FAQ: How can I reset a forgotten password?

https://service.elsevier.com/app/answers/detail/a_id/28452/supporthub/publishing/kw/editorial+manager/For further assistance, please visit our customer service site: <https://service.elsevier.com/app/home/supporthub/publishing/>. Here you can search for solutions on a range of topics, find answers to frequently asked questions, and learn more about Editorial Manager via interactive tutorials. You can also talk 24/7 to our customer support team by phone and 24/7 by live chat and email.

#AU_AEUE#

To ensure this email reaches the intended recipient, please do not delete the above code

In compliance with data protection regulations, you may request that we remove your personal registration details at any time. (Remove my information/details). Please contact the publication office if you have any questions.



Decision on submission to AEUE - International Journal of Electronics and Communications

4 pesan

AEUE - International Journal of Electronics and Communications <em@editorialmanager.com>

5 April 2023 pukul 23.05

Balas Ke: AEUE - International Journal of Electronics and Communications <support@elsevier.com>
Kepada: Teguh Firmansyah <teguhfiransyah@untirta.ac.id>

CC: andrea.morabito@unirc.it, sima_noghanian@ieee.org

Manuscript Number: AEUE-D-23-00484

Modeling of Quasi-tapered Microstrip Antenna Based on Expansion-exponential Tapered Method and Its Application for Wideband MIMO Structure

Dear Mr Firmansyah,

Thank you for submitting your manuscript to AEUE - International Journal of Electronics and Communications.

I have completed my evaluation of your manuscript. The reviewers recommend reconsideration of your manuscript following major revision. I invite you to resubmit your manuscript after addressing the comments below. Please resubmit your revised manuscript by May 05, 2023.

When revising your manuscript, please consider all issues mentioned in the reviewers' comments carefully: please outline every change made in response to their comments and provide suitable rebuttals for any comments not addressed. Please note that your revised submission may need to be re-reviewed.

To submit your revised manuscript, please log in as an author at <https://www.editorialmanager.com/aeue/>, and navigate to the "Submissions Needing Revision" folder.

AEUE - International Journal of Electronics and Communications values your contribution and I look forward to receiving your revised manuscript.

Research Elements (optional)

This journal encourages you to share research objects - including your raw data, methods, protocols, software, hardware and more – which support your original research article in a Research Elements journal. Research Elements are open access, multidisciplinary, peer-reviewed journals which make the objects associated with your research more discoverable, trustworthy and promote replicability and reproducibility. As open access journals, there may be an Article Publishing Charge if your paper is accepted for publication. Find out more about the Research Elements journals at https://www.elsevier.com/authors/tools-and-resources/research-elements-journals?dgcid=ec_em_research_elements_email.

Kind regards,
Shahram MINAEI
Editor-in-Chief

AEUE - International Journal of Electronics and Communications

Editor and Reviewer comments:

Reviewer #1:

1. A super wideband 2-port MIMO antenna is presented with the detailed analysis of the chosen tapered antenna geometry. Apart from the detailed analysis, the antenna lacks novelty. Also there is a major concern for the measurements carried out as single SMA connector is not capable of measuring the response at lower as well higher bands. Sub-6 GHz and mmwave bands need separate connectors.
2. List the novel contribution clearly and justify the need for the proposed antenna through extensive literature review.
3. Please refer to the attached file for more comments.

Reviewer #2:

The article entitled "Modeling of Quasi-tapered Microstrip Antenna Based on Expansion-exponential Tapered Method and Its Application for Wideband MIMO Structure" has been thoroughly reviewed and the current form of manuscript did not find suitable due to following comments:

Comment to the Authors:

1. Authors did not describe how to utilize the "Expansion-exponential Tapered Method" with the suggested design because it is a well known approach. It is a suggestion for authors to compare the results with simulation of the proposed design with the used tapered method.
2. From the results given in Fig. 12 & 13, the proposed design is a wideband antenna but authors have selected some specific bands only. Why?
3. From the results given in Fig 15, why are the cross-pol values high?
4. Channel capacity analysis of the proposed design is missing.
5. Authors did not disclose the name of software exploited for the analysis.

Associate Editor:

- Please clarify if ECC is calculated using the radiation patterns.
- The cross polarization patterns should be added to Fig. 15.
- Table I should include some references that propose MIMO wideband antennas.

More information and support

FAQ: How do I revise my submission in Editorial Manager?

https://service.elsevier.com/app/answers/detail/a_id/28463/supporthub/publishing/

You will find information relevant for you as an author on Elsevier's Author Hub: <https://www.elsevier.com/authors>

FAQ: How can I reset a forgotten password?

https://service.elsevier.com/app/answers/detail/a_id/28452/supporthub/publishing/kw/editorial+manager/

For further assistance, please visit our customer service site: <https://service.elsevier.com/app/home/supporthub/publishing/>. Here you can search for solutions on a range of topics, find answers to frequently asked questions, and learn more about Editorial Manager via interactive tutorials. You can also talk 24/7 to our

6/25/23, 9:16 PM


Email Sultan Ageng Tirtayasa University - Decision on submission to AEUE - International Journal of Electronics and Commu...

customer support team by phone and 24/7 by live chat and email.

#AU_AEUE#

To ensure this email reaches the intended recipient, please do not delete the above code

In compliance with data protection regulations, you may request that we remove your personal registration details at any time. ([Remove my information/details](#)). Please contact the publication office if you have any questions.

 **AEUE-D-23-00484_review comments.pdf**
14606K

Mail Delivery Subsystem <mailer-daemon@googlemail.com>
Kepada: teguhfirmansyah@untirta.ac.id

27 April 2023 pukul 10.15



Pesan terlalu besar

Pesan Anda tidak dapat dikirim ke **kondoh.jun@shizuoka.ac.jp** karena ukurannya melebihi batas. Coba kurangi ukuran pesan dan kirimkan kembali.

Tanggapan dari server jarak jauh adalah:

550 permanent failure for one or more recipients ([kondoh.jun@shizuoka.ac.jp:552](#) Message size exceeds fixed limit)

To:

May 16, 2023

Editor in Chief of AEU International Journal of Electronics and Communications

Prof. Dr. Shahram Minaei.

Re: Response to reviewers

Dear Professor,

I hope this email finds you well and healthy. First of all, we want to thank you for evaluating and allowing us an opportunity to address the reviewers' comments. We have carefully revised the manuscript, according to the reviewers' comments. We are uploading:

- 1) Cover Letter
- 2) Response to Reviewers
- 3) Conflict of Interest
- 4) Author Agreement
- 5) **Revised** manuscript (clean version)
- 6) **Revised** Manuscript with Marked changes (with **yellow highlights**)
- 7) Figures

Moreover, we also provide **additional data/figures** to enrich the paper's discussion. It can be seen in **Figs. 7(a-b), 15(a-j), 17(a-b), 18(a-c)**. Moreover, Jun Kondoh was included as an author to enhance the explanation and grammar evaluation.

Once again, we thank you for your valuable time reviewing and evaluating our paper. Please do not hesitate to contact me if there are any questions.

Sincerely Yours,
Teguh Firmansyah

Email:
teguhfirmansyah@untirta.ac.id

Journal : AEU International Journal of Electronics and Communications.
Manuscript ID : AEUE-D-23-00484
Title : Modeling of Quasi-tapered Microstrip Antenna Based on Expansion-exponential Tapered Method and Its Application for Wideband MIMO Structure

Response Letter

Journal : AEU International Journal of Electronics and Communications.
Manuscript ID : AEUE-D-23-00484
Title : Modeling of Quasi-tapered Microstrip Antenna Based on Expansion-exponential Tapered Method and Its Application for Wideband MIMO Structure

First of all, we would like to thank the reviewers for their in-depth and constructive reviews of our manuscript and the editor for his careful reading and suggestion to resubmit our manuscript. In this revised version of the manuscript, we did our best to address all comments raised by the reviewers. A detailed item-by-item responses to each of the reviewers' points are presented below.

Responses to reviewer 1

Concern # No. 1:

A super wideband 2-port MIMO antenna is presented with the detailed analysis of the chosen tapered antenna geometry. Apart from the detailed analysis, the antenna lacks novelty. Also there is a major concern for the measurements carried out as single SMA connector is not capable of measuring the response at lower as well higher bands. Sub-6 GHz and mmwave bands need separate connectors.

Author response: Many thanks to the reviewer for this feedback. **Regarding the novelty**, the study presented in this paper made several contributions, which are listed as follows:

1. A wideband antenna based on a quasi-tapered structure using a circular shape is proposed. A quasi-tapered characteristic was obtained by integrating a circular-shaped patch antenna with an inverted omega ground plane as shown in **Fig 1(a)**.
2. We also proposed an expansion-exponential tapered model to investigate the quasi-tapered structure based on a circular shape. This proposed model was utilized due to the limitation of the traditional linear, exponential, and Klopfenstein tapering methods. It is important to note that our circular tapered structure diverges from the conventional linear, exponential, or Klopfenstein shapes typically employed in tapering.
3. To obtain the mathematical model of for the circular shape tapered structure, we expand the the existing exponential shape tapered model. In detail, **Fig 1(b)** illustrates the proposed circular tapered structure which is divided into two halves circular shapes. It is seen that the physical dimension of the left-side of the half-circular shape is increasing. However, if we investigate the impedance characteristic, the impedance value is decreasing. Therefore, the left side structure

has a convergent behavior. Vice versa, the right side of the half-circular shape has a divergent characteristic.

4. The study employs the ABCD parameter based on the transmission line model to investigate the overall antenna structure. The proposed model was verified by the finite element method (FEM). Following the verification process, the proposed antenna was then applied to a MIMO structure. The fabrication of the antenna was carried out on a Rogers RT/Duroid 5880 substrate with $\epsilon_r = 2.2$, thickness of $h = 1.6$ mm, and dielectric loss $\tan \delta = 0.0009$.
5. In addition, we also proposed a multislot EBG structure to reduce the mutual coupling parameter in the MIMO antenna system. As a result, the proposed MIMO antenna demonstrated wide bandwidth and excellent performance across various communication bands. The antenna is capable of operating in the S-band to mmW band, effectively covering a broad frequency range. This wide frequency coverage enabled the antenna to support multiple communication standards, including 4G (3.3 GHz), mid-band 5G (3.4-3.8 GHz), WLAN (5.8 GHz), and high-band 5G (24.5-26 GHz) concurrently.

Table 1. Provides an overview of the proposed research positioning.

Table 1. Research position

Ref	Freq. (GHz)	Antenna structure	Proposed methods	Applications		MIMO antenna	Mutual coupling reduction	Advantages
				Narrow-band	Wide-band			
[26]	2.50	Microstrip slot dipole	Recursive convex optimization	Yes	-	-	-	The proposed model has the capability to make predictions for the near field.
[27]	30.0	Micro-coaxial collinear	Equivalent circuit modeling	Yes	-	-	-	The calculation model is capable of identifying the equivalent circuit.
[28]	2.47 - 2.56	Stacked Microstrip Ring	Cavity model	Yes	-	-	-	The proposed model can predict the near field.
[29]	1.50 - 2.50	Stepped-Impedance Slot Antenna	Stepped-Impedance Resonator	Yes	-	-	-	The proposed model is capable of predicting the dualband impedance characteristics.
[30]	2.00 - 8.00	CPW-fed slot antenna with monopole	Space-mapping with kriging surrogates	-	Yes	-	-	The proposed model has the ability to forecast the value of reflection coefficient.
[31]	3.00	Conventional dipole	Linear elements	-	Yes	-	-	The model can estimate the radiation pattern.
[32]	2.51 - 6.55	Linear tapered slot	Equivalent circuit model	-	Yes	-	-	The calculation model has the potential to determine the equivalent circuit.
[33]	3.50 - 8.50	Monopole UWB	Statistical analysis model	-	Yes	-	-	The proposed model can make predictions for the value of reflection coefficient.

[34]	2.20	Monopole	Equivalent circuit model	Yes	-	Yes	-	The network parameters can be utilized for the prediction of S-parameters performance.
[35]	5.15 - 5.35	Monopole	The effective length matrices	Yes	-	Yes	-	The effective length matrices demonstrate good agreement with the method of moments.
[36]	5.20	FIFA-monopole	Eigen-Analysis	Yes	-	Yes	-	The model can determine the radiation pattern.
[37]	2.90 - 18.00	Circular shaped monopole	N.R.	-	Yes	Yes	Yes	The proposed antenna exhibits wideband performance.
[38]	3.00 - 30.0	Monopole with slot	N.R.	-	Yes	Yes	Yes	The proposed antenna possesses good isolation.
[39]	3.30 - 8.50	L-shaped branch	N.R.	-	Yes	Yes	Yes	The proposed antenna has wideband performance.
This paper	3.30 - 26.0	Quasi-tapered using circular shaped	Expansion-exponential tapered model	-	Yes	Yes	Yes	The proposed antenna design combines wideband performance, a simple impedance calculation model, and low mutual coupling in a MIMO configuration.

Author action: We updated the manuscript by the yellow highlighted as shown on lines 90 - 137, and Table 1.

Regarding the connector,

Many thanks to the reviewer for this feedback. It should be noted when measuring the antenna performance. We use two scenarios. The first scenario combines conventional-SMA (low-freq) and End-lunch (high-freq with modified feed line) connectors. Meanwhile, the second scenario measurement uses the latest generation of SMA connectors. This connector can work up to 27 GHz. The measurement results of both scenarios are the same.

For an additional answer, this is the link for our connector.

<https://www.hasco-inc.com/connectors/sma-connectors/212-513sf-super-sma-jack-female-4-hole-375-square-flange-accepts-pin-dia-036/>

and

<https://www.hasco-inc.com/connectors/220-503sf-super-sma-jack-female-thread-in-accepts-pin-dia-036/>

SMA Female Connector 4 Hole .375" Square Flange - Accepts .036 Pin Dia., tested to 27 GHz

Part #: 212-5135P
 Brand: Southwest Microwave
 Weight: 0.50 Ounces
 Shipping: Calculated at checkout

For quantities greater than current stock levels, please contact customer service at 1-888-498-3242

Pricing by Quantity:

QUANTITY	PRICE
1 to 9	\$26.29
10 to 24	\$20.99
25 to 49	\$16.60
50 or above	\$13.67

ADD TO WISHLIST

SMA Female Connector Thread-In .425" Length - Accepts .036 Pin Dia., tested to 27 GHz

Part #: 200-9025P
 Brand: Southwest Microwave
 Weight: 0.30 Ounces
 Shipping: Calculated at checkout
 Current Stock: 23

For quantities greater than current stock levels, please contact customer service at 1-888-498-3242

Pricing by Quantity:

QUANTITY	PRICE
1 to 9	\$23.03
10 to 24	\$18.59
25 to 49	\$13.34
50 or above	\$10.05

Quantity: **ADD TO CART**

Data sheet :

ELECTRICAL	
Parameter	Specification
Frequency Range	DC - 27 GHz
VSWR	1.15:1 Max
Impedance	50 Ohms

MATERIALS	
Item	Specification (Note: All plating thickness values are in micro-inches)
Body	Passivated Stainless Steel
Contact Pin	Beryllium Copper (BeCu), UNS C17300 Per ASTM B196, Gold Plated Per MIL-G-45204 or ASTM B488
Center Contact Capture	High Temperature Ultem 1000 Per ASTM D5205
Connector Interface	Per MIL-STD-348, Figs. 310-1 and 310-2

Based on the data sheet, it can be seen that the connector has a good performance at a high frequency of 27 GHz. Therefore, our measurements are solid, with the same results in both scenarios. Moreover, as the reviewer suggested, we added this information to the main manuscript with a yellow highlight.

Author action:

The measurement of the proposed antenna's performance up to 26 GHz was facilitated by using the first-generation of super SMA female connectors from HASCO. Based on the data sheet, this connector has good performance from DC up to 27 GHz [45]. Furthermore, an R&S ZVA67 VNA is used to measure the antenna performance.

Reference :

- [45] L. Technologies, "SMA Connectors," *SMA Connectors*, 2012. [Online]. Available: <https://www.hasco-inc.com/categories/connectors/sma-connectors.html>.

Author action: We updated the manuscript by the yellow highlighted as shown on lines 378-381.

Concern # No. 2:

List the novel contribution clearly and justify the need for the proposed antenna through extensive literature review.

Author response: Thank you very much for the in-depth review. **Regarding the novelty**, the study presented in this paper made several contributions, which are listed as follows:

1. A wideband antenna based on a quasi-tapered structure using a circular shape is proposed. A quasi-tapered characteristic was obtained by integrating a circular-shaped patch antenna with an inverted omega ground plane as shown in **Fig 1(a)**.
2. We also proposed an expansion-exponential tapered model to investigate the quasi-tapered structure based on a circular shape. This proposed model was utilized due to the limitation of the traditional linear, exponential, and Klopfenstein tapering methods. It is important to note that our circular tapered structure diverges from the conventional linear, exponential, or Klopfenstein shapes typically employed in tapering.
3. To obtain the mathematical model of for the circular shape tapered structure, we expand the the existing exponential shape tapered model. In detail, **Fig 1(b)** illustrates the proposed circular tapered structure which is divided into two halves circular shapes. It is seen that the physical dimension of the left-side of the half-circular shape is increasing. However, if we investigate the impedance characteristic, the impedance value is decreasing. Therefore, the left side structure has a convergent behavior. Vice versa, the right side of the half-circular shape has a divergent characteristic.
4. The study employs the ABCD parameter based on the transmission line model to investigate the overall antenna structure. The proposed model was verified by the finite element method (FEM). Following the verification process, the proposed antenna was then applied to a MIMO structure. The fabrication of the antenna was carried out on a Rogers RT/Duroid 5880 substrate with $\epsilon_r = 2.2$, thickness of $h = 1.6$ mm, and dielectric loss $\tan \delta = 0.0009$.

5. In addition, we also proposed a multislot EBG structure to reduce the mutual coupling parameter in the MIMO antenna system. As a result, the proposed MIMO antenna demonstrated wide bandwidth and excellent performance across various communication bands. The antenna is capable of operating in the S-band to mmW band, effectively covering a broad frequency range. This wide frequency coverage enabled the antenna to support multiple communication standards, including 4G (3.3 GHz), mid-band 5G (3.4-3.8 GHz), WLAN (5.8 GHz), and high-band 5G (24.5-26 GHz) concurrently. **Table 1** provides an overview of the proposed research positioning.

Table 1. Research position

Ref	Freq. (GHz)	Antenna structure	Proposed methods	Applications		MIMO antenna	Mutual coupling reduction	Advantages
				Narrow-band	Wide-band			
[26]	2.50	Microstrip slot dipole	Recursive convex optimization	Yes	-	-	-	The proposed model has the capability to make predictions for the near field.
[27]	30.0	Micro-coaxial collinear	Equivalent circuit modeling	Yes	-	-	-	The calculation model is capable of identifying the equivalent circuit.
[28]	2.47 - 2.56	Stacked Microstrip Ring	Cavity model	Yes	-	-	-	The proposed model can predict the near field.
[29]	1.50 - 2.50	Stepped-Impedance Slot Antenna	Stepped-Impedance Resonator	Yes	-	-	-	The proposed model is capable of predicting the dualband impedance characteristics.
[30]	2.00 - 8.00	CPW-fed slot antenna with monopole	Space-mapping with kriging surrogates	-	Yes	-	-	The proposed model has the ability to forecast the value of reflection coefficient.
[31]	3.00	Conventional dipole	Linear elements	-	Yes	-	-	The model can estimate the radiation pattern.
[32]	2.51 - 6.55	Linear tapered slot	Equivalent circuit model	-	Yes	-	-	The calculation model has the potential to determine the equivalent circuit.
[33]	3.50 - 8.50	Monopole UWB	Statistical analysis model	-	Yes	-	-	The proposed model can make predictions for the value of reflection coefficient.
[34]	2.20	Monopole	Equivalent circuit model	Yes	-	Yes	-	The network parameters can be utilized for the prediction of S-parameters performance.
[35]	5.15 - 5.35	Monopole	The effective length matrices	Yes	-	Yes	-	The effective length matrices demonstrate good agreement with the method of moments.
[36]	5.20	FIFA-monopole	Eigen-Analysis	Yes	-	Yes	-	The model can determine the radiation pattern.
[37]	2.90 - 18.00	Circular shaped monopole	N.R.	-	Yes	Yes	Yes	The proposed antenna exhibits wideband performance.

[38]	3.00 – 30.0	Monopole with slot	N.R.	-	Yes	Yes	Yes	The proposed antenna possesses good isolation.
[39]	3.30 – 8.50	L-shaped branch	N.R.	-	Yes	Yes	Yes	The proposed antenna has wideband performance.
This paper	3.30 - 26.0	Quasi- tapered using circular shaped	Expansion- exponential tapered model	-	Yes	Yes	Yes	The proposed antenna design combines wideband performance, a simple impedance calculation model, and low mutual coupling in a MIMO configuration.

Author action: We updated the manuscript by the yellow highlighted as shown on lines 90 - 137, and Table 1.

Concern # No. 3:

Please refer to the attached file for more comments : Reply for the comments from the attached file

Concern # No. 4:

..... to support the Society 5.0?....

Author response: Many thanks to the reviewer for this comment. We have corrected the text as follows.

A massive communication network with high data-rate capability is required to support 5G technology [1], [2]. This challenging requirement has forced the development of 5G technology to work at the millimeter-wave (mmW) band to accommodate an enormous number of users with a wide bandwidth availability [3], [4]

References :

[1] B. Aghoutane, S. Das, M. EL Ghzaoui, B. T. P. Madhav, and H. El Faylali, “A novel dual band high gain 4-port millimeter wave MIMO antenna array for 28/37 GHz 5G applications,” *AEU - Int. J. Electron. Commun.*, vol. 145, no. December 2021, p. 154071, 2022, doi: 10.1016/j.aeue.2021.154071.

[2] B. Feng, Y. Tu, J. Chen, K. L. Chung, and S. Sun, “High-performance dual circularly-polarized antenna arrays using 3D printing for 5G millimetre-wave communications,” *AEU - Int. J. Electron. Commun.*, vol. 130, no. June 2020, p. 153569, 2021, doi: 10.1016/j.aeue.2020.153569.

[3] V. Yadav, R. S. Yadav, P. Yadav, B. Mishra, and A. Kumar, “Dual and wideband 6-port MIMO antenna for WiFi, LTE and carrier aggregation systems applications,” *AEU - Int. J. Electron. Commun.*, vol. 162, no. February, 2023, doi: 10.1016/j.aeue.2023.154576.

[4] K. Cuneray, N. Akcam, T. Okan, and G. O. Arican, “28/38 GHz dual-band MIMO antenna with wideband and high gain properties for 5G applications,” *AEU - Int. J. Electron. Commun.*, vol. 162, no. January, p. 154553, 2023, doi: 10.1016/j.aeue.2023.154553.

Author action: We updated the manuscript by the yellow highlighted as shown on lines 71-73.

Concern # No. 5:

Authors should emphasize that feeding needs to be optimized for an antenna to work at both lower and higher band simultaneously. The same feedline width and the connector cant be used for lower as well higher operational bands. At lower bands SMA connector can suffice the purpose however as the frequency increases the feedline will become thinner so end launch connectors are needed,

Author response: Many thanks to the reviewer for this feedback. It should be noted when measuring the antenna performance. We use two scenarios. The first scenario combines conventional-SMA (low-freq) and End-lunch (high-freq with modified feed line) connectors. Meanwhile, the second scenario measurement uses the latest generation of SMA connectors. This connector can work up to 27 GHz. The measurement results of both scenarios are the same.

For an additional answer, this is the link for our connector.

<https://www.hasco-inc.com/connectors/sma-connectors/212-513sf-super-sma-jack-female-4-hole-375-square-flange-accepts-pin-dia-036/>

and

<https://www.hasco-inc.com/connectors/220-503sf-super-sma-jack-female-thread-in-accepts-pin-dia-036/>





Data sheet :

ELECTRICAL	
Parameter	Specification
Frequency Range	DC - 27 GHz
VSWR	1.15:1 Max
Impedance	50 Ohms

MATERIALS	
Item	Specification (Note: All plating thickness values are in micro-inches)
Body	Passivated Stainless Steel
Contact Pin	Beryllium Copper (BeCu), UNS C17300 Per ASTM B196, Gold Plated Per MIL-G-45204 or ASTM B488
Center Contact Capture	High Temperature Uitem 1000 Per ASTM D5205
Connector Interface	Per MIL-STD-348, Figs. 310-1 and 310-2

Based on the data sheet, it can be seen that the connector has a good performance at a high frequency of 27 GHz. Therefore, our measurements are solid, with the same results in both scenarios. Moreover, as the reviewer suggested, we added this information to the main manuscript with a yellow highlight.

Author action:

The measurement of the proposed antenna's performance up to 26 GHz was facilitated by using the first-generation of super SMA female connectors from HASCO. Based on the data sheet, this connector has good performance from DC up to 27 GHz [45]. Furthermore, an R&S ZVA67 VNA is used to measure the antenna performance.

Reference :

[45] L. Technologies, "SMA Connectors," *SMA Connectors*, 2012. [Online]. Available: <https://www.hasco-inc.com/categories/connectors/sma-connectors.html>.

Author action: We updated the manuscript by the yellow highlighted as shown on lines 378-381.

Concern # No. 6:

The proposed **of** half-circular shape tapered configuration with expansion-exponential tapered model is shown in Fig. 2(a).

Author response: Thank you for your correction. We have remove the “**of**” at the main manuscript. Then, the corrected text is shown in as follows.

The proposed half-circular shape tapered configuration with expansion-exponential tapered model is shown in Fig. 2(a).

Author action: We updated the manuscript by the yellow highlighted as shown on lines 156-157.

Concern # No. 7:

Please use different color for the lines. Also only keep three very relevant results (shown in Fig. 8, now shown in Fig 9).

Author response:

Thank you very much for your comment. We agree with the reviwer, we have revised Fig 8. now shown in Fig 9 as shown in below.

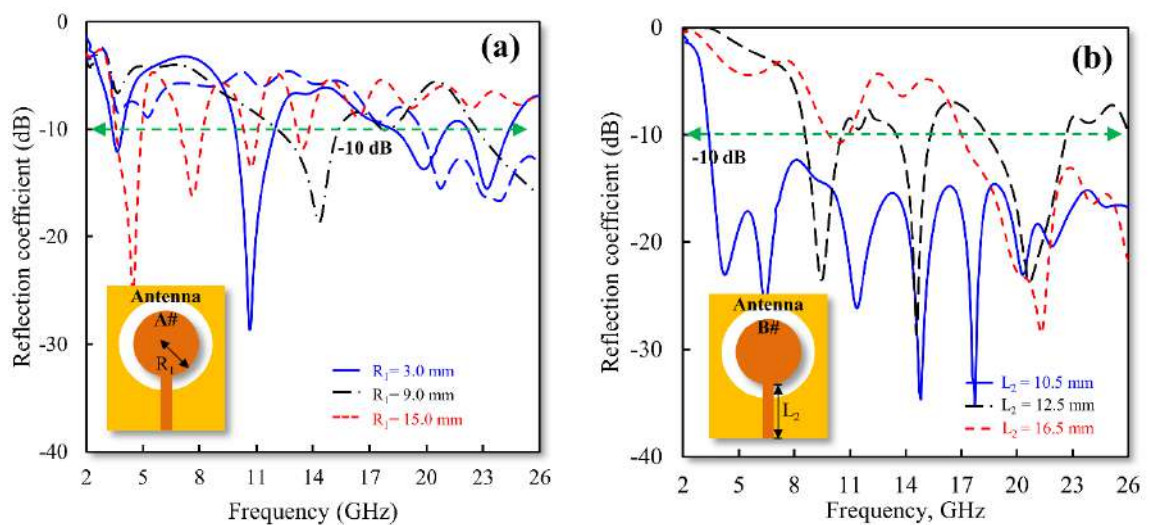


Fig. 9. (a) Reflection coefficient of antenna A# with varied of R_1 , (b) Reflection coefficient of antenna B# with varied of L_2

Author action: We updated the manuscript by the yellow highlighted as shown on lines 321-322.

Concern # No. 8:

No radiation pattern is shown here. (Fig 14. now shown in Fig 15)

Author response:

Thank you very much for pointing this out. We appologize for our mistakes by mention a wrong caption. We have revised the radiation pattern as shown in **Fig 15**.

Fig. 15 (a-j) presents the normalized co-and cross-polarization radiation patterns of the proposed antenna. Specifically, **Fig. 15 (a-e)** display the normalized co- and cross-polarization radiation patterns at the XOZ-plane for frequencies of 3.3 GHz, 5.8 GHz, 10 GHz, 24 GHz, and 26 GHz, respectively. It is seen at the XOZ-plane, the cross-polarization values are relatively large. However, the main beam at 0 degree exhibits a very low cross-polarization value. Moreover, **Fig. 15 (a-e)** show the normalized co- and cross-polarization radiation patterns at YOZ-plane for frequencies of 3.3 GHz, 5.8 GHz, 10 GHz, 24 GHz, and 26 GHz, respectively. At the YOZ-plane direction, the proposed antenna exhibits a very low cross-polarization value. Therefore, it can be concluded the proposed antenna has omni-directional pattern at the YOZ-plane.

As an additional explanation, there are several reasons that the monopole antenna can generate circular polarization such as ground-plane's position and antenna shape [46]–[48]. The ground-plane plays an important role in determining the polarization of an antenna. In the specific case of a monopole antenna, the ground plane can cause the polarization of the signal to change from its original orientation, with a larger ground plane providing more reflection and resulting in a more significant change in polarization [46]–[48].

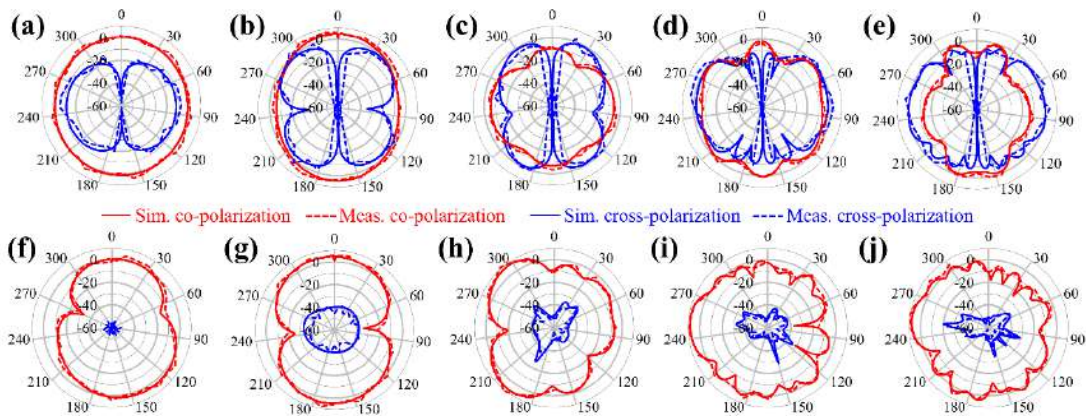


Fig. 15. Co- and cross-polarization normalized radiation patterns at XOZ-plane at frequency of (a) 3.3 GHz, (b) 5.8 GHz, (c) 10 GHz, (d) 24 GHz, and (e) 26 GHz. Then, Co- and cross-polarization normalized radiation patterns at YOZ-plane at frequency of (f) 3.3 GHz, (g) 5.8 GHz, (h) 10 GHz, (i) 24 GHz, and (j) 26 GHz.

Author action: We updated the manuscript by the yellow highlighted as shown on lines 406-426.

Concern # No. 9:

Include simulated and measured gain and efficiency results of the antenna.

Author response: Thank you very much for your comment. We agree with the reviewer. We have added the data as shown in **Fig 17 (a)**. However, we apologize only give a simulation data for the efficiency. We hope this data do not reduce our main proposed content such as a modeling of quasi-tapered microstrip antenna based on expansion-exponential tapered method and its application for wideband MIMO structure.

A realized gain and efficiency of MIMO antenna C4# is shown in **Fig 17(a)**. As depicted in the graph, the antenna has a realized gain ranging from 2.0 dBi to 9.5 dBi. The efficiency value range from 95.4% to 98.2 %. It is important to note that only simulation data for efficiency are presented due to the limitations of the measurement device. However, the obtained results indicate good performance in terms of efficiency. This is attributed due to the low loss of Rogers RT/Duroid 5880 substrate which has a dielectric loss tangent ($\tan \delta$) of 0.0009.

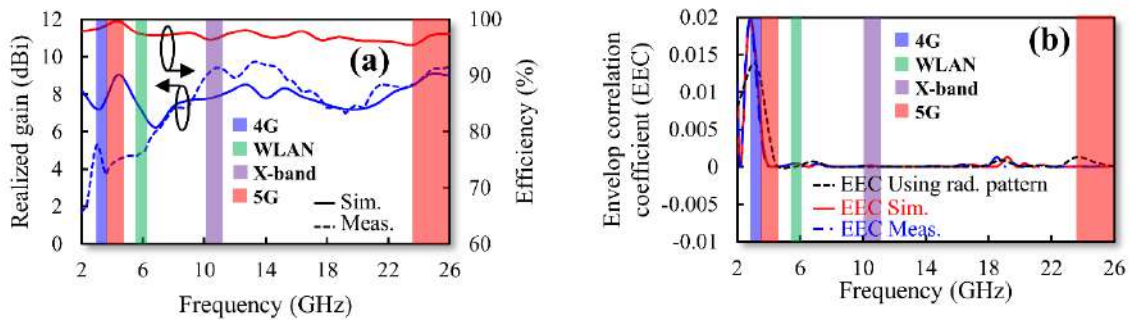


Fig. 17. Comparison result of (a) realized gain and efficiency, (b) enveloped correlation coefficient

Author action: We updated the manuscript by the yellow highlighted as shown on lines 441-452.

Concern # No. 10:

Table 2. Include the size of the antennas in terms of lambda and the shape of radiation pattern.

Author response:

Thank you very much for your comment. We agree with the reviewer. Therefore, we have revised **Table 2**, including the size of the antennas in terms of lambda and the shape of the radiation pattern. In detail, **Table 2** shows a performance comparison of the proposed antenna with published antennas. It can be seen that the proposed antenna has wide bandwidth with good MIMO performance. Moreover, it should be mentioned here we have re-measured our co- and cross-polarization data as shown in **Fig. 15**.

Author action: We updated the manuscript by the yellow highlighted as shown on lines 423-426.

Table 2. Performance comparison of the proposed antenna with published antennas

Ref.	Antenna structure	f_c / BW (GHz)	Proposed application	Size (λ_0)	Substratae	Shape of rad. pattern	Port	Isolation (dB)	Realized Gain (dBi)	Efficiency (%)	CCL	EEC	DG
[51]	Quasi self complementary	6.85/7.50	WLAN, UWB	0.73×0.73	FR4, $\epsilon_r = 4.4$, $h = 1.57$, $\tan \delta = 0.02$	Omni directional	4	< -15	1.7 – 4.2	60 - 90	N.R	N.R	N.R
[52]	Planar-monopole	7.40/9.20	UWB	0.64×0.76	RTDuroid4350B, $\epsilon_r = 3.5$, $h = 0.8$, $\tan \delta = 0.004$	Omni directional	2	< -20	-2 – 5.8	95 - 99	N.R	N.R	N.R
[53]	Koch fractal monopole	7.5/9.0	C-Band, UWB	1.12×0.62	FR4, $\epsilon_r = 4.4$, $h = 1.57$, $\tan \delta = 0.02$	Omni directional	2	< -19	1.0 – 5.0	N.R	N.R	0.17	N.R
[54]	Monopole with floating parasitic	6.85/7.50	UWB	0.80×0.91	RTDuroid4003, $\epsilon_r = 4.3$, $h = 1.57$, $\tan \delta = 0.0024$	Omni directional	2	< -16	3.4 – 6.5	N.R	N.R.	0.2	N.R
[55]	Single-dipole	3.65/0.30	5G	1.70×2.06	FR4, $\epsilon_r = 4.4$, $h = 1$, $\tan \delta = 0.02$	Directional	2	< -18	N.R.	80 -90	N.R.	0.1	N.R.
[56]	Dual monopole	7.55/8.90	WLAN and 5G	0.55×0.90	RTDuroid5880, $\epsilon_r = 2.2$, $h = 1.57$, $\tan \delta = 0.0009$	Omni directional	2	< -18	N.R	N.R	N.R	0.35	N.R.
[57]	Monopole with EBG	2.42/0.15	WLAN	0.23×0.30	FR4, $\epsilon_r = 4.4$, $h = 1$, $\tan \delta = 0.02$	Directional	2	< -24	~ 4.25	50 – 58	N.R	0.008	9.99
[58]	Circular monopole	2.50/0.60	WLAN	0.58×0.33	JC, $\epsilon_r = 1.6$, $h = 1$, $\tan \delta = 0.02$	Omni directional	2	< -16	~ 3.0	N.R	N.R	0.05	N.R
[59]	CPW Asymmetric EBG	4.75/2.90	Sub-6 GHz 5G	0.34×0.66	FR4, $\epsilon_r = 4.4$, $h = 1.57$, $\tan \delta = 0.02$	Omni directional	2	< -18	N.R	N.R	N.R	0.025	~ 10.0
[60]	O-shaped monopole	4.10/3.40	WLAN and 5G	0.13×0.62	FR4, $\epsilon_r = 4.4$, $h = 1.57$, $\tan \delta = 0.02$	Omni directional	2	< -23	2 – 4	20.0 - 65.0	N.R	N.R	N.R
[61]	Octagonal-elips shaped	11.0/18.0	UWB and 5G	1.46×1.61	FR4, $\epsilon_r = 4.4$, $h = 1.57$, $\tan \delta = 0.02$	Omni directional	2	< -15	~ 10.0	90 -92	N.R	0.02	9.80 - 10.00
[62]	Octagonal-shaped radiating	6.85/7.50	UWB with nocth	0.43×0.68	FR4, $\epsilon_r = 4.4$, $h = 1.57$, $\tan \delta = 0.02$	Omni directional	2	< -18	1.2 – 2.91	70 - 90	<0.05	<0.02	9.40 - 10.00
[63]	Metamaterial and SIW	9.00/14.00	UWB	1.05×1.08	FR4, $\epsilon_r = 4.4$, $h = 1.57$, $\tan \delta = 0.02$	Omni directional	2	< -23	3.7 – 4.3	65 -80	<0.04	0.04	1.5-10
This paper	Quasi-tapered using circular shaped	14.65/22.70	4G / Mid-band 5G / WLAN /X-Band / High band 5G	4.15×2.09	RTDuroid5880, $\epsilon_r = 2.2$, $h = 1.57$, $\tan \delta = 0.0009$	Omni directional	2	< -20	2.0 - 9.5	95.4 – 98.2	<0.04	<0.02	9.88 - 10

Note : f_c = frequency center, BW = bandwidth, CCL = channel capacity loss, EEC = envelop correlation coefficient, DG = diversity gain, and N.R = not reported.

Responses to reviewer 2

Concern # No. 1:

Authors did not describe how to utilize the "Expansion-exponential Tapered Method" with the suggested design because it is an well known approach. It is a suggestion for authors to compare the results with simulation of the proposed design with the used tapered method.

Author response: Many thanks to the reviewer for this fruitful feedback and insightful suggestion. We have added the comparison between the proposed expansion-exponential tapered and conventional tapered methods of circular convergent-taper and circular divergent-taper, as shown in **Fig 7(a) and 7(b)**, respectively.

Fig. 7(a) and 7(b) show the results comparison between the expansion-exponential tapered method and conventional tapered method for circular convergent-taper and circular divergent-taper configurations, respectively. MATLAB software was used to perform the calculations for both the expansion-exponential and conventional tapered methods. In addition to MATLAB, the transmission line electromagnetics modeling tool suite of TNT 1.2.2 was utilized for the FEM based calculations. It is observed that the proposed method exhibited greater consistency and better fit with the FEM results. These results look similar for circular-convergent taper and circular-divergent taper. However, if we compare it with the conventional tapered methods, the deviation is significant. This results suggests that the proposed expansion-exponential tapered method offers distinct advantages and a more suitable design approach compared to conventional methods. Additionally, it is important to note that further detailed investigations of the antenna characteristics were conducted using CST Microwave Studio software.

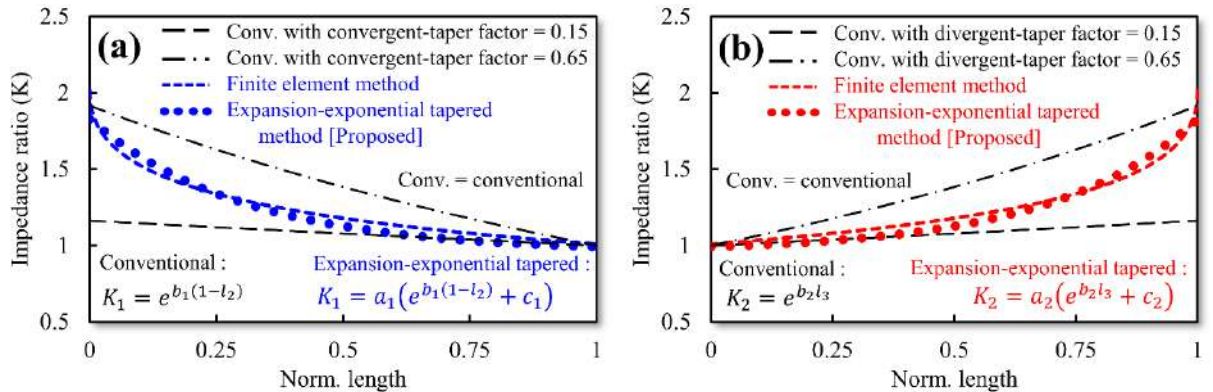


Fig. 7. Results comparison between the proposed method expansion-exponential tapered method and conventional tapered method (a) circular convergent-taper, and (b) circular divergent-taper.

Author action: We updated the manuscript by the yellow highlighted as shown on lines 282-298.

Concern # No. 2:

From the results given in Fig. 12 & 13, the proposed design is a wideband antenna but authors have selected some specific bands only. Why?.

Author response: Thank you very much for your comment.

It should be noted that, in principle, this antenna has the potential to operate across wide frequency bands. However, in this paper, the focus was directed towards specific frequency bands in order to position the study within the context of future communication technologies. We have selected several specific bands such as the 4G (3.3 ghz), mid-band 5G (3.4-3.8 ghz), WLAN (5.8 ghz), X-band (10-11 ghz), and high-band 5G (24.5-26 ghz) communications.

Moreover, this paper is also focused on development and modeling of quasi-tapered microstrip antenna based on expansion-exponential tapered method and its application for wideband MIMO structure.

Author action: We updated the manuscript by the yellow highlighted as shown on lines 400-405.

Concern # No. 3:

From the results given in Fig 15, why are the cross-pol values high?

Author response: Thank you very much for your comment. We have re-evaluated our data regarding the radiation patterns. Therefore, we have re-measured of our co- and cross-polarization data. It can be clearly seen at **Fig. 15**.

Fig. 15 (a-j) presents the normalized co-and cross-polarization radiation patterns of the proposed antenna. Specifically, **Fig. 15 (a-e)** display the normalized co- and cross-polarization radiation patterns at the XOZ-plane for frequencies of 3.3 GHz, 5.8 GHz, 10 GHz, 24 GHz, and 26 GHz, respectively. It is seen at the XOZ-plane, the cross-polarization values are relatively large. However, the main beam at 0 degree exhibits a very low cross-polarization value. Moreover, **Fig. 15 (a-e)** show the normalized co- and cross-polarization radiation patterns at YOZ-plane for frequencies of 3.3 GHz, 5.8 GHz, 10 GHz, 24 GHz, and 26 GHz, respectively. At the YOZ-plane direction, the proposed antenna exhibits a very low cross-polarization value. Therefore, it can be concluded the proposed antenna has omni-directional pattern at the YOZ-plane.

As an additional explanation, there are several reasons that the monopole antenna can generate circular polarization such as ground-plane's position and antenna shape [46]–[48]. The ground-plane plays an important role in determining the polarization of an antenna. In the specific case of a monopole antenna, the ground plane can cause the polarization of the signal to change from its original orientation, with a larger ground

plane providing more reflection and resulting in a more significant change in polarization [46]–[48].

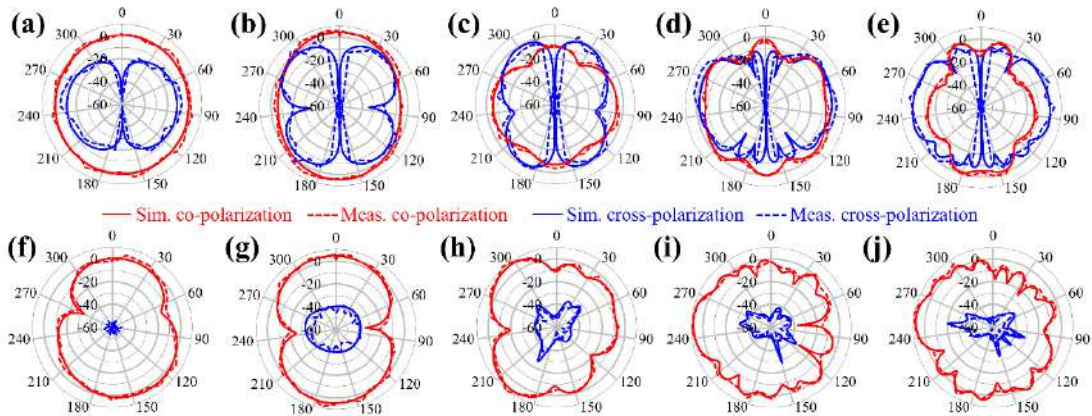


Fig. 15. Co- and cross-polarization normalized radiation patterns at XOZ-plane at frequency of (a) 3.3 GHz, (b) 5.8 GHz, (c) 10 GHz, (d) 24 GHz, and (e) 26 GHz. Then, Co- and cross-polarization normalized radiation patterns

Author action: We updated the manuscript by the yellow highlighted as shown on lines 406-426.

Concern # No. 4:

Channel capacity analysis of the proposed design is missing.

Author response: Thank you very much for the in-depth review. As a reviewer suggested, we have added the channel capacity analysis as shown in **Fig 18 (c)**

Fig. 18(a-c) show comparison result of diversity gain (DG), total active reflection coefficient (TARC), and channel capacity loss (CCL) of the MIMO antenna C4#, respectively. Moreover, we can also calculate the DG value using the EEC obtained from the radiation patterns. The DG maximum value achieved is 10 dB, while the proposed MIMO antenna C4# has a high DG of above 9.9 dB. This means the proposed antenna performs well in terms of MIMO performance. Additionally, the TARC value which is a metric to relates the reflection power an N-port microwave component can be calculated using equations from [4], [49], [50]. The TARC value of the proposed antenna is lower than -10 dB which indicates that the reflection power is very low. Then, the CCL value is lower than 0.4, which is suitable for MIMO applications. **Table 2** shows the comparison between our proposed design and previous published antennas. The result shows that the proposed structure has many advantages that are suitable for 5G applications.

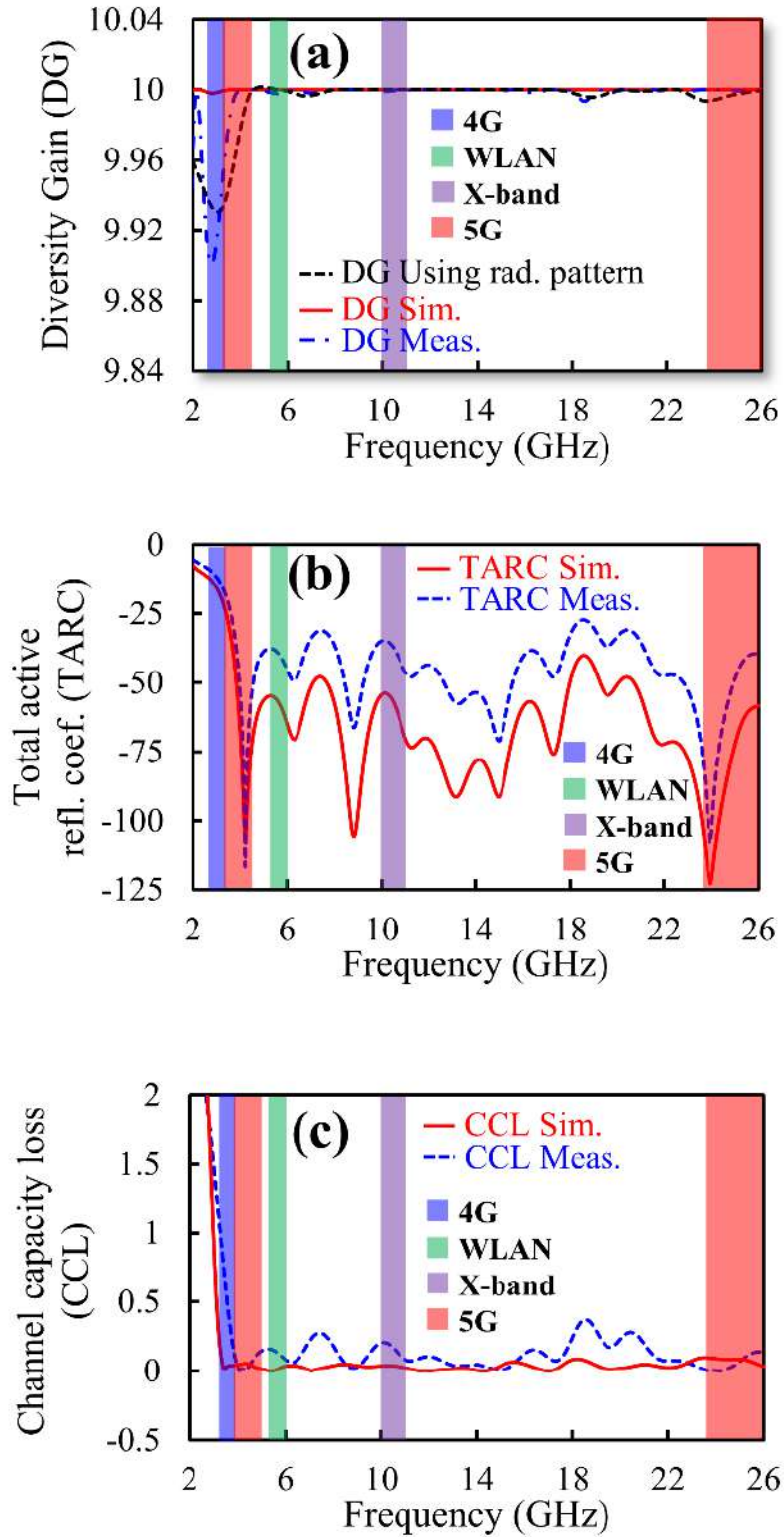


Fig. 18. Comparison result of (a) diversity gain, (b) total active reflection coefficient, and (c) channel capacity loss

Author action: We updated the manuscript by the yellow highlighted as shown on lines 456-469.

Concern # No. 5:

Authors did not disclose the name of software exploited for the analysis.

Author response: Thank you very much for your comment. We agree with this suggestion.

MATLAB software was used to perform the calculations for both the expansion-exponential and conventional tapered methods. In addition to MATLAB, the transmission line electromagnetics modeling tool suite of TNT 1.2.2 was utilized for the FEM based calculations. It is observed that the proposed method exhibited greater consistency and better fit with the FEM results. These results look similar for circular-convergent taper and circular-divergent taper. However, if we compare it with the conventional tapered methods, the deviation is significant. This results suggests that the proposed expansion-exponential tapered method offers distinct advantages and a more suitable design approach compared to conventional methods. Additionally, it is important to note that further detailed investigations of the antenna characteristics were conducted using CST Microwave Studio software.

Author action: We updated the manuscript by the yellow highlighted as shown on lines 285-293.

Responses to Associate Editor

Concern # No. 1:

Please clarify if ECC is calculated using the radiation patterns.

Author response: Many thanks to the reviewer for this fruitful feedback. We agree with the comments. We have added the ECC data by calculating the radiation patterns. It can be seen in Fig 17 (b).

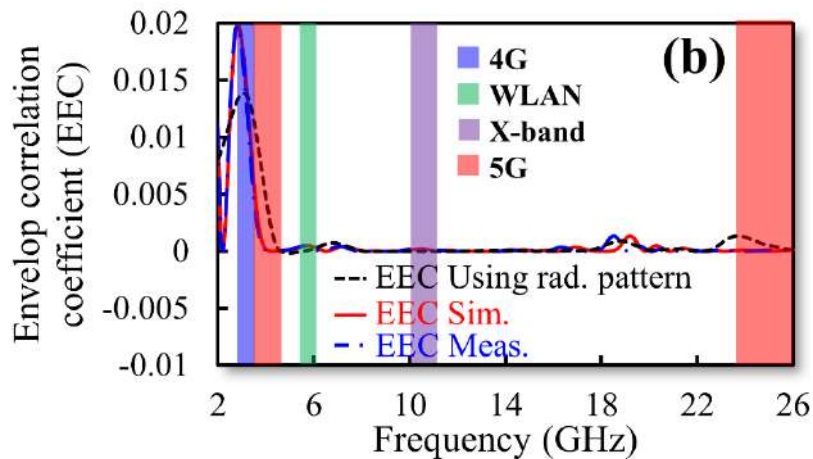


Fig. 17 (b). Comparison result of (b) enveloped correlation coefficient

Author action: We updated the manuscript by the yellow highlighted as shown on lines 452-455.

Concern # No. 2:

The cross polarization patterns should be added to Fig. 15

Author response: Thank you very much for your comment. We have re-evaluated our data regarding the radiation patterns. Therefore, we have re-measured of our co- and cross-polarization data. It can be clearly seen at Fig. 15.

Fig. 15 (a-j) presents the normalized co- and cross-polarization radiation patterns of the proposed antenna. Specifically, Fig. 15 (a-e) display the normalized co- and cross-polarization radiation patterns at the XOZ-plane for frequencies of 3.3 GHz, 5.8 GHz, 10 GHz, 24 GHz, and 26 GHz, respectively. It is seen at the XOZ-plane, the cross-polarization values are relatively large. However, the main beam at 0 degree exhibits a very low cross-polarization value. Moreover, Fig. 15 (a-e) show the normalized co- and cross-polarization radiation patterns at YOZ-plane for frequencies of 3.3 GHz, 5.8 GHz, 10 GHz, 24 GHz, and 26 GHz, respectively. At the YOZ-plane direction, the proposed antenna exhibits a very low cross-polarization value. Therefore, it can be concluded the proposed antenna has omni-directional pattern at the YOZ-plane.

As an additional explanation, there are several reasons that the monopole antenna can generate circular polarization such as ground-plane's position and antenna shape [46]–[48]. The ground-plane plays an important role in determining the polarization of an antenna. In the specific case of a monopole antenna, the ground plane can cause the polarization of the signal to change from its original orientation, with a larger ground plane providing more reflection and resulting in a more significant change in polarization [46]–[48].

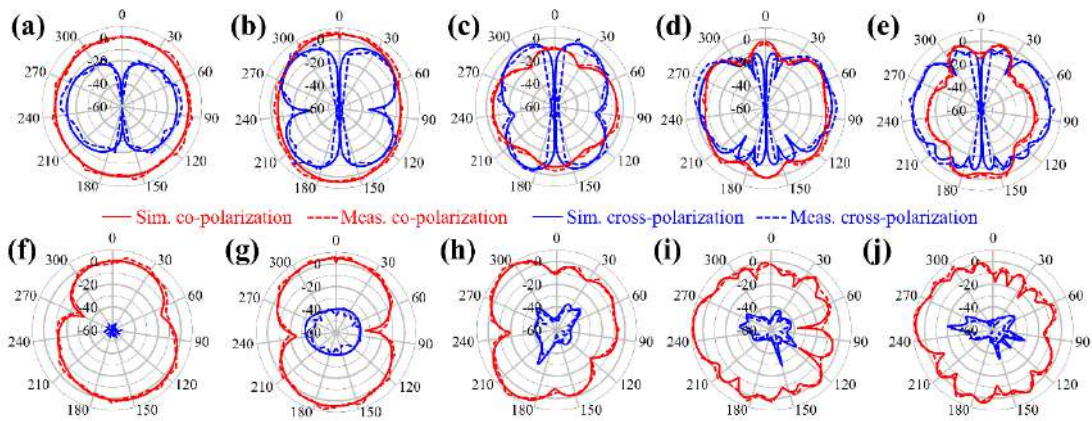


Fig. 15. Co- and cross-polarization normalized radiation patterns at XOZ-plane at frequency of (a) 3.3 GHz, (b) 5.8 GHz, (c) 10 GHz, (d) 24 GHz, and (e) 26 GHz. Then, Co- and cross-polarization normalized radiation patterns

Author action: We updated the manuscript by the yellow highlighted as shown on lines 406-426.

Concern # No. 3:

Table I should include some references that propose MIMO wideband antennas.

Author response: Thank you very much for your comment. We agree with this suggestion. We have added some references that propose MIMO wideband antennas. **Table 1** provides an overview of the proposed research positioning.

Table 1. Research position

Ref	Freq. (GHz)	Antenna structure	Proposed methods	Applications		MIMO antenna	Mutual coupling reduction	Advantages
				Narrow-band	Wide-band			
[26]	2.50	Microstrip slot dipole	Recursive convex optimization	Yes	⋮	⋮	⋮	The proposed model has the capability to make predictions for the near field.
[27]	30.0	Micro-coaxial collinear	Equivalent circuit modeling	Yes	⋮	⋮	⋮	The calculation model is capable of identifying the equivalent circuit.
[28]	2.47 - 2.56	Stacked Microstrip Ring	Cavity model	Yes	⋮	⋮	⋮	The proposed model can predict the near field.

[29]	1.50 - 2.50	Stepped-Impedance Slot Antenna	Stepped-Impedance Resonator	Yes	-	-	-	The proposed model is capable of predicting the dualband impedance characteristics.
[30]	2.00 - 8.00	CPW-fed slot antenna with monopole	Space-mapping with kriging surrogates	-	Yes	-	-	The proposed model has the ability to forecast the value of reflection coefficient.
[31]	3.00	Conventional dipole	Linear elements	-	Yes	-	-	The model can estimate the radiation pattern.
[32]	2.51 - 6.55	Linear tapered slot	Equivalent circuit model	-	Yes	-	-	The calculation model has the potential to determine the equivalent circuit.
[33]	3.50 - 8.50	Monopole UWB	Statistical analysis model	-	Yes	-	-	The proposed model can make predictions for the value of reflection coefficient.
[34]	2.20	Monopole	Equivalent circuit model	Yes	-	Yes	-	The network parameters can be utilized for the prediction of S-parameters performance.
[35]	5.15 - 5.35	Monopole	The effective length matrices	Yes	-	Yes	-	The effective length matrices demonstrate good agreement with the method of moments.
[36]	5.20	FIFA-monopole	Eigen-Analysis	Yes	-	Yes	-	The model can determine the radiation pattern.
[37]	2.90 - 18.00	Circular shaped monopole	N.R.	-	Yes	Yes	Yes	The proposed antenna exhibits wideband performance.
[38]	3.00 - 30.0	Monopole with slot	N.R.	-	Yes	Yes	Yes	The proposed antenna possesses good isolation.
[39]	3.30 - 8.50	L-shaped branch	N.R.	-	Yes	Yes	Yes	The proposed antenna has wideband performance.
This paper	3.30 - 26.0	Quasi-tapered using circular shaped	Expansion-exponential tapered model	-	Yes	Yes	Yes	The proposed antenna design combines wideband performance, a simple impedance calculation model, and low mutual coupling in a MIMO configuration.

Author action: We updated the manuscript by the yellow highlighted as shown on lines 90 - 137, and Table 1.

Again, we thank you for the valuable time you put into reviewing and evaluating our paper. Finally, please do not hesitate to contact me if there are any questions.

Yours Sincerely,

Teguh Firmansyah

Email:

teguhfirmansyah@untirta.ac.id



Teguh Firmansyah <teguhfirmansyah@untirta.ac.id>

Decision on submission to AEUE - International Journal of Electronics and Communications

3 pesan

AEUE - International Journal of Electronics and Communications <em@editorialmanager.com>

24 Mei 2023 pukul 15.12

Balas Ke: AEUE - International Journal of Electronics and Communications <support@elsevier.com>
Kepada: Teguh Firmansyah <teguhfirmansyah@untirta.ac.id>CC: andrea.morabito@unirc.it

Manuscript Number: AEUE-D-23-00484R1

Modeling of Quasi-tapered Microstrip Antenna Based on Expansion-exponential Tapered Method and Its Application for Wideband MIMO Structure

Dear Mr Firmansyah,

Thank you for submitting your manuscript to AEUE - International Journal of Electronics and Communications.

I am pleased to inform you that your manuscript has been accepted for publication.

My comments, and any reviewer comments, are below.

Your accepted manuscript will now be transferred to our production department. We will create a proof which you will be asked to check, and you will also be asked to complete a number of online forms required for publication. If we need additional information from you during the production process, we will contact you directly.

We appreciate and value your contribution to AEUE - International Journal of Electronics and Communications. We regularly invite authors of recently published manuscript to participate in the peer review process. If you were not already part of the journal's reviewer pool, you have now been added to it. We look forward to your continued participation in our journal, and we hope you will consider us again for future submissions.

We encourage authors of original research papers to share the research objects – including raw data, methods, protocols, software, hardware and other outputs – associated with their paper. More information on how our open access Research Elements journals can help you do this is available at https://www.elsevier.com/authors/tools-and-resources/research-elements-journals?dgcid=ec_em_research_elements_email.Kind regards,
Shahram MINAEI
Editor-in-Chief

AEUE - International Journal of Electronics and Communications

Editor and Reviewer comments:

Area Editor:

All reviewers' comments have been addressed. The revised manuscript can now be accepted.

Reviewer #1:

The comments are well addressed and implemented.

More information and support

FAQ: When and how will I receive the proofs of my article?

https://service.elsevier.com/app/answers/detail/a_id/6007/p/10592/supporthub/publishing/related/You will find information relevant for you as an author on Elsevier's Author Hub: <https://www.elsevier.com/authors>

FAQ: How can I reset a forgotten password?

https://service.elsevier.com/app/answers/detail/a_id/28452/supporthub/publishing/kw/editorial+manager/For further assistance, please visit our customer service site: <https://service.elsevier.com/app/home/supporthub/publishing/>. Here you can search for solutions on a range of topics, find answers to frequently asked questions, and learn more about Editorial Manager via interactive tutorials. You can also talk 24/7 to our customer support team by phone and 24/7 by live chat and email.

#AU_AEUE#

To ensure this email reaches the intended recipient, please do not delete the above code

**PLEASE TAKE ACTION - Share your article [AEUE_154745]**

4 pesan

Elsevier - Article Status <Article_Status@elsevier.com>
Kepada: teguhfirmansyah@untirta.ac.id

9 Juni 2023 pukul 00.21

ELSEVIER**Share your article!**

Dear Dr. Firmansyah,

We are pleased to let you know that the final version of your article *Modeling of Quasi-tapered Microstrip Antenna Based on Expansion-exponential Tapered Method and Its Application for Wideband MIMO Structure* is now available online, containing full bibliographic details.

To help you access and share this work, we have created a Share Link – a personalized URL providing **50 days' free access** to your article. Anyone clicking on this link before July 28, 2023 will be taken directly to the final version of your article on ScienceDirect, which they are welcome to read or download. No sign up, registration or fees are required.



Your personalized Share Link:
<https://authors.elsevier.com/a/1hDMC56FhxSXTI>

Click on the icons below to share with your network:



We encourage you to use this Share Link to download a copy of the article for your own archive. The URL is also a quick and easy way to share your work with colleagues, co-authors and friends. And you are welcome to add the Share Link to your homepage or social media profiles, such as Facebook and Twitter.

You can find out more about Share Links on [Elsevier.com](https://www.elsevier.com).

Did you know, as an author, you can use your article for a wide range of scholarly, non-commercial purposes, and share and post your article online in a variety of ways? For more information visit www.elsevier.com/sharing-articles.

Kind regards,
Elsevier Researcher Support

Increase your article's impact

Our [Get Noticed](#) guide contains a range of practical tips and advice to help you maximize visibility of your article.

Publishing Lab

Do you have ideas on how we can improve the author experience? Sign up for the [Elsevier Publishing Lab](#) and help us develop our publishing innovations!

Have questions or need assistance?

Please do not reply to this automated message.

For further assistance, please visit our [Elsevier Support Center](#) where you can search for solutions on a range of topics and find answers to frequently asked questions.

From here you can also contact our Researcher Support team via 24/7 live chat, email or phone support.

© 2023 Elsevier Ltd | Privacy Policy <http://www.elsevier.com/privacypolicy>

Elsevier Limited, The Boulevard, Langford Lane, Kidlington, Oxford, OX5 1GB, United Kingdom, Registration No. 1982084. This e-mail has been sent to you from Elsevier Ltd. To ensure delivery to your inbox (not bulk or junk folders), please add Article_Status@elsevier.com to your address book or safe senders list.

Modeling of quasi-tapered microstrip antenna based on expansion-exponential tapered method and its application for wideband MIMO structure

by Teguh Firmansyah

Submission date: 26-Jun-2023 01:07PM (UTC+0700)

Submission ID: 2122800637

File name: 1-s2.0-S1434841123002194-main.pdf (8.41M)

Word count: 8839

Character count: 45722



Regular paper

Modeling of quasi-tapered microstrip antenna based on expansion-exponential tapered method and its application for wideband MIMO structure

Teguh Firmansyah^{a,*}, Supriyanto Praptodiyono^a, Jaka Permana^a, Syah Alam^b,
Toto Supriyanto^c, Ken Paramayudha^d, Yuyu Wahyu^d, Mudrik Alaydrus^e, Jun Kondoh^{f,g}

^a Department of Electrical Engineering, Universitas Sultan Ageng Tirtayasa, Cilegon, Indonesia

^b Department of Electrical Engineering, Universitas Trisakti, Jakarta, Indonesia

^c Department of Telecommunication Engineering, Politeknik Negeri Jakarta, Jakarta, Indonesia

^d Research Center for Electronics and Telecommunication, Indonesian Institute of Sciences, Bandung, Indonesia

^e Department of Electrical Engineering, Universitas Mercu Buana, Jakarta, Indonesia

^f Graduate School of Science and Technology, Shizuoka University, 3-5-1 Johoku, Naka-ku, Hamamatsu-shi 432-8561, Japan

^g Graduate School of Integrated Science and Technology, Shizuoka University, 3-5-1 Johoku, Naka-ku, Hamamatsu-shi, Shizuoka 432-8561, Japan



ARTICLE INFO

Keywords:

4G/WLAN/X-band/5G

Expansion-exponential

MIMO antenna

Quasi-tapered structure

ABSTRACT

In this paper, a quasi-tapered wideband antenna using a circular-shaped with an inverted-omega ground structure is presented. A tapered antenna is usually developed based on linear-shape, exponential-shape, or Klopfenstein-shape taper. Here, we proposed an expansion of the exponential tapered model to investigate the circular-shaped tapered structure. In detail, the proposed antenna is divided into circular divergent and circular convergent-tapered sections. Then, the impedance ratio is utilized to analyze the tapered structure. Moreover, the ABCD parameter based on the transmission line model is used to investigate the overall antenna structure. The proposed model was verified by finite element method and a step impedance resonance evaluation. Furthermore, the proposed wideband antenna is also developed with multiple input multiple output (MIMO) and mutual coupling reduction structure. The antenna was fabricated on Rogers RT/Duroid 5880 substrate with $\epsilon_r = 2.2$, thickness of $h = 1.6$ mm, and dielectric loss $\tan \delta = 0.0009$. As a result, the proposed MIMO antenna can successfully cover the 4G (3.3 GHz), mid-band (3.4–3.8 GHz), WLAN (5.8 GHz), X-band (10–11 GHz), and high-band 5G (24.5–26 GHz) communications. A good agreement between the simulated and measured results validates the proposed method.

1. Introduction

A massive communication network with high data-rate capability is required to support 5G technology [1,2]. This challenging requirement has forced the development of 5G technology to work at the millimeter-wave (mmW) band to accommodate an enormous number of users with a wide bandwidth availability [3,4]. Several interesting methods of wideband antenna design working at mmW band have been investigated such as the substrate integrated cavity (SIC) antenna [5] and double-sided substrate-integrated waveguide (SIW) antenna [6]. They operate at the mmW band with a gain of 12 dBi and 8 dBi, respectively. Moreover, a monopole-like antenna structure [7] and a magneto-electric antenna [8] were introduced to combine 4G/WLAN and 5G

communications. Furthermore, antennas based on a tapered structure were proposed in [9–12].

In addition, another fundamental characteristic of 5G antennas is the multiple-input multiple-output (MIMO) capability. A well-designed MIMO antenna should deliver excellent particular performances, such as mutual coupling (MC), envelope correlation coefficient (ECC), and diversity gain (DG) [13–15]. Several methods were proposed for development of MIMO antennas including quasi-Yagi structure [16], metal frame structure [17], vertical stubs [18], fractal [19], and Y-shape structure [20]. Nonetheless, although these methods offer a good MIMO performance, they were only applicable for a single band 5G application. Then, a dual-loop antenna structure [21], step impedance [22], and a double-oval shaped antenna [23] were introduced for 4G and 5G

58

* Corresponding author.

E-mail address: teguhfirmansyah@untirta.ac.id (T. Firmansyah).

<https://doi.org/10.1016/j.ijele.2023.154745>

Received 7 March 2023; Accepted 24 May 2023

Available online 2 June 2023

1434-8411/© 2023 Elsevier GmbH. All rights reserved.

implementation with MIMO capability [24,25]. Nevertheless, these antennas did not target the mmWave band. Therefore, we can see the gap in the development of the MIMO antenna that can handle 4G, WLAN, X-band, and mid-high band 5G communications from S-band to mmW-band.

In addition to wideband performance and MIMO capability, the modeling of an antenna is essential for understanding and investigating its behavior. Therefore, many researchers proposed and derived models for antennas based on recursive convex optimization [26], equivalent circuit modeling [27], cavity model [28], and stepped-impedance resonator [29]. However, these proposed modeling techniques were focused on a narrow bandwidth antenna. To model wideband antennas, other methods such as space-mapping with kriging surrogates [30], linear elements [31], equivalent circuit model [32] have been successfully applied with slightly complex calculations. Furthermore, the MIMO antenna applications were investigated using various modeling techniques, namely a statistical analysis model [33], equivalent circuit model [34], effective length matrices [35], and eigen-analysis [36]. Nevertheless, these models were applied for narrowband applications. It is important to note that the design of antennas with wideband characteristics and suitable MIMO capability remains an open issue in antenna engineering. The study presented in this paper made several contributions, which are listed as follows:

1. A wideband antenna based on a quasi-tapered structure using a circular shape is proposed. A quasi-tapered characteristic was obtained by integrating a circular-shaped patch antenna with an inverted omega ground plane as shown in Fig. 1(a).
2. We also proposed an expansion-exponential tapered model to investigate the quasi-tapered structure based on a circular shape. This proposed model was utilized due to the limitation of the traditional linear, exponential, and Klopfenstein tapering methods. It is important to note that our circular tapered structure diverges from the conventional linear, exponential, or Klopfenstein shapes typically employed in tapering.
3. To obtain the mathematical model of for the circular shape tapered structure, we expand the existing exponential shape tapered model. In detail, Fig. 1(b) illustrates the proposed circular tapered structure which is divided into two halves circular shapes. It is seen that the physical dimension of the left-side of the half-circular shape is increasing. However, if we investigate the impedance characteristic, the impedance value is decreasing. Therefore, the left side structure has a convergent behavior. Vice versa, the right side of the half-circular shape has a divergent characteristic.
4. The study employs the ABCD parameter based on the transmission line model to investigate the overall antenna structure. The proposed model was verified by the finite element method (FEM). Following

the verification process, the proposed antenna was then applied in a MIMO structure. The fabrication of the antenna was carried out on a Rogers RT/Duroid 5880 substrate with $\epsilon_r = 2.2$, thickness of $h = 1.6$ mm, and dielectric loss $\tan \delta = 0.0009$. In addition, we also proposed a multislot defected ground structure (DGS) structure to reduce the mutual coupling parameter in the MIMO antenna system. As a result, the proposed MIMO antenna demonstrated wide bandwidth and excellent performance across various communication bands. The antenna is capable of operating in the S-band to mmW band, effectively covering a broad frequency range. This wide frequency coverage enabled the antenna to support multiple communication standards, including 4G (3.3 GHz), mid-band 5G (3.4–3.8 GHz), WLAN (5.8 GHz), and high-band 5G (24.5–26 GHz) concurrently. Table 1 provides an overview of the proposed research positioning.

This article has structures as follows. The first section describes the research position and the proposed method. The second section focuses on the quasi-tapered investigation based on the convergent/divergent tapered model with ABCD parameters. The third section highlights the design and measurement of the proposed quasi-tapered MIMO antenna. Then, it is followed by the results/discussions and the MIMO performance investigation. Finally, the last section concludes this research.

2. Quasi-tapered antenna based on circular-shaped patch with inverted-omega ground structure

Several methods have been studied to predict the operation frequency of an antenna, namely the lumped circuit modelling [40,41] and the transmission line approach [13]–[17]. Fig. 1(a) shows the main part of the antenna structure including the patch plane, ground plane, and excitation port. It should be noted that the proposed antenna has a direct excitation configuration. Hence, we can extract the antenna structure as several parts: a source impedance (Z_S), an excitation line, a convergent-tapered section, a divergent-tapered section, and a load-impedance (Z_L). Here, we use air impedance as the load impedance [42,43], as depicted in Fig. 1(b). The followed section describes the expanded exponential-shape taper to get the circular-shape taper model.

2.1. Half-circular shaped tapered with expansion-exponential tapered model

The proposed half-circular shape tapered configuration with the expansion-exponential tapered model is shown in Fig. 2(a). It has a radius of R and has convergent-tapered behavior. The input part is directly connected to the source impedance of $Z_{S(2)}$ and the end part is connected to the load impedance of $Z_{L(2)}$. It has a length of l_A from the

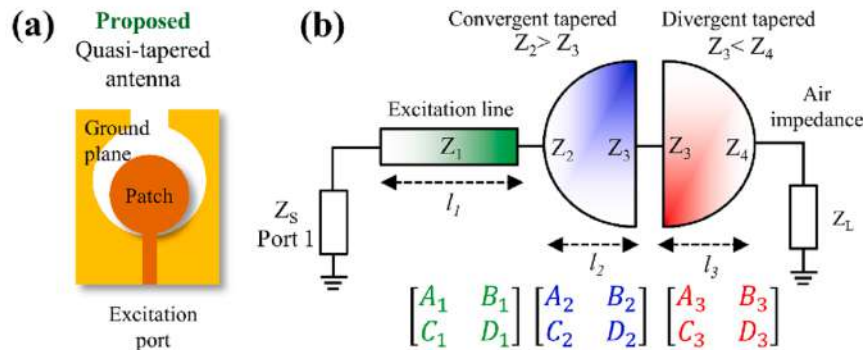


Fig. 1. (a) the proposed antenna based on quasi-tapered structure using circular-shaped patch with inverted-omega ground, (b) the ABCD parameters of proposed quasi-tapered antenna based on exponential tapered transmission lines approach.

Table 1
Research position.

Ref	Freq. (GHz)	Antenna structure	Proposed methods	Applications Narrow-band	Wide-band	MIMO antenna	Mutual coupling reduction	Advantages
[26]	2.50	Microstrip slot dipole	Recursive convex optimization	Yes	-	-	-	The proposed model has the capability to make predictions for the near field.
[27]	30.0	Micro-coaxial collinear	Equivalent circuit modeling	Yes	-	-	-	The calculation model is capable of identifying the equivalent circuit.
[28]	2.47-2.56	Stacked Microstrip Ring	Cavity model	Yes	-	-	-	The proposed model can predict the near field.
[29]	1.50-2.50	Stepped-Impedance Slot Antenna	Stepped-Impedance Resonator	Yes	-	-	-	The proposed model is capable of predicting the dualband impedance characteristics.
[30]	2.00-8.00	CPW-fed slot antenna with monopole	Space-mapping with kriging surrogates	-	Yes	-	-	The proposed model has the ability to forecast the value of reflection coefficient.
[31]	3.00	Conventional dipole	Linear elements	-	Yes	-	-	The model can estimate the radiation pattern.
[32]	2.51-6.55	Linear tapered slot	Equivalent circuit model	-	Yes	-	-	The calculation model has the potential to determine the equivalent circuit.
[33]	3.50-8.50	Monopole UWB	Statistical analysis model	Yes	Yes	-	-	The proposed model can make predictions for the value of reflection coefficient.
[34]	2.20	Monopole	Equivalent circuit model	Yes	-	Yes	-	The network parameters can be utilized for the prediction of S-parameters performance.
[35]	5.15-5.35	Monopole	The effective length matrices	Yes	-	Yes	-	The effective length matrices demonstrate good agreement with the method of moments.
[36]	5.20	FIFA-monopole	Eigen-Analysis	Yes	-	Yes	-	The model can determine the radiation pattern.
[37]	2.90-18.00	Circular shaped monopole	N.R.	-	Yes	Yes	-	The proposed antenna exhibits wideband performance.
[38]	3.00 - 30.0	Monopole with slot	N.R.	-	Yes	Yes	-	The proposed antenna possesses good isolation.
[39]	3.30 -8.50	L-shaped branch	N.R.	-	Yes	Yes	-	The proposed antenna has wideband performance.
This paper	3.30-26.0	Quasi-tapered using circular shaped	Expansion-exponential tapered model	-	Yes	Yes	Yes	The proposed antenna design combines wideband performance, a simple impedance calculation model, and low mutual coupling in a MIMO configuration.

Note: N.R = not reported.

input-port to the output-port. Moreover, Fig. 2(b). show the approximation characteristic of the impedance ratio (K) with different length of the taper. Here, we used the widest dimension of taper as the reference hence it has a unity value. Then, we can see that the impedance is increasing due to the decrease in the taper width.

To investigate the half-circular tapered configuration, we expand the exponential tapered model by introduce the term of impedance ratio with the expansion-exponential tapered model. The K can be written as:

$$K = a(e^{b(1-l_A)} + c) \tag{1}$$

where the a , b , and c are the adjustable constant parameters that follow the impedance curve of the circular shape. The intrinsic characteristic of the exponential-taper model is defined by the taper factor (b). Therefore, the impedance value of $Z_{l=l_A}$ at the length of l_A can be determined as:

$$Z_{l=l_A} = Z_{l=0} a(e^{b(1-l_A)} + c) \tag{2}$$

where $Z_{l=0}$ is the impedance at the initial position. Here, we state the initial impedance value as Z_0 . Then, the ABCD matrix of the half circular taper can be determined by:

$$\begin{bmatrix} A & B \\ C & D \end{bmatrix} = \frac{1}{\sqrt{Z_A Z_B}} \times \begin{bmatrix} Z_A \cosh \gamma l_A - Z_A \frac{d}{2\gamma} \sinh \gamma l_A & j Z_A Z_B \frac{\beta}{\gamma} \sinh \gamma l_A \\ j \frac{\beta}{\gamma} \sinh \gamma l_A & Z_B \cosh \gamma l_A + Z_B \frac{d}{2\gamma} \sinh \gamma l_A \end{bmatrix} \tag{3}$$

where

$$\gamma = \sqrt{\beta^2 - \left(\frac{d}{2}\right)^2} \tag{4}$$

$$d = \frac{\ln(a(e^{b(1-l_A)} + c))}{l_A} \tag{5}$$

$$\beta = \frac{2\pi}{\lambda} \tag{6}$$

with γ is the propagation constant. Moreover, the input impedance $Z_{IN(A)}$ can be calculated as:

$$Z_{IN(A)} = Z_A \frac{2Z_L \gamma + (j2Z_B \beta - Z_L d) \tanh \gamma l_A}{2Z_B \gamma + (j2Z_L \beta + Z_B d) \tanh \gamma l_A} \tag{7}$$

The next step is to investigate the antenna structure using the expansion-exponential taper model approximation, as depicted in Fig. 3 (a)-(b).

2.2. Quasi-tapered antenna with expansion-exponential tapered model

In detail, the proposed antenna structure can be separated into three important [40]s including excitation line, convergent-taper, and divergent taper, as shown in Fig. 3(a). It is important to note that eventhough the physical dimension becomes narrow or converging the impedance value becomes higher or diverging. Therefore, we called it as a divergent-taper and vice versa. Fig. 3(b) shows that the excitation line width is constant. Therefore, the impedance ratio is also constant. In addition, we introduce K_1 and K_2 as the impedance ratio for convergent-taper and divergent-taper, respectively. In detail, the investigation of the structure will be started by the excitation line followed by the convergent taper and divergent taper.

2.2.1. The excitation line

For more convenience and detail of the tapered structure, we can see Fig. 3(a)-(3b). The excitation line has directly connected to the input

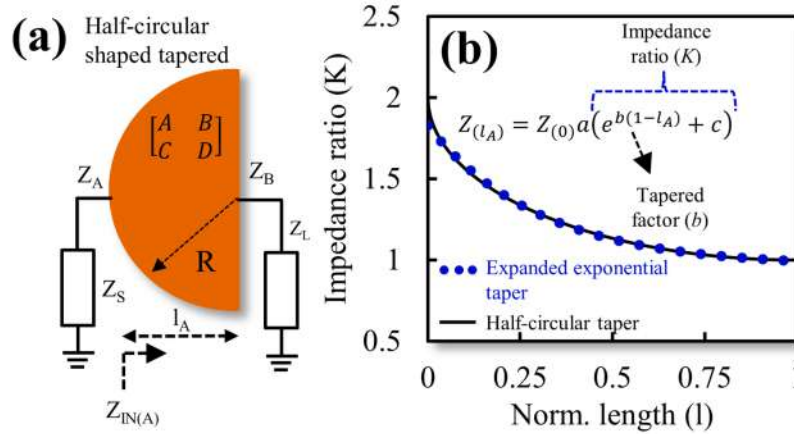


Fig. 2. (a) The proposed of half-circular shaped taper configuration with convergent tapered behavior. (b) Approximation of impedance ratio with widest dimension of taper as the reference.

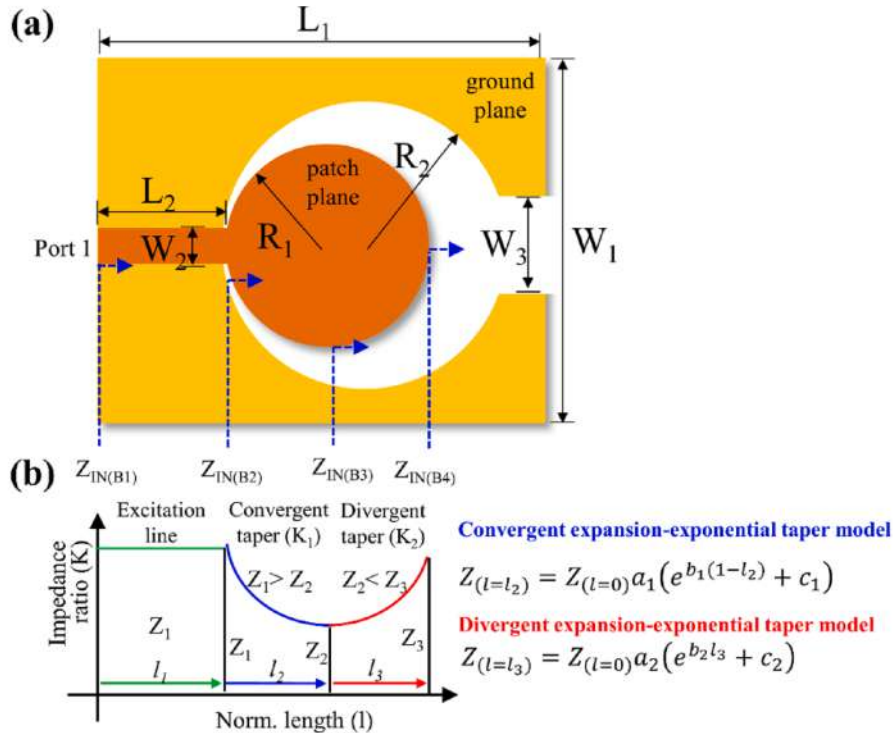


Fig. 3. (a) Quasi-tapered antenna based on circular-shaped with inverted-omega ground structure, (b) the approximation of impedance ratio and the electrical length of the proposed antenna structure.

impedance (Z_S) which is usually called as port 1. Moreover, the excitation line has the impedance characteristic (Z_1) and electrical length (l_1). They correspond to the width (W_2) and the length (L_1), respectively. To simplify the investigation, we assume the impedance of the excitation line (Z_1) is equal to the source impedance (Z_S).

2.2.2. The half-circular shaped convergent-tapered

The convergent-tapered is focused on decreasing of impedance values. Therefore, the impedance ratio (K_1) for the convergent taper of

the proposed antenna is determined by:

$$K_1 = a_1 (e^{b_1(1-l_2)} + c_1) \tag{8}$$

where the a_1 , b_2 , and c_2 are constant parameters and the value a_1 follows the impedance curve. Moreover, b_2 is the convergent taper ratio for the proposed antenna.

Then, the impedance value of $Z_{(l=l_2)}$ at the length of l_2 can be calculated as:

$$Z_{l=l_2} = Z_{l=0} a_1 (e^{b_1(1-l_2)} + c_1) \tag{9}$$

where $Z_{l=0}$ is the impedance at the initial position. The ABCD matrix of half-circular taper with convergent structure can be determined by:

$$\begin{bmatrix} A_2 & B_2 \\ C_2 & D_2 \end{bmatrix} = \frac{1}{\sqrt{Z_1 Z_2}} \times \begin{bmatrix} Z_1 \cosh \gamma_2 l_2 - Z_1 \frac{d_1}{2\gamma} \sinh \gamma_2 l_2 & j Z_1 Z_2 \frac{\beta}{\gamma} \sinh \gamma_2 l_2 \\ j \frac{\beta}{\gamma} \sinh \gamma_2 l_2 & Z_2 \cosh \gamma_2 l_2 + Z_2 \frac{d_1}{2\gamma} \sinh \gamma_2 l_2 \end{bmatrix} \tag{10}$$

where

$$\gamma_2 = \sqrt{\beta^2 - \left(\frac{d_1}{2}\right)^2} \tag{11}$$

$$d_1 = \frac{\ln(a_1 (e^{b_1(1-l_2)} + c_1))}{l_2} \tag{12}$$

with γ_2 is the propagation constant of the convergent taper with circular shape. Then, Fig. 4(a)-4(c) show the relation between normalized length (l_2) with the impedance ratio (K_I) for convergent taper with different value of a_1 , c_1 , and b_1 .

In det 18 the normalized length of l_2 value was analyzed between 0 and 1. It can be seen that the a_1 and c_1 have a similar effect to the impedance ratio (K_I). The a_1 and c_1 have linear effects to the impedance ratio value. Moreover, K_I was highly influenced by coefficient b_1 . Therefore, by adjusting the value of a_1 , c_1 , and b_1 , we can obtain the impedance ratio that is similar to the circular part.

2.2.3. The half-circular shaped divergent-tapered

The impedance ratio (K_2) for the divergent taper part of the proposed antenna design is determined by:

$$K_2 = a_2 (e^{b_2 l_2} + c_2) \tag{13}$$

where a_1 , b_2 , and c_2 are the adjustable constant parameters that 4 lows the impedance curve. Moreover, b_2 is the convergent to 4r ratio for the proposed antenna. The impedance value of $Z_{l=l_2}$ at the length of l_2 can be calculated as:

$$Z_{l=l_2} = Z_{l=0} a_2 (e^{b_2 l_2} + c_2) \tag{14}$$

Then, the ABCD matrix of half-circular taper with convergent structure can be determined by:

$$\begin{bmatrix} A_3 & B_3 \\ C_3 & D_3 \end{bmatrix} = \frac{1}{\sqrt{Z_2 Z_3}} \times \begin{bmatrix} Z_2 \cosh \gamma_3 l_3 + Z_2 \frac{d_2}{2\gamma_3} \sinh \gamma_3 l_3 & j Z_2 Z_3 \frac{\beta}{\gamma_3} \sinh \gamma_3 l_3 \\ j \frac{\beta}{\gamma_3} \sinh \gamma_3 l_3 & Z_3 \cosh \gamma_3 l_3 - Z_3 \frac{d_2}{2\gamma_3} \sinh \gamma_3 l_3 \end{bmatrix} \tag{15}$$

where

$$\gamma_3 = \sqrt{\beta^2 - \left(\frac{d_2}{2}\right)^2} \tag{16}$$

$$d_2 = \frac{\ln(a_3 (e^{b_2 l_3} + c_2))}{l_3} \tag{17}$$

with γ_2 is the propagation constant of the circular shape. Moreover, Fig. 5(a)-5(c) show the relation between normalized length (l_2) with the impedance ratio (K_I) of the convergent taper for different value of a_1 , c_1 , and b_1 , respectively. In details, the normalized length l_2 value was plotted from 0 to 1. Then, a_1 is varied from 0.028 to 0.038 with a step value of 0.002. Therefore, we can see that the value of K_I decreases exponentially.

Overall, by adjusting the values of a_1 , b_1 , and c_1 , we can get the impedance ratio values of half-circular shaped using exponential taper model approach.

3. Comparison model

26 To verify the proposed model, the comparison of the impedance ratio of the expanded exponential model and finite element method (FEM) is presented in Fig. 6(a). We can see that the models are in good agreement and fit with each other. This means that the proposed model can be used to calculate the impedance ratio of circular-shaped taper. Moreover, the proposed model can be also implemented and verified using simple case, such as when $K = 1$ and the length of l between 0.5 and 1, d_1 and d_2 will become 0 as shown in Fig. 6(b). The model can be also utilized for the calculation of input impedance of step impedance resonator. In detail, by using $d = 0$ and the loss-less case of $\gamma = j\beta$, it will lead to the equation of input impedance of step impedance resonator as follows:

$$Z_{IN(B1)} = Z_1 \frac{Z_{IN(B2)} + j Z_1 \tan \beta l_1}{Z_1 + j Z_{IN(B2)} \tan \beta l_1} \tag{18}$$

$$Z_{IN(B2)} = Z_1 \frac{Z_{IN(B3)} + j Z_2 \tan \beta l_2}{Z_2 + j Z_{IN(B3)} \tan \beta l_2} \tag{19}$$

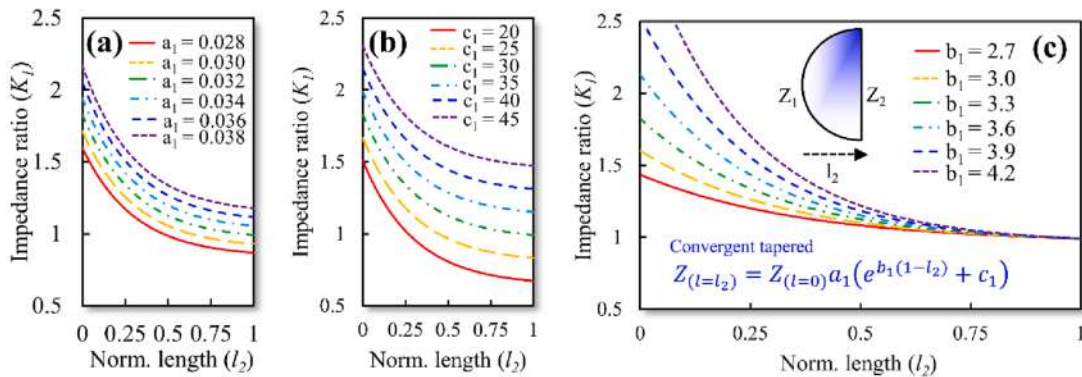


Fig. 4. (a) The relation between normalized length (l_2) with the impedance ratio (K_I) for different value of (a) a_1 , (b) c_1 , and (c) b_1 .

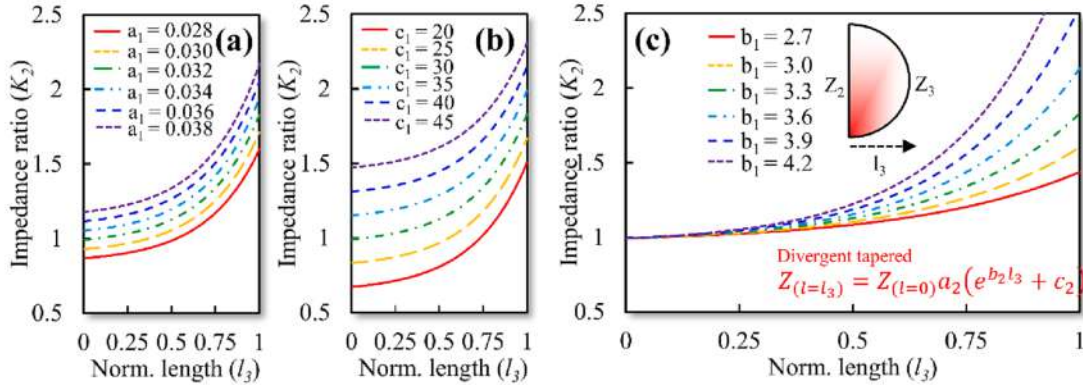


Fig. 5. (a) The relation between normalized length (l_3) with the impedance ratio (K_2) for different value of (a) a_2 , (b) c_2 and (c) b_1 .

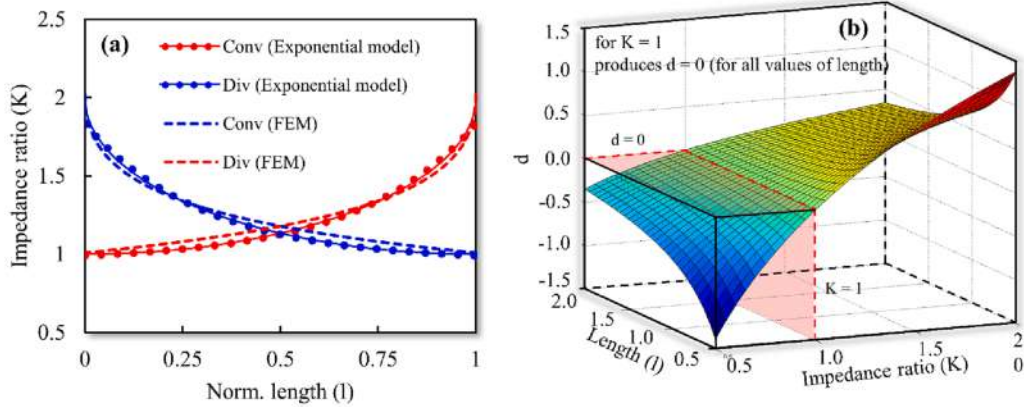


Fig. 6. (a) Comparison of circular shape-taper using expanded exponential model, and finite element method (FEM) (b) a generalized for case $K = 1$ and its relations between l and d value.

$$Z_{IN(B3)} = Z_2 \frac{Z_{IN(B4)} + jZ_3 \tan \beta l_3}{Z_3 + jZ_{IN(B4)} \tan \beta l_3} \quad (20)$$

$$Z_{IN(B4)} = Z_L \quad (21)$$

Finally, the proposed exponential tapered transmission line model can be used for impedance calculation of circular shape resonator and step impedance resonator.

Fig. 7(a) and 7(b) show the results comparison between the expansion-exponential tapered method and conventional tapered method for circular convergent-taper and circular divergent-taper configurations, respectively. MATLAB software was used to perform the calculations for both the expansion-exponential and conventional tapered methods. In addition to MATLAB, the transmission line electromagnetics modeling tool suite of TNT 1.2.2 was utilized for the FEM based calculations. It is observed that the proposed method exhibited greater consistency and better fit with the FEM results. These results look similar for circular-convergent taper and circular-divergent taper. However, if we compare it with the conventional tapered methods, the deviation is significant. This results suggests that the proposed expansion-exponential tapered method offers distinct advantages and a more suitable design approach compared to conventional methods. Additionally, it is important to note that further detailed investigations of the antenna characteristics were conducted using CST Microwave Studio software.

The next step is antenna dimension optimization and MIMO

characterization. The antenna dimension can be optimized to obtain working frequencies ranging from S-band to mmWave band with $|S_{11}| < -10$ dB. To reduce the mutual coupling effect of this proposed MIMO antenna, we include a structure that is based on multi-slot configuration. This multi-slot structure was positioned at the middle part of the antenna ground plane. To evaluate the MIMO performance of the antenna, several additional parameters should also be considered. The parameters $|S_{21}|$, ECC, and DG. ECC can be determined using S-parameters [44]. Then, the DG can be derived from the ECC equation [44].

4. Design of quasi-tapered wideband MIMO antenna

The design steps of the proposed antenna can be divided into two main parts. The first part focuses on the modelling of the quasi-tapered antenna using the transmission line model approach. Then, the second part focuses on the optimization of the MIMO antenna. In detail, the design procedures of the quasi-tapered antennas have several steps including a conventional circular shape monopole microstrip antenna design, feeding length modification, and ground-plane modification into an inverted omega-ground structure as illustrated as antenna A#, B#, and C# in Fig. 8(a)-8(c), respectively.

The substrate geometry of antenna A# is rectangular with a length of L_1 and a width of W_1 . The radiating part of the antenna A# structure is developed from a circular-shaped patch with radius of R_1 and is fed by a direct-excitation feed with a length of L_{3A} and width of W_2 . At the

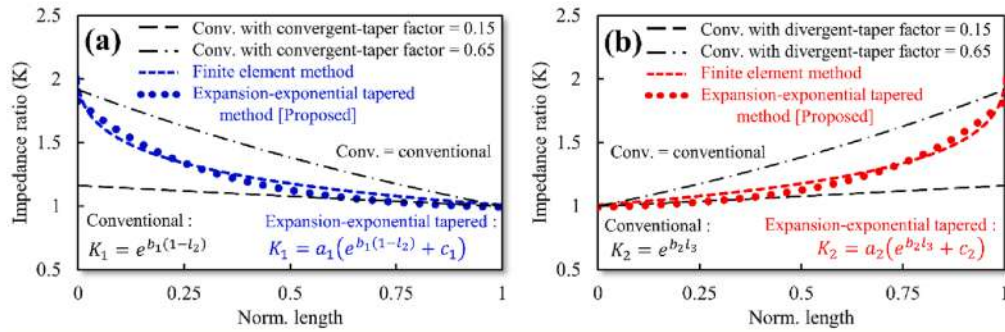


Fig. 7. Results comparison between the proposed method expansion-exponential tapered method and conventional tapered method (a) circular convergent-taper, and (b) circular divergent-taper.

ground plane side, a circular ground slot with the radius of R_2 is included. This ground slot is positioned at distances of L_2 and L_4 from the bottom and the top side of the substrate, respectively. It should be mentioned that the position of the circular patch and the circular ground slot are centrally aligned. Fig. 9(a) shows the reflection coefficient of antenna A# with variation of R_1 . In this scenario, R_1 is varied from 3 mm to 15 mm. We can see that the change of R_1 leads to the variation of antenna frequency and the return loss. However, we note that the antenna still has a poor matching impedance at several desired frequencies as shown in the reflection coefficient value. Hence, in the next step we investigate the effect of excitation length (L_2) variation on the resonant frequency as antenna B#. The simulation result of the effect of L_2 variation is shown in Fig. 9(b). The result indicates that the length of L_2 has a significant effect on the return loss of the antenna. Next, we add an upper part slot with a width of W_3 . This antenna is called antenna C#.

Fig. 10(a) shows that by using this additional slot, the antenna has a better reflection coefficient compared to antenna B#. Furthermore, Fig. 10(b) shows the comparison of the return loss of antenna A#/B#/C#. We can see that antenna C# has a better reflection coefficient compared to antenna A# or B#. Therefore, we decide to expand antenna C# into a MIMO structure. The design evolution of the MIMO antenna structure is shown in Fig. 11(a), 11(b), 11(c), and 11(d) as MIMO antenna C1#, C2#, C3#, and C4#. The C1# antenna represents a conventional MIMO antenna which comprises two identical antennas without any structural modification as depicted in Fig. 11(a).

In MIMO antenna C2#, an additional single DGS slot-ground

structure with a length of L_{D1} and width of W_{D1} is introduced at the top part of the ground plane as depicted in Fig. 11(b). The MIMO antenna C3# has a dual slot-ground structure. The additional slot is positioned at the middle part of the ground plane with a length of L_{D2} and a width of W_{D2} , as shown in Fig. 11(c). Finally, a third ground slot is included in MIMO antenna C4#. This slot is introduced at the bottom part of the ground plane with a length of L_{D3} and width of W_{D3} , as illustrated in Fig. 11(d). The complete dimension and 3D view of MIMO antenna C4# can be seen in Fig. 12(a) and Fig. 12(b), respectively.

Moreover, Fig. 13(a) shows the comparison of the reflection coefficient of the MIMO antennas. We can see that a return loss of under -10 dB at the desired frequencies is achieved for all MIMO antennas C1#/C2#/C3#/C4#. This indicates that the proposed MIMO configurations have no significant effect on the operation frequency of the antenna. Lastly, Fig. 13(b) shows the comparison of the mutual coupling of MIMO antenna C1#/C2#/C3#/C4#. The results indicate that the MIMO antenna C4# provides the best isolation with a mutual coupling lower than -20 dB. Next, the proposed antenna is fabricated and measured to verify the simulation results.

5. Result and discussion

The proposed antennas C# and C4# were fabricated on Rogers RT/Duroid 5880 substrate with $\epsilon_r = 2.2$, thickness of $h = 1.6$ mm, and dielectric loss $\tan \delta = 0.0009$. The complete dimensions are as follows (in millimeter): $R_1 = 9$, $R_2 = 15$, $W_1 = 40$, $W_2 = 2.6$, $W_3 = 10$, $W_T = 85$,

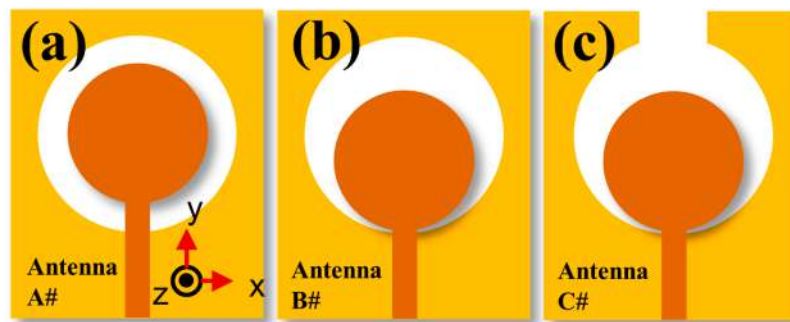


Fig. 8. (a) Conventional circular shape antenna, (b) modification the feeding length of L_2 , (c) modification of ground-plane and became inverted omega-ground structure by added W_3 .

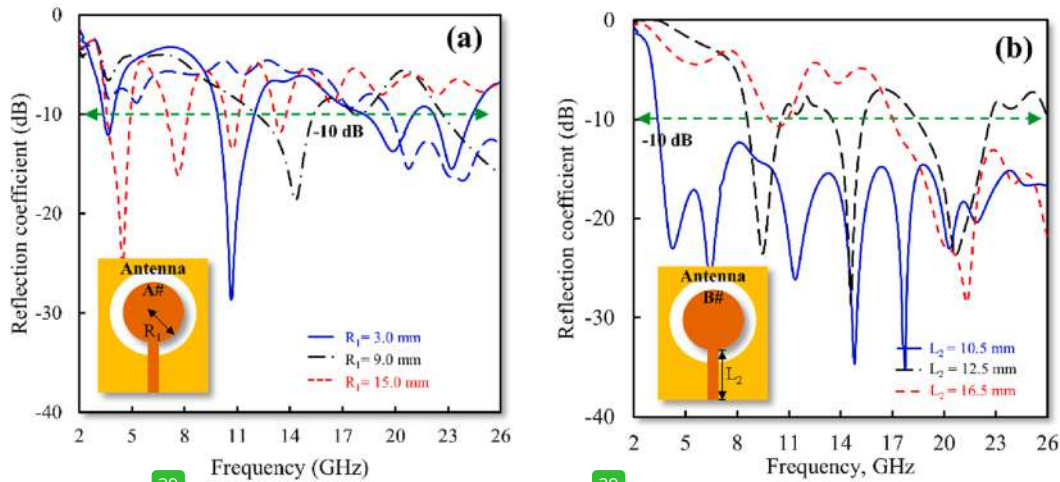


Fig. 9. (a) Reflection coefficient of antenna A# with varied of R_1 , (b) Reflection coefficient of antenna B# with varied of L_2 .

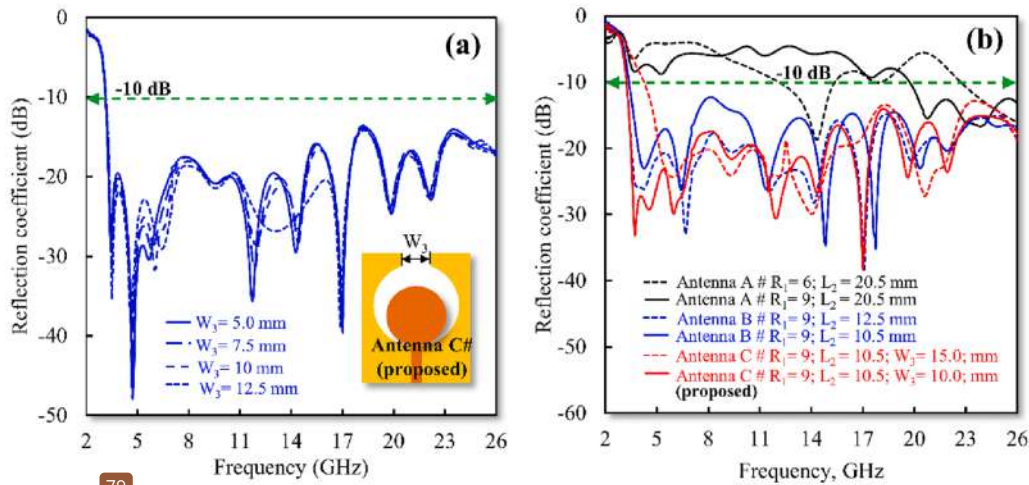


Fig. 10. (a) Reflection coefficient of antenna C# with varied of W_3 , (b) comparison of reflection coefficient of antenna A#/B#/C#.

$W_{D1} = 5$, $W_{D2} = 5$, $W_{D3} = 5$, $L_1 = 45$, $L_2 = 10.4$, $L_3 = 4.6$, $L_{3A} = 15.5$, $L_{3B} = 10.5$, $L_{D1} = 6$, $L_{D2} = 29.5$, $L_{D3} = 5$. In detail, Fig. 14(a), 14(b), 14(c), and 14(d) show the photographs of fabricated antenna C# and C4# with view from the patch and the ground side. The measurement of the proposed antenna's performance up to 26 GHz was facilitated by using the first-generation of super SMA female connectors from HASCO. Based on the data sheet, this connector has good performance from DC up to 27 GHz [45]. Furthermore, an R&S ZVA67 VNA is used to measure the antenna performance.

Fig. 14(e) shows the reflection coefficient comparison between the simulation and measurement of antenna C#. We can see that at several frequencies points the measured return losses are higher than those from the simulation. Nevertheless, they are still under -10 dB and hence the antenna C# can successfully cover a wide range from S-band to mmW band. Fig. 14(f) shows a comparison of the reflection coefficient between the simulation and measurement of MIMO antenna C4#. In line with the antenna C#, the MIMO configuration does not change the reflection

coefficients significantly. The return loss of the proposed MIMO antenna is still under -10 dB.

The mutual coupling (MC) comparison between simulation and measurement of MIMO antenna C4# is depicted in Fig. 14(g). In MIMO antenna, MC is generally used to evaluate the interaction of the antennas. We can see that the MIMO antenna C4# has MC values lower than -20 dB in all desired frequencies. Therefore, we can conclude that the interferences between antennas are insignificant. It should be noted that, in principle, this antenna has the potential to operate across wide frequency bands. However, in this paper, the focus was directed towards specific frequency bands in order to position the study within the context of future communication technologies. We have selected several specific bands such as the 4G (3.3 GHz), mid-band 5G (3.4–3.8 GHz), WLAN (5.8 GHz), X-band (10–11 GHz), and high-band 5G (24.5–26 GHz) communications.

Fig. 15 (a-j) presents the normalized co- and cross-polarization radiation patterns of the proposed antenna. Specifically, Fig. 15 (a-e) display

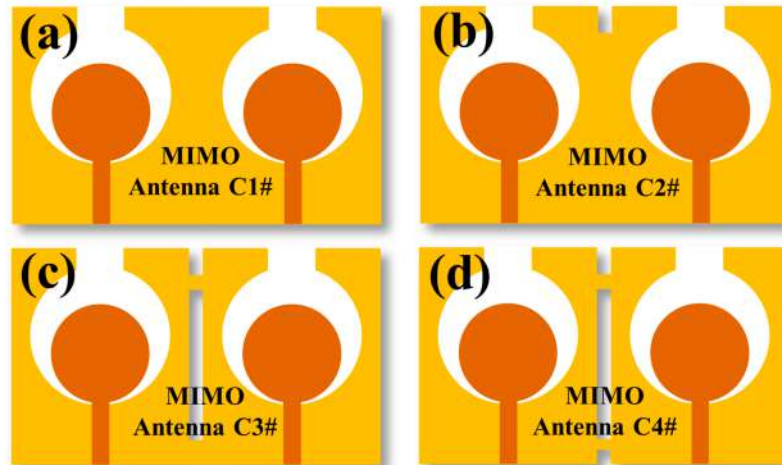


Fig. 11. (a) MIMO antenna C4#, and (b) 3D view of proposed MIMO antenna C4#.

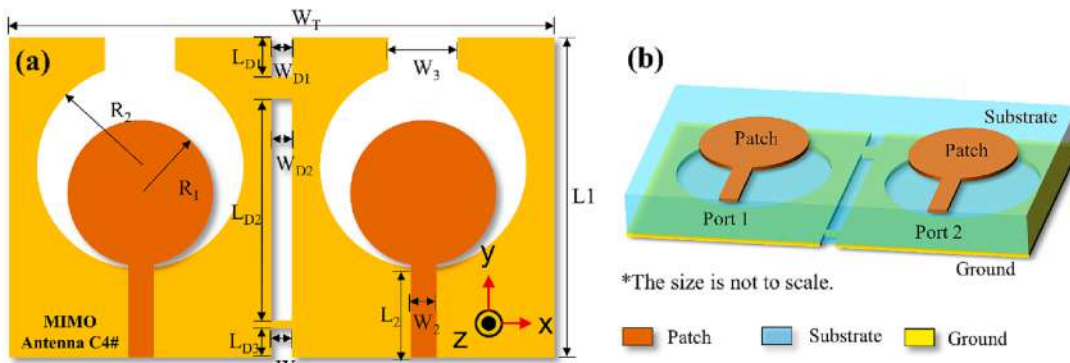


Fig. 12. (a) MIMO antenna C4#, and (b) 3D view of proposed MIMO antenna C4#.

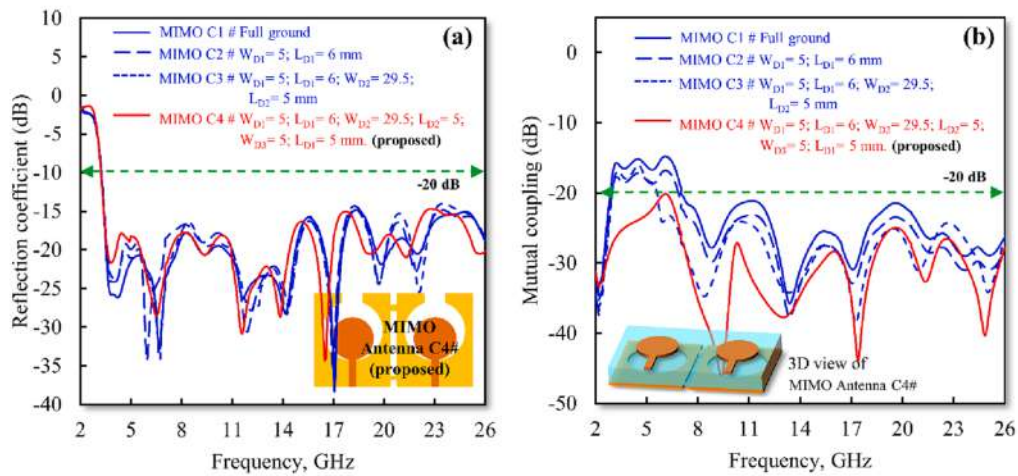


Fig. 13. (a) A comparison of reflection coefficient of MIMO antenna C1#/C2#/C3#/C4#, (b) comparison of mutual coupling of MIMO antenna C1#/C2#/C3#/C4#.

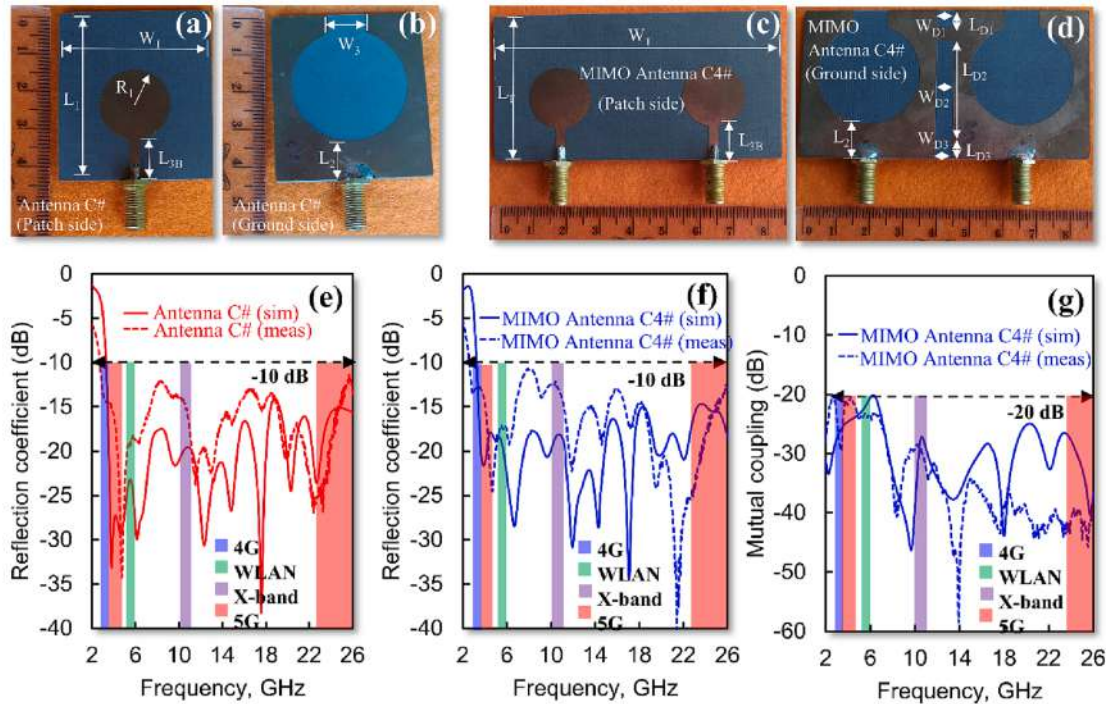


Fig. 14. (a) Fabrication result of antenna C# (a) view [11](#) patch side, (b) view from ground side. Fabrication result of MIMO antenna C4# (c) view from patch side, (d) view from ground side. The reflection coefficient [42](#) between simulation and measurement of (e) antenna C#, (f) MIMO antenna C4#, (g) a mutual coupling comparison between simulation and measurement of MIMO antenna C4#.

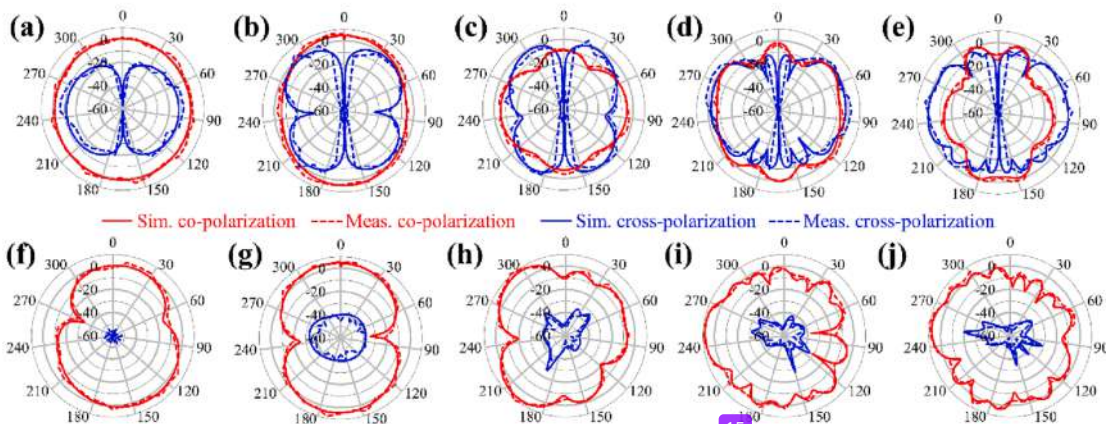


Fig. 15. Co- and cross-polarization normalized radiation patterns at XOZ-plane at frequency of (a) 3.3 GHz, [15](#) 8 GHz, (c) 10 GHz, (d) 24 GHz, and (e) 26 GHz. Then, Co- and cross-polarization normalized radiation patterns at YOZ-plane at frequency of (f) 3.3 GHz, (g) 5.8 GHz, (h) 10 GHz, (i) 24 GHz, and (j) 26 GHz.

the normalized co- and [12](#) s-polarization radiation patterns at the XOZ-plane for frequencies of 3.3 GHz, 5.8 GHz, 10 GHz, 24 GHz, and 26 GHz, respectively. It is seen at the XOZ-plane, the cross-polarization values are relatively large. However, the main beam at 0 degree exhibits a very low [6](#) ss-polarization value. Moreover, Fig. 15 (a-e) show the normalized co- and [12](#) s-polarization radiation patterns at YOZ-plane for frequencies of 3.3 GHz, 5.8 GHz, 10 GHz, 24 GHz, and 26 GHz, respectively. At the YOZ-plane direction, the [8](#) s-polarization antenna exhibits a very low cross-polarization value. Therefore, it can be concluded the proposed antenna has omni-directional pattern at the YOZ-plane.

As an additional explanation, there are several reasons that the monopole antenna can generate circular polarization such as [2](#) ound-plane's position and antenna shape [46-48](#). The ground-plane plays an important role in determining the po [80](#) sition of an antenna. In the specific case of a monopole antenna, the ground plane can cause the polarization of the signal to change from its original orientation, with a larger ground plane providing more reflection and resulting in a more significant change in polarization [46-48](#).

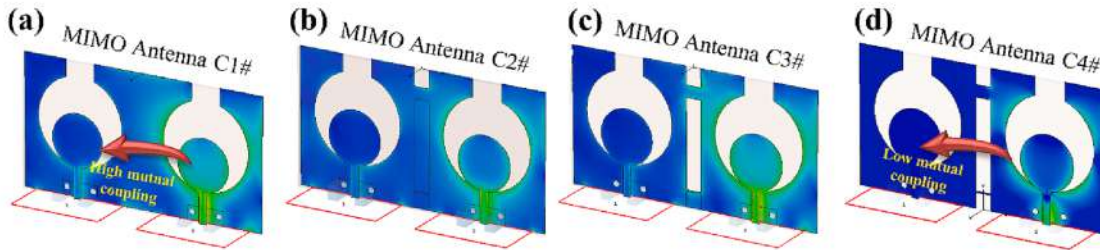


Fig. 16. Surface current density of (a) MIMO antenna C1#, (b) MIMO antenna C2#, (c) MIMO antenna C3#, (d) MIMO antenna C4#.

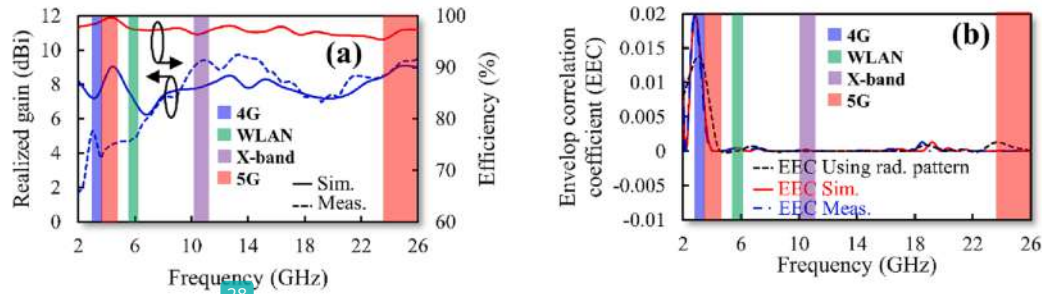


Fig. 17. Comparison result of (a) realized gain and efficiency, (b) enveloped correlation coefficient.

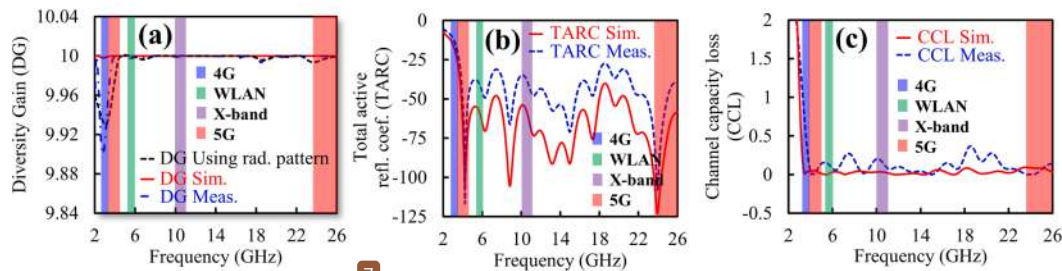


Fig. 18. Comparison result of (a) diversity gain, (b) total active reflection coefficient, and (c) channel capacity loss.

6. MIMO performances

The evaluation of surface current density distribution is crucial to understand the behavior of the proposed MIMO antenna. This surface current density distribution can be used to explain the MC between closely spaced antennas. Fig. 16(a), 16(b), 16(c), and 16(d) illustrate the surface current density of MIMO antenna C1#, C2#, C3#, and C4#, respectively. We can see that the MIMO antenna C1# has the highest mutual coupling among others. The MCs are qualitatively decreased after ground slots were included. This can be seen in Fig. 16(d) where the MIMO antenna C4# generates the lowest mutual coupling, as indicated by the blue color in the subsequent antenna. Then, Fig. 17 (a-b) show the results comparison of realized gain and efficiency, and enveloped correlation coefficient, respectively.

A realized gain and efficiency of MIMO antenna C4# shown in Fig. 17(a). As depicted in the graph, the antenna has a realized gain ranging from 2.0 dBi to 9.5 dBi. The efficiency value range from 95.4% to 98.2%. It is important to note that only simulation data for efficiency are presented due to the limitations of the measurement device. However, the obtained results indicate good performance in terms of efficiency. This is attributed to the low loss of Rogers RT/Duroid 5880 substrate which has a dielectric loss tangent ($\tan \delta$) of 0.0009. Furthermore, the envelope correlation coefficient (EEC) of the antenna

is illustrated in Fig. 17(b). The EEC value can be calculated using radiation patterns or scattering parameters [4,49,50]. The result shows that the EEC is slightly increased around the S-band. This occurrence is correlated with the MC, as a higher MC between antennas will have a more significant effect on the EEC. Nonetheless, we can see that the ECCs are still under 0.02 at all frequencies. Therefore, it is indicated that the antenna has a small correlation coefficient.

Fig. 18(a-c) show comparison result of diversity gain (DG), total active reflection coefficient (TARC), and channel capacity loss (CCL) of the MIMO antenna C4#, respectively. Moreover, we can also calculate the DG value using the EEC obtained from radiation patterns. The DG maximum value achieved is 10 dB, while the proposed MIMO antenna C4# has a high DG of above 9.9 dB. This means the proposed antenna performs well in terms of MIMO performance. Additionally, the TARC value which is a metric that relates the reflection power in an N-port microwave component can be calculated using equations from [4,49,50]. The TARC value of the proposed antenna is lower than -10 dB which indicates that the reflection power is very low. Then, the CCL value is lower than 0.4, which is suitable for MIMO applications. Table 2 shows the comparison between our proposed design and previous published antennas. The result shows that the proposed structure has many advantages that are suitable for 5G applications.

39
Table 2
Performance comparison of the proposed antenna with published antennas.

Ref.	Antenna structure	f_c / BW (GHz)	Proposed application	Size (λ_0)	Substrate	Shape of rad. pattern	Port	Isolation (dB)	Realized Gain (dBi)	Efficiency (%)	CCL	EEC	DG
[51]	Quasi self complementary	6.85/7.50	WLAN, UWB	0.73×0.73	FR4, $\epsilon_r = 4.4$, $h = 1.57$, $\tan \delta = 0.02$	Omni	4	< -15	1.7 - 4.2	60-90	10	N.R	10
[52]	Planar-monopole	7.40/9.20	UWB	0.73×0.64	RTDuroid4350B, $\epsilon_r = 3.5$, $h = 0.8$, $\tan \delta = 0.004$	directional	2	< -20	-2 - 5.8	95-99	N.R	N.R	N.R
[53]	Koch fractal monopole	7.5/9.0	C-Band, UWB	0.76×1.12	FR4, $\epsilon_r = 4.4$, $h = 1.57$, $\tan \delta = 0.02$	directional	2	< -19	1.0 - 5.0	N.R	N.R	0.17	N.R
[54]	Monopole with floating parasitic	6.85/7.50	UWB	0.62×0.80	RTDuroid4003, $\epsilon_r = 4.3$, $h = 1.57$, $\tan \delta = 0.0024$	directional	2	< -16	3.4 - 6.5	N.R	N.R	0.2	N.R
[55]	Single-dipole	3.65/4.00	5G	0.91×1.70	FR4, $\epsilon_r = 4.4$, $h = 1$, $\tan \delta = 0.02$	Directional	2	< -18	N.R.	80-90	N.R.	0.1	N.R.
[56]	Dual monopole	7.55/8.90	WLAN and 5G	2.06×0.55	RTDuroid5880, $\epsilon_r = 2.2$, $h = 1.57$, $\tan \delta = 0.0009$	directional	2	< -18	N.R	N.R	N.R	0.35	N.R.
[57]	Monopole with EBG	2.42/2.90	WLAN	0.90×0.23	FR4, $\epsilon_r = 4.4$, $h = 1$, $\tan \delta = 0.02$	Directional	2	< -24	-4.25	50 - 58	N.R	0.008	9.99
[58]	Circular monopole	2.50/3.40	WLAN	0.15×0.30	JC, $\epsilon_r = 1.6$, $h = 1$, $\tan \delta = 0.02$	directional	2	< -16	-3.0	N.R	N.R	0.05	N.R
[59]	CPW Asymmetric EBG	4.75/5.40	Sub-6 GHz 5G	0.33×0.34	FR4, $\epsilon_r = 4.4$, $h = 1.57$, $\tan \delta = 0.02$	directional	2	< -18	N.R	N.R	N.R	0.025	-10.0
[60]	O-shaped monopole	4.10/4.75	WLAN and 5G	2.90×0.13	FR4, $\epsilon_r = 4.4$, $h = 1.57$, $\tan \delta = 0.02$	directional	2	< -23	2 - 4	20.0-65.0	N.R	N.R	N.R
[61]	Octagonal-dips shaped	11.0/18.0	UWB and 5G	3.40×1.46	FR4, $\epsilon_r = 4.4$, $h = 1.57$, $\tan \delta = 0.02$	directional	2	< -15	-10.0	90-92	N.R	0.02	9.80-10.00
[62]	Octagonal-shaped radiating	6.85/7.50	UWB with notch	1.61×0.43	FR4, $\epsilon_r = 4.4$, $h = 1.57$, $\tan \delta = 0.02$	directional	2	< -18	1.2 - 2.91	70-90	<0.05	<0.02	9.40-10.00
[63]	Metamaterial and SIW	9.00/14.00	UWB	0.68×1.05	FR4, $\epsilon_r = 4.4$, $h = 1.57$, $\tan \delta = 0.02$	directional	2	< -23	3.7 - 4.3	65-80	<0.04	0.04	1.5-10
This paper	Quasi-tapered using circular shaped	14.65/22.70	4G / Mid-band 5G / WLAN /X-Band / High band 5G	1.08×4.15	RTDuroid5880, $\epsilon_r = 2.2$, $h = 1.57$, $\tan \delta = 0.0009$	directional	2	< -20	2.0-9.5	95.4 - 98.2	<0.04	<0.02	9.88-10

Note: f_c = frequency center, BW = bandwidth, CCL = channel capacity loss, EEC = envelop correlation coefficient, DG = diversity gain, and N.R = not reported.

7. Conclusion

We have successfully designed a quasi-tapered wideband MIMO antenna by combining a circular-shaped patch and an inverted omega ground structure. An expansion of the exponential tapered model was used to investigate the circular-shaped tapered structure. In detail, the proposed antenna is divided into circular divergent and circular convergent-tapered sections. Then, a transmission lines approach was utilized to analyze and optimize the antenna structure. The proposed model was verified by FEM simulation and also step impedance calculation. Moreover, the proposed MIMO antenna can successfully cover the at 4G (3.3 GHz), mid-band 5G (3.4–3.8 GHz), WLAN (5.8 GHz), X-band (10–11 GHz), and high-band 5G (24.5–26 GHz) communications. A good agreement between the simulated and measured results validates the proposed method. A good agreement between the simulated and measured results validates the proposed method.

3 Declaration of Competing Interest

The authors declare that they have no known competing financial interests or personal relationships that could have appeared to influence the work reported in this paper.

Data availability

Data will be made available on request.

Acknowledgment

This work is supported by the Kementerian Pendidikan, Kebudayaan, Riset, dan Teknologi of Indonesia. Universitas Sultan Ageng Tirtayasa. 2023.

References

- [1] B. Aghoutane, S. Das, M. El Ghzaoui, B. T. P. Madhav, and H. El Faylali, "A novel dual band high gain 4-port millimeter wave MIMO antenna array for 28/37 GHz 5G applications," *AEU - Int. J. Electron. Commun.*, vol. 145, no. December 2021, p. 154071, 2022, <https://doi.org/10.1016/j.aeue.2021.154071>.
- [2] B. Feng, Y. Tu, J. Chen, K. L. Chung, and S. Sun, "High-performance dual circularly-polarized antenna arrays using 3D printing for 5G millimeter-wave communications," *AEU - Int. J. Electron. Commun.*, vol. 130, no. June 2020, p. 153569, 2021, <https://doi.org/10.1016/j.aeue.2020.153569>.
- [3] Yadav V, Yadav RS, Yadav P, Mishra B, Kumar A. "Dual and wideband 6-port MIMO antenna for WiFi, LTE and carrier aggregation systems applications", *AEU - Int J Electron Commun* 2023;162. <https://doi.org/10.1016/j.aeue.2023.154576>.
- [4] Cumeray K, Akcam N, Okan T, Arican GO. "28/38 GHz dual-band MIMO antenna with wideband and high gain properties for 5G applications", *AEU - Int J Electron Commun* 2023;vol. 162:154553. <https://doi.org/10.1016/j.aeue.2023.154553>.
- [5] Mao CX, Khalily M, Xiao P, Brown TWC, Gao S. Planar sub-millimeter-wave array antenna with enhanced gain and reduced sidelobes for 5G broadcast applications. *IEEE Trans Antennas Propag* 2019;67(1):160–8. <https://doi.org/10.1109/TAP.2018.2874796>.
- [6] Di Renza RB, Magri Souza VPR, Ferreira TN, Matos LJ, Souza JAM, Siqueira GL. A new double-sided substrate-integrated waveguide slot array antenna for 5G applications. *Microw Opt Technol Lett* 2019;61(3):682–7. <https://doi.org/10.1002/mop.31617>.
- [7] Wen S, Dong Y. A low-profile wideband antenna with monopolelike radiation characteristics for 4G/5G indoor micro base station application. *IEEE Antennas Wirel Propag Lett* 2020;19(12):2305–9. <https://doi.org/10.1109/LAWP.2020.3030968>.
- [8] Sun K, Yang D, Liu S. A wideband hybrid feeding circularly polarized magneto-electric dipole antenna for 5G Wi-Fi. *Microw Opt Technol Lett* 2018;60(8): 1837–42. <https://doi.org/10.1002/mop.31259>.
- [9] Al-Rawi A, Hussain A, Yang J, Franzen M, Orlenius C, Kishk AA. A new compact wideband MIMO antenna - the double-sided tapered self-grounded monopole array. *IEEE Trans Antennas Propag* 2014;62(6):3365–9. <https://doi.org/10.1109/TAP.2014.2309985>.
- [10] Ma TG, Jeng SK. A printed dipole antenna with tapered slot feed for ultrawide-band applications. *IEEE Trans Antennas Propag* 2005;53(11):3833–6. <https://doi.org/10.1109/TAP.2005.858819>.
- [11] Allen CM, Eldek AA, Elsherbeni AZ, Smith CE, Huang CWP, Lee KF. Dual tapered meander slot antenna for radar applications. *IEEE Trans Antennas Propag* 2005;53(7):2324–8. <https://doi.org/10.1109/TAP.2005.850757>.
- [12] Ren J, et al. Large Frequency Ratio Vivaldi Antenna System With Low-Frequency Gain Enhancement Utilizing Dual-Function Taper Slot. *IEEE Trans Antennas Propag* 2022;70(6):4854–9.
- [13] Ding T, Wang M, Xiao J, Shu J, Ye Q. A Wrench-Shaped Monopole-Like Slot Antenna For UWB Applications. *Cross Strait Radio Science & Wireless Technology Conference (CSRSWTC)*:9–11. <https://doi.org/10.1109/CSRSWTC50769.2020.9372582>.
- [14] Ling CW, Lo WH, Yan RH, Chung SJ. Planar binomial curved monopole antennas for ultrawideband communication. *IEEE Trans Antennas Propag* 2007;55(9): 2622–4. <https://doi.org/10.1109/TAP.2007.904140>.
- [15] Wang L, et al. Compact UWB MIMO antenna with high isolation using fence-type decoupling structure. *IEEE Antennas Wirel Propag Lett* 2019;18(8):1641–5. <https://doi.org/10.1109/LAWP.2019.2925857>.
- [16] Nouri M, Abazari Aghdam S, Jafarieh A, Bagby J, Sahebghalam S. A wideband millimeter-wave antenna based on quasi-Yagi antenna with MIMO circular array antenna beamforming for 5G wireless networks. *Microw Opt Technol Lett* 2019;61(7):1810–4. <https://doi.org/10.1002/mop.31790>.
- [17] Chen HD, Tsai YC, Sim CYD, Kuo C. Broadband eight-antenna array design for Sub-6 GHz 5G NR bands metal-frame smartphone applications. *IEEE Antennas Wirel Propag Lett* 2020;19(7):1078–82. <https://doi.org/10.1109/LAWP.2020.2988898>.
- [18] Zhao A, Ren Z. Size reduction of self-isolated MIMO antenna system for 5G mobile phone applications. *IEEE Antennas Wirel Propag Lett* 2019;18(1):152–6. <https://doi.org/10.1109/LAWP.2018.2883428>.
- [19] S. Alam, I. Surjati, A. Ferawan, and T. Firmansyah, "Design and realization of compact microstrip antenna using fractal sierpinski carpet for wireless fidelity application," *Indones. J. Electr. Eng. Informatics*, vol. 6, no. 1, pp. 70–78, 2018, [10.11591/ije.v6i1.390](https://doi.org/10.11591/ije.v6i1.390).
- [20] Multi-output Y.S.M. Three wideband monopolar patch antennas in a Y-shape structure for 5G multi-input-multi-output access points. *IEEE Antennas Wirel Propag Lett* 2020;19(3):393–7. <https://doi.org/10.1109/LAWP.2020.2967354>.
- [21] Hu WEI, et al. Dual-Band Eight-Element MIMO Array Using Multi-Slot Decoupling Technique for 5G Terminals. *IEEE Access* 2019;7:153910–20. <https://doi.org/10.1109/ACCESS.2019.2948639>.
- [22] Wibisono G, Firmansyah T. "Concurrent multiband low noise amplifier with multisection impedance transformer", in *Asia-Pacific Microwave Conference Proceedings*. APMC 2012. <https://doi.org/10.1109/APMC.2012.6421776>.
- [23] Hua Q, Huang Yi, Member S, Alieldin A. A dual-band dual-polarized base station antenna using a novel feeding structure for 5G communications. *IEEE Access* 2020; 8:63710–7. <https://doi.org/10.1109/ACCESS.2020.2984199>.
- [24] Mohanty A, Sahu S. "Bio-inspired maple-leaf viburnum shaped 4-port compact wideband MIMO antenna with reinforced interleaved SIW cavity integration", *AEU - Int J Electron Commun* 2022;vol. 156:154383. <https://doi.org/10.1016/j.aeue.2022.154383>.
- [25] Wu T, Wang MJ, Chen J. Decoupling of MIMO antenna array based on half-mode substrate integrated waveguide with neutralization lines. *AEU - Int J Electron Commun* 2022;157:154416. <https://doi.org/10.1016/j.aeue.2022.154416>.
- [26] Yang SJ, Kim YD, Yun DJ, Yi DW, Myung NH. Antenna modeling using sparse infinitesimal dipoles based on recursive convex optimization. *IEEE Antennas Wirel Propag Lett* 2018;17(4):662–5. <https://doi.org/10.1109/LAWP.2018.2810289>.
- [27] S. Lin, H. Dong, Y. Liu, X. Y. Zhang, and X. Zhang, "Equivalent Circuit Modeling and Radiation Analysis of a Micro-Coaxial Collinear Antenna," *2022 IEEE Int. Symp. Antennas Propag. Ust. Radio Sci. Meet. AP-S/URSI 2022 - Proc.*, pp. 199–200, 2022, [10.1109/AP-S/USNC-URSI47032.2022.9886416](https://doi.org/10.1109/AP-S/USNC-URSI47032.2022.9886416).
- [28] Gómez-Tagle J, Christodoulou CG. Extended cavity model analysis of stacked microstrip ring antennas. *IEEE Trans Antennas Propag* 1997;45(11):1626–35. <https://doi.org/10.1109/8.650074>.
- [29] Wang CJ, Chen LT. Modeling of stepped-impedance slot antenna. *IEEE Trans Antennas Propag* 2014;62(2):955–9. <https://doi.org/10.1109/TAP.2013.2291906>.
- [30] S. Koziel, S. Ogurtsov, and J. P. Jacobs, "Modeling of wideband antennas using space-mapping-corrected kriging surrogates," *2013 7th Eur. Conf. Antennas Propagation, EuCAP 2013*, pp. 1540–1543, 2013.
- [31] Lu G, Korisch I, Greenstein L, Spasojevic P. "Antenna modelling using linear elements, with applications to UWB", *IEEE Antennas Propag. Soc AP-S Int Symp* 2004;3:2544–7. <https://doi.org/10.1109/aps.2004.1331892>.
- [32] Nayak U, Chongder P, Biswas A. "Novel filtering and diplexing linear tapered slot antenna with high-selectivity", *AEU - Int J Electron Commun* 2022;156. <https://doi.org/10.1016/j.aeue.2022.154363>.
- [33] Roblin C, D'Errico R. Statistical analysis of a parametric model of a 'population' of UWB antennas. *Eur Conf Antennas Propagation, EuCAP 2009:3343–7*.
- [34] Wallace JW, Mehmood R. On the accuracy of equivalent circuit models for multi-antenna systems. *IEEE Trans Antennas Propag PART 1* 2012;vol. 60(2):540–7. <https://doi.org/10.1109/TAP.2011.2152339>.
- [35] Papamichael V, Soras C. MIMO antenna modelling using the effective length matrices. *Prog Electromagn Res C* 2009;10:111–27. <https://doi.org/10.2528/PIERC09061903>.
- [36] Papamichael VC. Eigen-analysis of lossy compact multielement antenna systems. *IEEE Antennas Wirel Propag Lett* 2009;8:1334–6. <https://doi.org/10.1109/LAWP.2009.2038288>.
- [37] S. Kareemulla and V. Kumar, "Diversity performance of band notched ultrawideband MIMO antenna," *Optik*, vol. 272, no. August 2022, p. 170128, 2023, <https://doi.org/10.1016/j.ijleo.2022.170128>.
- [38] F. Wang, Z. Duan, Q. Li, Y. Wei, and Y. Gong, "Compact wideband MIMO antenna for 5G communication," *2017 IEEE Antennas Propag. Soc. Int. Symp. Proc.*, vol. 2017-Janua, no. c, pp. 939–940, 2017, [10.1109/APUSNRCURSINRSM.2017.8072512](https://doi.org/10.1109/APUSNRCURSINRSM.2017.8072512).

- [39] Chen Z, Yuan XT, Ren J, Yuan T. "An ultra-wideband MIMO antenna for 5G smartphone", *AEU - Int J Electron Commun* 2022;vol. 154:154301. <https://doi.org/10.1016/j.aeue.2022.154301>.
- [40] Ansarizadeh M, Ghorbani A, Abd-Allahmeed RA. An approach to equivalent circuit modeling of rectangular microstrip antennas. *Prog Electromagn Res B* 2008;8:77-86. <https://doi.org/10.2528/pterb08050403>.
- [41] Adams JJ, Bernhard JT. Broadband equivalent circuit models for antenna impedances and fields using characteristic modes. *IEEE Trans Antennas Propag* 2013;61(8):3985-94. <https://doi.org/10.1109/TAP.2013.2261852>.
- [42] N. M. Din, C. K. Chakrabarty, A. Bin Ismail, K. K. A. Devi2, and W.-Y. Chen, "Design of RF Energy Harvesting System for energizing low power devices," *Prog. Electromagn. Res.*, vol. 132, no. July, pp. 49-69, 2012.
- [43] Devi KKA, Sadasivam S, Din NM, Chakrabarthy CK, Rajib SK. Design of a wideband 377 Ohm E-Shaped patch antenna for RF energy harvesting. *Microw Opt Technol Lett* 2013;55(3):569-73. <https://doi.org/10.1002/mop>.
- [44] Iqbal A, Saraereh OA, Ahmad AW, Bashir S. Mutual Coupling Reduction Using F-Shaped Stubs in UWB-MIMO Antenna. *IEEE Access* 2017;6:2755-9. <https://doi.org/10.1109/ACCESS.2017.2785232>.
- [45] Technologies L. SMA Connectors [Online]. Available: SMA Connectors 2012. <https://www.hasco-inc.com/categories/connectors/sma-connectors.html>.
- [46] Chang TN, Lin JM. Dual-band circularly polarized monopole antenna. *J Electromagn Waves Appl* 2015;29(7):843-57. <https://doi.org/10.1080/09205071.2015.1022265>.
- [47] Liang Z, Li Y, Long Y. Multiband monopole mobile phone antenna with circular polarization for GNSS application. *IEEE Trans Antennas Propag* 2014;62(4):1910-7. <https://doi.org/10.1109/TAP.2014.2299821>.
- [48] M. H. Shih, K. L. Hsiao, and C. J. Wang, "A monopole antenna with circular polarization," *ISAP 2014 - 2014 Int. Symp. Antennas Propagation, Conf. Proc.*, pp. 609-610, 2015, 10.1109/ISANP.2014.7026798.
- [49] Li Y, et al. "Mutual coupling reduction for monopole MIMO antenna using L-shaped stubs, defective ground and chip resistors", *AEU - Int J Electron Commun* 2023; vol. 160:154524. <https://doi.org/10.1016/j.aeue.2022.154524>.
- [50] A. Khan, A. Wakeel, L. Qu, and Z. Zahid, "Dual-band 8 × 8 MIMO antenna with enhanced isolation and efficiency for 5G smartphone applications," *AEU - Int. J. Electron. Commun.*, vol. 163, no. December 2022, p. 154600, 2023, 10.1016/j.aeue.2023.154600.
- [51] Liu L, Cheung SW, Yuk TI. Compact MIMO antenna for portable devices in UWB applications. *IEEE Trans Antennas Propag* 2013;61(8):4257-64. <https://doi.org/10.1109/TAP.2013.2263277>.
- [52] Zhu J, Li S, Feng B. Compact dual-polarized UWB quasi-self-complementary MIMO / Diversity. *IEEE Antennas Wirel Propag Lett* 2016;15:905-8. <https://doi.org/10.1109/LAWP.2015.2479622>.
- [53] Irene G, Rajesh A. A penta-band reject inside cut Koch fractal hexagonal monopole UWB MIMO antenna for portable devices. *Prog Electromagn Res C* 2018;82:225-35. <https://doi.org/10.2528/pterc18020604>.
- [54] Khan MS, Capobianco A, Najam AI, Shoab I, Autizi E, Shafique MF. Compact ultra-wideband diversity antenna with a floating parasitic digitated decoupling structure. *IET Microwaves, Antennas Propag* 2014;8(10):747-53. <https://doi.org/10.1049/iet-map.2013.0672>.
- [55] Qu L, Piao H. A dual-port single-dipole MIMO antenna pair based on selective modal excitation for 5G metal-rimmed terminals. *IEEE Access* 2022;10:100208-14. <https://doi.org/10.1109/ACCESS.2022.3188017>.
- [56] A. Qudus and R. Saleem, "Dual Port UWB Diversity/MIMO Antenna with Dual Band-Notch Characteristics," in *International Conference on Signal Processing and Communication Systems (ICSPCS)*, 2016, pp. 7-10. <https://doi.org/10.1109/ICSPCS.2016.7843320>.
- [57] Sharma K, Pandey GP. Two port compact MIMO antenna for ISM band applications. *Prog Electromagn Res C* 2020;100:173-85. <https://doi.org/10.2528/pterc20011504>.
- [58] Raviteja GV, Kumar PP, Ramesh G, Prasad BG, Sai RV. Wearable Dual-port MIMO antenna for On-body applications," in *International Conference on Elect. Electron Inform Commun Technol (ICEEICT)* 2022:7-11. <https://doi.org/10.1109/ICEEICT53079.2022.9768416>.
- [59] A. I. Afifi, A. S. Abd El-Hameed, A. Allam, S. M. Ahmed, and A. B. Abdel-Rahman, "Dual Port MIMO Antenna with Low Mutual Coupling Based on Asymmetric EBG Decoupling Structure," *15th Eur. Conf. Antennas Propagation, EuCAP 2021*, pp. 5-9, 2021, 10.23919/EuCAP51087.2021.9411149.
- [60] Soltani S, Lotfi P, Murch RD. Design of compact dual-band dual-port WLAN MIMO antennas using slots. *IEEE Antennas Propag Soc AP-S Int Symp* 2015;vol. 2015:924-5. <https://doi.org/10.1109/APS.2015.7304849>.
- [61] Gireesh P, Sandeep Kumar P, Malathi K, Khanra I, Agarwal A, Sivakumar K. Design and analysis of dual port super wideband antenna set for MIMO applications. *J Phys Conf Ser* 2021;1964(6):pp. <https://doi.org/10.1088/1742-6596/1964/6/062051>.
- [62] Kumar A, Ansari AQ, Kanaujia BK, Kishor J, Kumar S. An ultra-compact two-port UWB-MIMO antenna with dual band-notched characteristics. *AEU - Int J Electron Commun* 2020;114:152997. <https://doi.org/10.1016/j.aeue.2019.152997>.
- [63] Anand S, Theetharappan R. "Metamaterial and SIW inspired isolating fences for lateral de-coupling in MIMO antenna", *AEU - Int J Electron Commun* 2023;vol. 166:154667. <https://doi.org/10.1016/j.aeue.2023.154667>.

Modeling of quasi-tapered microstrip antenna based on expansion-exponential tapered method and its application for wideband MIMO structure

ORIGINALITY REPORT

18%

SIMILARITY INDEX

13%

INTERNET SOURCES

16%

PUBLICATIONS

%

STUDENT PAPERS

PRIMARY SOURCES

1	Michael Kerr, Fengling Han, Xun Yi, Andrei Kelarev, Ron Van Schyndel. "A non-invasive method for the cataloguing and authentication of surveillance video using on-camera blockchain participation, machine learning and signal analysis", Forensic Science International: Digital Investigation, 2023 Publication	1%
2	ebin.pub Internet Source	1%
3	faculty.ksu.edu.sa Internet Source	1%
4	"Optical and Wireless Technologies", Springer Science and Business Media LLC, 2020 Publication	1%
5	academic.hep.com.cn Internet Source	1%
6	livrepository.liverpool.ac.uk Internet Source	1%

7	www.hindawi.com Internet Source	1 %
8	dspace.dtu.ac.in:8080 Internet Source	<1 %
9	eprints.untirta.ac.id Internet Source	<1 %
10	Jin Cheng, Robert J. Adams, John C. Young, Michael A. Khayat. "Augmented EFIE With Normally Constrained Magnetic Field and Static Charge Extraction", IEEE Transactions on Antennas and Propagation, 2015 Publication	<1 %
11	A. Moradikordalivand, T. A. Rahman, S. Ebrahimi, S. Hakimi. "An Equivalent Circuit Model for Broadband Modified Rectangular Microstrip-Fed Monopole Antenna", Wireless Personal Communications, 2014 Publication	<1 %
12	www.freepatentsonline.com Internet Source	<1 %
13	Ultra-Wideband Short Pulse Electromagnetics 9, 2010. Publication	<1 %
14	curve.carleton.ca Internet Source	<1 %

hal.archives-ouvertes.fr

15

Internet Source

<1 %

16

www.scilit.net

Internet Source

<1 %

17

Majid Shokri, Changiz Ghobadi, Javad Nourinia, Pedro Pinho et al. "A Compact Four Elements Self-Isolated MIMO Antenna for C-Band Applications", 2023 IEEE 27th Workshop on Signal and Power Integrity (SPI), 2023

Publication

<1 %

18

Wu, J., Z. Zhao, Z. Nie, and Q. Liu. "A Broadband Unidirectional Antenna Based on Closely Spaced Loading Method", IEEE Transactions on Antennas and Propagation, 2012.

Publication

<1 %

19

eprints.utm.edu.my

Internet Source

<1 %

20

thesai.org

Internet Source

<1 %

21

ijece.iaescore.com

Internet Source

<1 %

22

Yue Zhao. "A N77/78/79 Self-Decoupled Antenna Pair for 5G Smartphones", 2020 IEEE Asia-Pacific Microwave Conference (APMC), 2020

Publication

<1 %

satellite applications", International Journal of Communication Systems, 2022

Publication

79

Amjad Iqbal, Abdul Basir, Amor Smida, Nazih Khaddaj Mallat, Issa Elfergani, Jonathan Rodriguez, Sunghwan Kim. "Electromagnetic Bandgap Backed Millimeter-Wave MIMO Antenna for Wearable Applications", IEEE Access, 2019

Publication

<1 %

80

Saswati Ghosh, Ajay Chakrabarty. "Dual Band Circularly Polarized Monopole Antenna Design for RF Energy Harvesting", IETE Journal of Research, 2015

Publication

<1 %

Exclude quotes Off

Exclude matches Off

Exclude bibliography On

Modeling of quasi-tapered microstrip antenna based on expansion-exponential tapered method and its application for wideband MIMO structure

GRADEMARK REPORT

FINAL GRADE

/0

GENERAL COMMENTS

Instructor

PAGE 1

PAGE 2

PAGE 3

PAGE 4

PAGE 5

PAGE 6

PAGE 7

PAGE 8

PAGE 9

PAGE 10

PAGE 11

PAGE 12

PAGE 13

PAGE 14

Lampiran Tambahan :

Print screen :

AEU - International Journal of Electronics
and Communications

terindex Web of Science dengan

Impact Factor 3.169

Print screen :

List jurnal sudah di scopus-author

Print screen :

SCIMAGO SJR = 0.753 dan Quartil nya

Search results > Journal profile

Favorite Export

JCR YEAR

2021

AEU-INTERNATIONAL JOURNAL OF ELECTRONICS AND COMMUNICATIONS

ISSN

1434-8411

EISSN

1618-0399

JCR ABBREVIATION

AEU-INT J ELECTRON C

ISO ABBREVIATION

AEU-Int. J. Electron. Commun.

Journal information

EDITION

Science Citation Index Expanded (SCIE)

CATEGORY

TELECOMMUNICATIONS - SCIE
ENGINEERING, ELECTRICAL & ELECTRONIC - SCIE

LANGUAGES

Multi-Language

REGION

GERMANY (FED REP GER)

231 ELECTRONIC JCR YEAR

1997

Publisher information

PUBLISHER

ELSEVIER GMBH

ADDRESS

HACKERBRUCKE 6, 80335
MUNICH, GERMANY

PUBLICATION FREQUENCY

15 issues/year

Journal's performance

Journal Impact Factor

The Journal Impact Factor (JIF) is a journal-level metric calculated from data indexed in the Web of Science Core Collection. It should be used with careful attention to the many factors that influence citation rates, such as the volume of publication and citations characteristics of the subject area and type of journal. The Journal Impact Factor can complement expert opinion and informed peer review. In the case of academic evaluation for tenure, it is inappropriate to use a journal-level metric as a proxy measure for individual researchers, institutions, or articles. [Learn more](#)

2021 JOURNAL IMPACT FACTOR

3.169

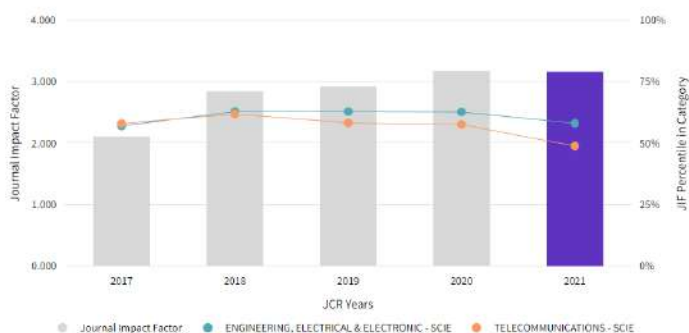
[View calculation](#)

JOURNAL IMPACT FACTOR WITHOUT SELF CITATIONS

2.483

[View calculation](#)

Journal Impact Factor Trend 2021



[View all years](#)

Journal Impact Factor contributing items

[Export](#)

Citable items (787)	Citing Sources (397)
TITLE	CITATION COUNT
Novel method of mobile edge computation offloading based on evolutionary game strategy for IoT devices	25
Energy Aware Cluster Based Multi-hop Energy Efficient Routing Protocol using Multiple Mobile Nodes (MEACBM) in Wireless Sensor Networks	24
Compact and low-frequency broadband microwave metamaterial absorber based on meander wire structure loaded resistors	21
Printed millimeter-wave MIMO-based slot antenna arrays for 5G networks	20
A review of GaN HEMT broadband power amplifiers	17
Improving the electrical characteristics of nanoscale triple-gate junctionless FinFET using gate oxide engineering	17
Non-ideal memristor synapse-coupled bi-neuron Hopfield neural network: Numerical simulations and breadboard experiments	16
Neutralization technique based two and four port high isolation MIMO antennas for UWB communication	15
Outage probability of NOMA system with wireless power transfer at source and full-duplex relay	15
Reconfigurable chaotic pseudo random number generator based on FPGA	15

[View All in Web of Science](#)

Journal Citation Indicator (JCI)

[Export](#)

0.83

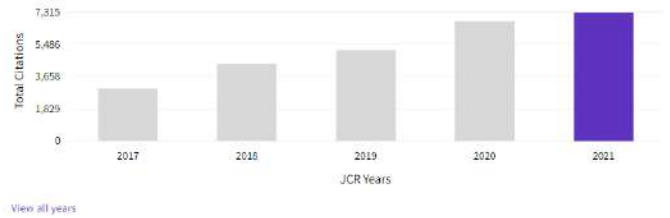
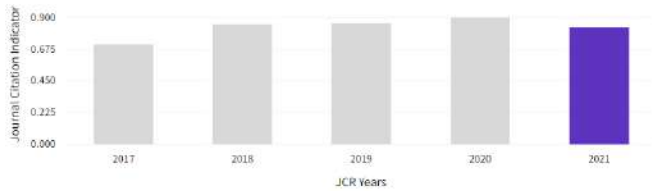
The Journal Citation Indicator (JCI) is the average Category Normalized Citation Impact (NCI) of citable items (articles & reviews) published by a journal over a recent three year period. The average JCI in a category is 1. Journals with a JCI of 1.5 have 50% more citation impact than the average in that category. It may be used alongside other metrics to help you evaluate journals. [Learn more](#)

Total Citations

[Export](#)

7,315

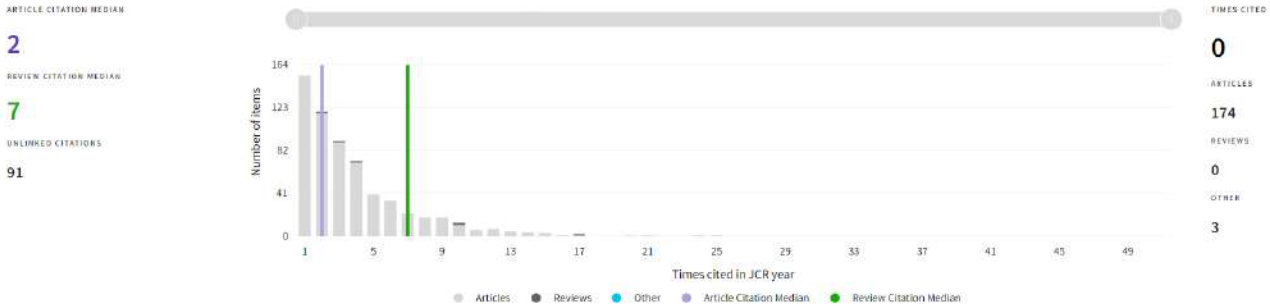
The total number of times that a journal has been cited by all journals included in the database in the JCR year. Citations to journals listed in JCR are compiled annually from the JCR years combined database, regardless of which JCR edition lists the journal.



Citation distribution

Export

The Citation Distribution shows the frequency with which items published in the year or two years prior were cited in the JCR data year (i.e., the component of the calculation of the JIF). The graph has similar functionality as the JIF Trend graph, including hover-over data descriptions for each data point, and an interactive legend where each data element's legend can be used as a toggle. You can view Articles, Reviews, or Non-Citable (other) items to the JIF numerator. [Learn more](#)



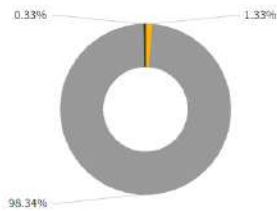
Open Access (OA)

Export

The data included in this tile summarizes the items published in the journal in the JCR data year and in the previous two years. For example, in the 2020 JCR data, released in June 2021, the Open Access (OA) data show the publication model (Gold OA or subscription) of materials published in 2018, 2019 and 2020, and citations in 2020 to these items. This three-year set of published items is used to provide descriptive analysis of the content and community of the journal. [Learn more](#)

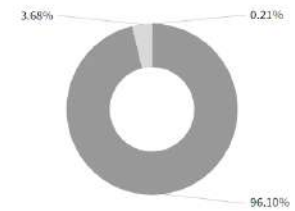
Items

TOTAL CITABLE 1,200
% OF CITABLE OA 1.33%



Citations*

TOTAL CITABLE 2,720
% OF CITABLE OA 0.22%



UNLINKED CITATIONS 104 / 3.68%

*Citations in 2021 to items published in [2019-2021]

Rank by Journal Impact Factor

Journals within a category are sorted in descending order by Journal Impact Factor (JIF) resulting in the Category Ranking below. A separate rank is shown for each category in which the journal is listed in JCR. Data for the most recent year is presented at the top of the list, with other years shown in reverse chronological order. [Learn more](#)

EDITION
Science Citation Index Expanded (SCIE)
CATEGORY
ENGINEERING, ELECTRICAL & ELECTRONIC
116/276

JCR YEAR	JIF RANK	JIF QUARTILE	JIF PERCENTILE
2021	116/276	Q2	58.15
2020	102/273	Q2	62.82
2019	99/266	Q2	62.97
2018	99/266	Q2	62.97
2017	112/260	Q2	57.12

EDITION
Science Citation Index Expanded (SCIE)
CATEGORY
TELECOMMUNICATIONS
48/93

JCR YEAR	JIF RANK	JIF QUARTILE	JIF PERCENTILE
2021	48/93	Q3	45.92
2020	39/91	Q2	57.69
2019	38/90	Q2	58.33
2018	34/88	Q2	61.93
2017	37/87	Q2	58.05

Rank by Journal Citation Indicator (JCI) [Ⓞ]

Journals within a category are sorted in descending order by Journal Citation Indicator (JCI) resulting in the Category Ranking below. A separate rank is shown for each category in which the journal is listed in JCR. Data for the most recent year is presented at the top of the list, with other years shown in reverse chronological order. [Learn more](#)

CATEGORY
ENGINEERING, ELECTRICAL & ELECTRONIC
118/344

JCR YEAR	JCI RANK	JCI QUARTILE	JCI PERCENTILE	
2021	118/344	Q2	65.84	
2020	98/319	Q2	69.44	
2019	108/318	Q2	66.19	
2018	114/312	Q2	63.62	
2017	133/306	Q2	56.70	

CATEGORY
TELECOMMUNICATIONS
47/115

JCR YEAR	JCI RANK	JCI QUARTILE	JCI PERCENTILE	
2021	47/115	Q2	59.57	
2020	37/105	Q2	65.24	
2019	37/105	Q2	65.24	
2018	43/104	Q2	59.13	
2017	44/102	Q2	57.35	

Citation network

Cited Half-life

3.5 years

The Cited Half-Life is the median age of the items in this journal that were cited in the JCR year. Half of a journal's cited items were published more recently than the cited half-life.

TOTAL NUMBER OF CITES

7,315

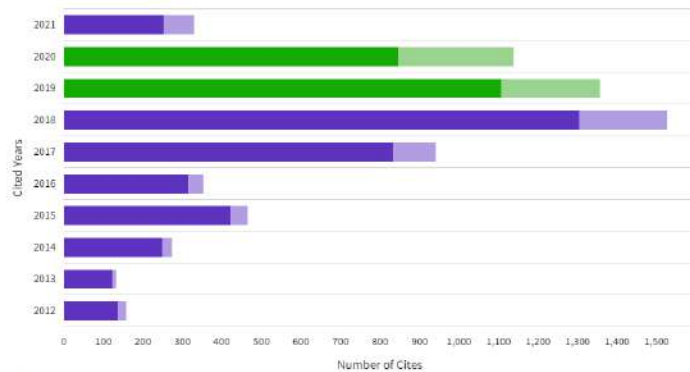
NON SELF-CITATIONS

6,149

SELF-CITATIONS

1,166

Cited Half-life Data



- Non-self citations: citations to the journal from the items in other sources
- Citations to items in the journal from items in the same journal
- Citations used to calculate the Impact Factor

Citing Half-life

5.7 years

The Citing Half-Life is the median age of items in other publications cited by this journal in the JCR year.

TOTAL NUMBER OF CITES

12,887

NON SELF-CITATIONS

11,721

SELF-CITATIONS

1,166

Citing Half-life Data

[Export](#)

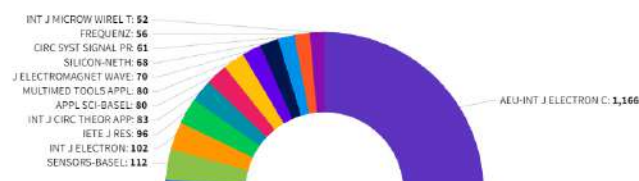
CITED YEAR	# OF CITES FROM 2021	CUMULATIVE %	# OF CITING SOURCES
All years	7,315 citations	100.00%	811 sources
2021	330 citations	4.51%	95 sources
2020	1,138 citations	20.07%	259 sources
2019	1,356 citations	38.61%	296 sources
2018	1,526 citations	59.47%	308 sources
2017	940 citations	72.32%	284 sources
2016	353 citations	77.14%	168 sources
2015	465 citations	83.50%	209 sources
2014	274 citations	87.25%	146 sources
2013	132 citations	89.05%	88 sources
2012	158 citations	91.21%	90 sources
Older	643 citations		

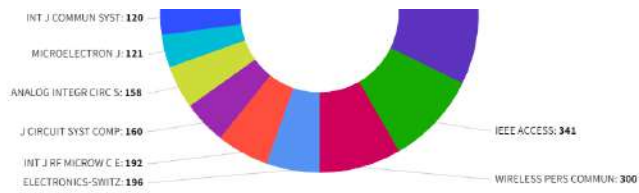
Journal Citation Relationships

Cited Data

Citing Data

Top 20 journals citing AEU-INT J ELECTRON C by number of citations:





Content metrics

Source data

This tile shows the breakdown of document types published by the journal. Citable Items are Articles and Reviews. For the purposes of calculating JIF, a JCR year considers the publications of that journal in the two prior years. [Learn more](#)

413 total citable items

	ARTICLES	REVIEWS	COMBINED(C)	OTHER DOCUMENT TYPES(D)	PERCENTAGE
NUMBER IN JCR YEAR 2022 (A)	410	3	413	1	100%
NUMBER OF REFERENCES (B)	12,734	152	12,886	1	100%
RATIO (B/A)	31.1	50.7	31.2	1.0	

Average JIF Percentile

Export

The Average Journal Impact Factor Percentile takes the sum of the JIF Percentile rank for each category under consideration, then calculates the average of those values. [Learn more](#)

ALL CATEGORIES AVERAGE	53.54
EDITION	Science Citation Index Expanded
ENGINEERING, ELECTRICAL & ELECTRONIC	58.15
TELECOMMUNICATIONS	48.92

Contributions by organizations

Export

Organizations that have contributed the most papers to the journal in the most recent three-year period. [Learn more](#)

RANK	ORGANIZATION	COUNT
1	NATIONAL INSTITUTE OF TECHNOLOGY (NIT SYSTEM)	86
2	INDIAN INSTITUTE OF TECHNOLOGY SYSTEM (IIT SYSTEM)	59
3	EGYPTIAN KNOWLEDGE BANK (EKB)	55
4	ISLAMIC AZAD UNIVERSITY	41
5	DELHI TECHNOLOGICAL UNIVERSITY	19
6	TON DUC THANG UNIVERSITY	18
7	JAWAHARLAL NEHRU UNIVERSITY, NEW DELHI	15
-	KING MONGKUTS INSTITUTE OF TECHNOLOGY LADKRABANG	15
-	SHAHID BEHESHTI UNIVERSITY	15
10	BIRNO UNIVERSITY OF TECHNOLOGY	14

Contributions by country/region

Export

Countries or Regions that have contributed the most papers to the journal in the most recent three-year period. [Learn more](#)

RANK	COUNTRY / REGION	COUNT
1	India	384
2	Iran	243
3	CHINA MAINLAND	187
4	Turkey	68
5	Egypt	59
6	Spain	44
7	Canada	36
8	USA	33
9	Malaysia	32
10	Brazil	30

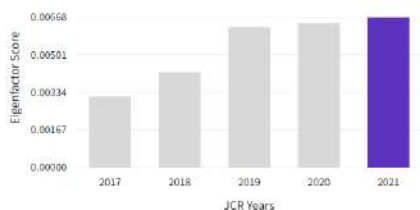
Additional metrics

Eigenfactor Score

Export

0.00668

The Eigenfactor Score is a reflection of the density of the network of citations around the journal using 5 years of cited content as cited by the Current Year. It considers both the number of citations and the source of those citations, so that highly cited sources will influence the network more than less cited sources. The Eigenfactor calculation does not include journal self-citations. [Learn more](#)

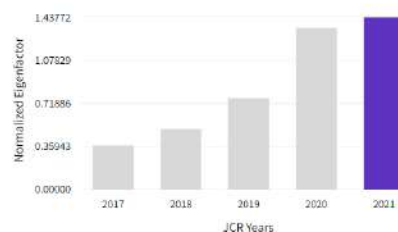


Normalized Eigenfactor

Export

1.43772

The Normalized Eigenfactor Score is the Eigenfactor score normalized, by rescaling the total number of journals in the JCR each year, so that the average journal has a score of 1. Journals can then be compared and influence measured by their score relative to 1. [Learn more](#)

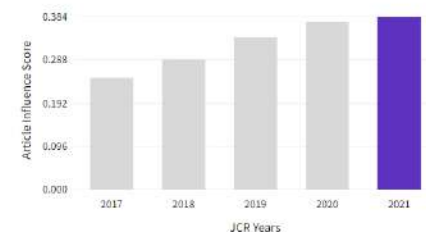


Article influence score

Export

0.384

The Article Influence Score normalizes the Eigenfactor Score according to the cumulative size of the cited journal across the prior five years. The mean Article Influence Score for each article is 1.00. A score greater than 1.00 indicates that each article in the journal has above-average influence. [Learn more](#)



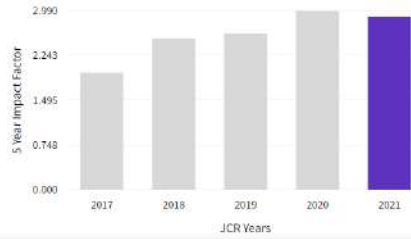
5 Year Impact Factor



2.895

[View Calculation](#)

The 5-year Impact Factor is the average number of times articles from the journal published in the past five years have been cited in the JCR year. It is calculated by dividing the number of citations in the JCR year by the total number of articles published in the five previous years.



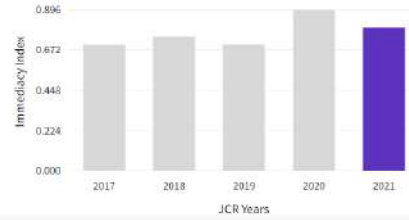
Immediacy Index



0.799

[View Calculation](#)

The Immediacy Index is the count of citations in the current year to the journal that reference content in this same year. Journals that have a consistently high Immediacy Index attract citations rapidly. [Learn more](#)



How likely are you to recommend Journal Citation Reports to a friend or coworker?

Not at all likely 0 1 2 3 4 5 6 7 8 9 10 Extremely likely





This author profile is generated by Scopus. Learn more

Firmansyah, Teguh

Universitas Sultan Ageng Tirtayasa, Serang, Indonesia © 54971241500 <https://orcid.org/0000-0002-9000-9337> View more

286

Citations by 230 documents

58

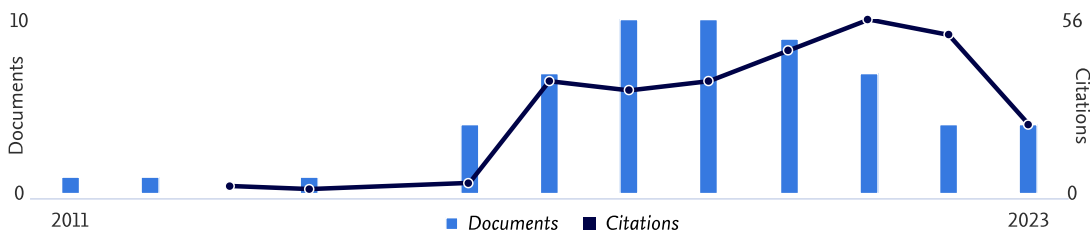
Documents

11

h-index View h-graph

Set alert Save to list Edit profile More

Document & citation trends



Analyze author output Citation overview

Most contributed Topics 2018–2022

Stepped Impedance Resonator; Bandpass Filters; Compact

7 documents

Multiple-Input Multiple-Output (MIMO); Antenna; Antenna Arrays

3 documents

Radio over Fiber; Sidebands; Optics

2 documents

View all Topics

58 Documents Cited by 230 documents 1 Preprint 113 Co-Authors 27 Topics 0 Awarded Grants

Beta

58 documents

Export all Save all to list

Sort by Date (...

Article

Modeling of quasi-tapered microstrip antenna based on expansion-exponential tapered method and its application for wideband MIMO structure

0

Citations

Firmansyah, T., Praptodiyono, S., Permana, J., ...Alaydrus, M., Kondoh, J.

AEU - International Journal of Electronics and Communications, 2023, 169, 154745

Show abstract View at Publisher Related documents

Article

Multifunctional of dual-band permittivity sensors with antenna using multicascode T-shaped resonators for simultaneous measurement of solid materials and data transfer capabilities

0

Citations

Alam, S., Zakaria, Z., Surjati, I., ...Alaydrus, M., Firmansyah, T.

Measurement: *Journal of the International Measurement Confederation*, 2023, 217,

113078

Show abstract [▼](#) View at Publisher [↗](#) Related documents

Article • Article in Press

Integrated Microwave Sensor and Antenna Sensor Based on Dual T-Shaped Resonator Structures for Contact and Non-Contact Characterization of Solid Material

0

Citations

Alam, S., Zakaria, Z., Surjati, I., ...Alaydrus, M., Firmansyah, T.

IEEE Sensors Journal, 2023

Show abstract [▼](#) View at Publisher [↗](#)

Conference Paper

Highly Independent Dual-Band Permittivity Sensors for Simultaneous Measurement of Solid Materials

0

Citations

Alam, S., Zakaria, Z., Surjati, I., ...Alaydrus, M., Firmansyah, T.

2023 33rd International Conference Radioelektronika, RADIOELEKTRONIKA 2023, 2023

Show abstract [▼](#) View at Publisher [↗](#) Related documents

Article

Dual-Band Independent Permittivity Sensor Using Single-Port with a Pair of U-Shaped Structures for Solid Material Detection

8

Citations

Alam, S., Zakaria, Z., Surjati, I., ...Alaydrus, M., Firmansyah, T.

IEEE Sensors Journal, 2022, 22(16), pp. 16111–16119

Show abstract [▼](#) View at Publisher [↗](#) Related documents

Article • Open access

Bandwidth Enhancement and Circular Polarization Microstrip Antenna Using L Slot and Rectangular Parasitic Stacked | Мікросмуужкова антена з розширенням смуги пропускання та круговою поляризацією з використанням L-слоту та стопкою прямокутних паразитних елементів

0

Citations

Alam, S., Surjati, I., Sari, L., ...Zakaria, Z., Shairi, N.A.

Journal of Nano- and Electronic Physics, 2022, 14(4), 04029

Show abstract [▼](#) View at Publisher [↗](#) Related documents

Article • Open access

Triple Band Notched Microstrip Antenna Using Planar Series 2x2 Element Array for 5G Communication System

1

Citations

Alam, S., Surjati, I., Sari, L., ...Hikmaturokhman, A., Firmansyah, T.

Journal of Nano- and Electronic Physics, 2022, 14(1), 01019

Show abstract [▼](#) View at Publisher [↗](#) Related documents

Article

Reconfigurable localized surface plasmon resonance spectrum based on acousto-dynamic coupling in arrays gold nanoparticles induced by shear horizontal vibration

0

Citations

Firmansyah, T., Wibisono, G., Tjipto Rahardjo, E., Kondoh, J.

Applied Surface Science, 2022, 571, 151331

Show abstract [▼](#) View at Publisher [↗](#) Related documents

Article

Multifunctional and Sensitivity Enhancement of Hybrid Acoustoplasmonic Sensors Fabricated on 36XY-LiTaO₃ with Gold Nanoparticles for the Detection of Permittivity, Conductivity, and the Refractive Index

4

Citations

Firmansyah, T., Wibisono, G., Rahardjo, E.T., Kondoh, J.

ACS Applied Materials and Interfaces, 2021, 13(11), pp. 13822–13837

Article


A highly independent and controllable dual-band bandpass filter based on source-load coupling with stub-block isolation structure

2


Citations

Denny, Y.R., Firmansyah, T.

Microwave and Optical Technology Letters, 2021, 63(3), pp. 729–735

Show abstract  View at Publisher  Related documents

< Previous 1 2 3 4 5 6 Next >

Display 10 results 

[Back to top](#)

[> View list in search results format](#)

[> View references](#)

[!\[\]\(e9474ce1d70442456f8fe9c393ea149c_img.jpg\) Set document alert](#)

About Scopus

[What is Scopus](#)

[Content coverage](#)

[Scopus blog](#)

[Scopus API](#)

[Privacy matters](#)

Language

[日本語版を表示する](#)

[查看简体中文版本](#)

[查看繁體中文版本](#)

[Просмотр версии на русском языке](#)

Customer Service

[Help](#)

[Tutorials](#)

[Contact us](#)

ELSEVIER

[Terms and conditions ↗](#) [Privacy policy ↗](#)

Copyright © Elsevier B.V. ↗. All rights reserved. Scopus® is a registered trademark of Elsevier B.V.

We use cookies to help provide and enhance our service and tailor content. By continuing, you agree to the use of cookies ↗.



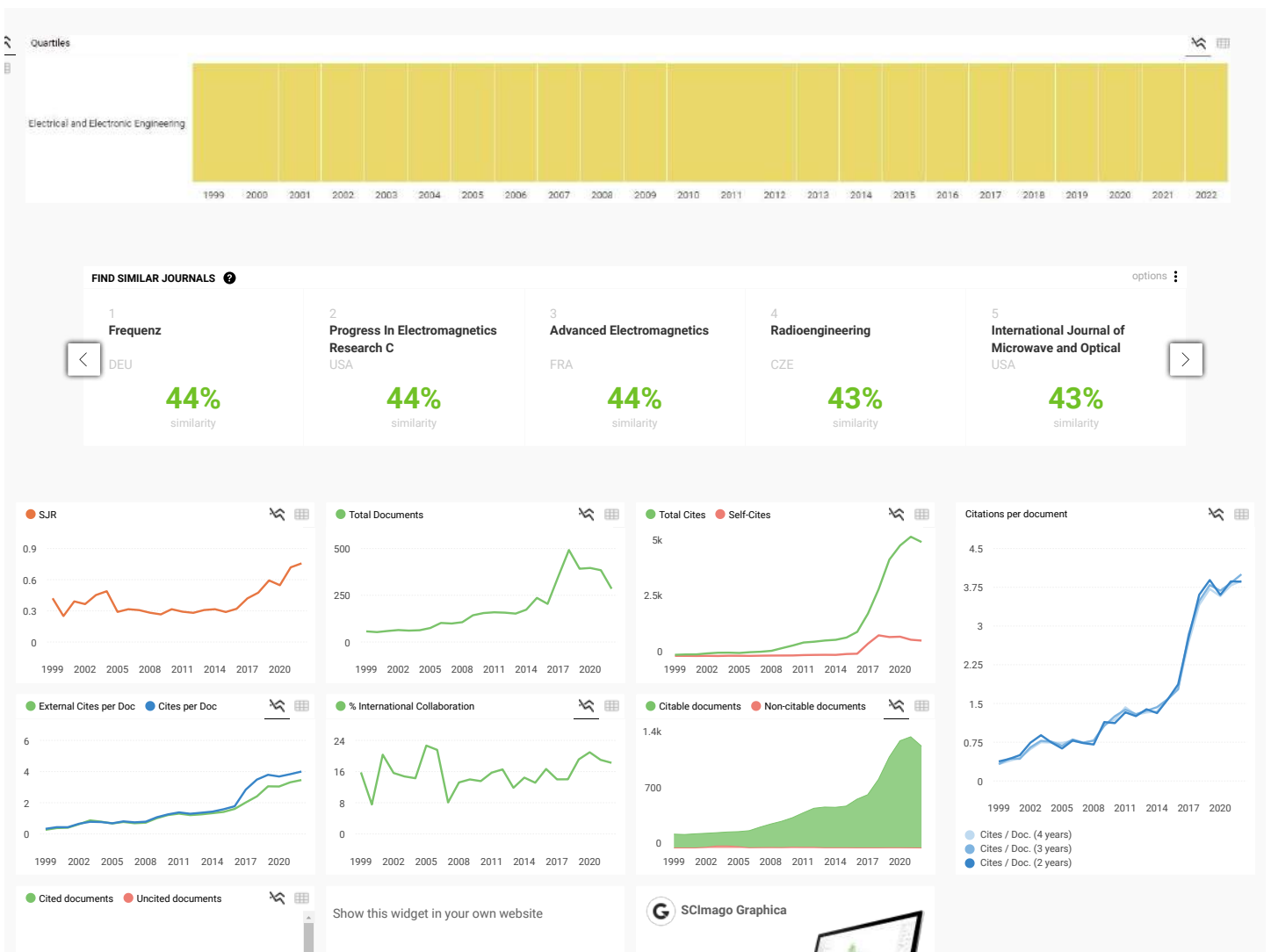
AEU - International Journal of Electronics and Communications

COUNTRY Germany Universities and research institutions in Germany Media Ranking in Germany	SUBJECT AREA AND CATEGORY Engineering Electrical and Electronic Engineering	PUBLISHER Urban und Fischer Verlag Jena	H-INDEX 72
PUBLICATION TYPE Journals	ISSN 16180399, 14348411	COVERAGE 2001-2022	INFORMATION Homepage How to publish in this journal Contact

SCOPE

AEU is an international scientific journal which publishes original works, invited tutorials, and special issues on the state-of-the-art research areas. The journal's scope covers design and implementation of electronic devices, circuits, and communication systems, including but not limited to: circuit theory and applications analog and digital integrated circuit design electronic components and devices RF circuits analog, digital, and mixed signal processing building blocks and systems (filters, oscillators, VCOs, PLLs, etc.) biomedical circuits memristors and memristive circuits neuromorphic circuits power electronic circuits integrated circuits for communications circuits for optical communication systems realization of microwave, radar, and sonar systems realization of antenna systems keywords: circuit theory, integrated circuits, analog circuits, digital circuits, mixed signal circuits, electronic components, electronic devices, memristors, filters, oscillators, biomedical circuits, neuromorphic circuits, RF circuits, optical communication systems, microwave systems, antenna systems.

Join the conversation about this journal





AEU - International Journal of Electronics and...

Q2 Electrical and Electronic Engineering

Best Quartile

SJR 2022 0.76

← Just copy the code below and paste within your html code:

<a href="https://www.scimag

Explore, visually communicate and make sense of data with our [new data visualization tool](#).



Metrics based on Scopus® data as of April 2023

Leave a comment

Name

Email

(will not be published)

I'm not a robot

The users of Scimago Journal & Country Rank have the possibility to dialogue through comments linked to a specific journal. The purpose is to have a forum in which general doubts about the processes of publication in the journal, experiences and other issues derived from the publication of papers are resolved. For topics on particular articles, maintain the dialogue through the usual channels with your editor.

Developed by: Scimago

Powered by: Scopus